THE UNIVERSITY *of* EDINBURGH

External fire spread

from

timber lined compartments

Georgios Kanellopoulos

Doctor of philosophy

The University of Edinburgh

2021

This page intentionally left blank.

External fire spread

from

timber lined compartments

Georgios Kanellopoulos

This thesis has been supervised by

Dr Angus Law

&

Dr Rory Hadden

The examining committee consisted of

Dr Colleen Wade

&

Dr Richard Carvel

Στο Μανώλη

Στη Μαρία

Στο Στέλιο

This page intentionally left blank.

Contents

Declaration

This thesis and the work described herein have been undertaken solely by Georgios Kanellopoulos, at the University of Edinburgh, unless otherwise stated. This work has not been submitted for any other degree or professional qualification.

The experimental work described in Chapter 4 was undertaken by Georgios Kanellopoulos and Alastair Bartlett, as part of the "*Fire Spread from Mass Timber Buildings"* project.

The external thermocouple tree, herein referred to as Tiresias, which was repurposed and used in Chapters 5 and 6 was the original design and construction of Adam Glew.

The image processing code, which was modified and used in Chapters 5 and 6, was based on the original code of Alastair Bartlett.

All analysis presented herein was undertaken by Georgios Kanellopoulos.

Georgios Kanellopoulos

July 2021

This page intentionally left blank.

Abstract

Mass timber or engineered timber products have become increasingly high profile in the past decade. They are advocated by the construction industry as structural elements, or elements of the building envelope that perform well in terms of sustainability, energy efficiency, and aesthetics. Nevertheless, these novel materials, since they are comprised of timber and adhesives, contribute in a fire scenario. The contribution of timber has been addressed so far by the use of plasterboard, in order to protect the timber; however, architects and stakeholders push towards more timber surfaces to be exposed. At present day, research has developed an understanding about the way timber behaves during a fire from a structural perspective, how it affects the compartment fire dynamics, and what are the critical values in order to achieve auto-extinction. The external fire spread aspect has not been addressed in the community to the same extent; this project aimed to understand the hazards of external fire spread from timber-lined compartments.

A series of experimental programmes was undertaken. Experiments were performed to record a “traditional” (i.e., non-combustible internal linings) compartment behaviour, as a baseline; following that, differences on the external fire spread, presented by the internal timber linings, could be quantified. The first experimental campaign established a clear difference in external fire dynamics. Heat fluxes on a façade above the opening were 20-30% (for one exposed timber lining) and up to 60% (for two exposed timber linings) higher than a compartment with non-combustible linings; heat fluxes opposite are dependent on distance from the opening; near-field values are approximately equal; far-field plumes from timber compartments recorded higher values compared to the inert ones. Heat release and mass loss rates were 20-30% and 35-40% higher, respectively, when timber surfaces were exposed.

After the preliminary experiments, a following experimental series attempted to isolate the contribution of timber from that of the fuel source. At the first stage, a baseline was created using exclusively non-combustible insulation as linings. A novel experimental system was used; the fuel source was a propane burner (thus excluding a heat feedback aspect); an external thermocouple tree was used to measure plume temperatures; calorimetry was performed in total and at the compartment opening; calibrated cameras were used. The gas phase temperatures of the external plume and the overall shape of the plume were quantified. With respect to classic plume theory correlations, the compartment presented a comparable behaviour; this baseline was later used to compare results with exposed timber linings.

The final experimental campaign revealed differences in plume behaviour from the baseline. Exposed timber ceilings, depending on the amount of exposed surface, affected the plume trajectory, and deviated from the baseline; exposed back wall, regardless of the amount of exposed surface, performed more similarly to the inert compartment baseline. With exposed ceilings heat fluxes on the façade were higher; on the other hand, the exposed wall led to higher heat fluxes opposite the compartment. Momentum and buoyancy increased as more timber was exposed. The Lee et al. model, which was modified by Gorska, was expanded for datasets of both under- and well-ventilated compartments with the full thesis' dataset.

Understanding the hazards of timber-lined compartments will allow architects and engineers to deliver safer, more sustainable, and aesthetically pleasing buildings to the public.

Lay summary

Mass timber or engineered timber products have become increasingly high profile in the past decade. They are advocated by the construction industry as parts of the bearing structure, or elements of the building envelope. This is mainly due to timber's performance in terms of sustainability, energy efficiency, and aesthetics. The construction industry promotes, for the last decade, engineered timber products for mid- and high-rise buildings (i.e. timber skyscrapers). Nevertheless, these novel materials, since they consist of timber and adhesives, contribute in a building fire. To avoid that, timber, so far, has been protected with the use of plasterboard. However, architects and stakeholders want to expose more timber surfaces, as the end result is aesthetically pleasing. At present day, research has established how timber performs from a structural perspective, some of the changes on fires in the interior of buildings when timber is exposed, and under which conditions a fire can burn out in rooms with timber linings. Despite the above, more research is needed in how fire spreads externally from a burning room (or compartment) and how timber affects this phenomenon. This project aimed to address this issue.

Initially, a series of medium-scale compartment fires was conducted. This experimental programme established that timber presents an additional hazard for external fire spread. More exposed timber meant that more fuel was available to burn. Timber presence was shown that affected: (1) the building of fire origin, as measurements above the compartment opening were higher when timber was exposed; (2) the surrounding at a distance, as flames were taller and more radiative compared to "traditional" non-combustible buildings.

The second experimental campaign aimed to: (1) create a baseline of an inert compartment, that would then be compared with compartments with timber linings; (2) improve the experimental setup by additional measuring tools and improvement of previously used equipment. These improvements on the setup

made possible a comparison of these experiments with the established theories on external fire spread.

The final experimental campaign included timber linings in the compartment. The contribution of timber was isolated; the effects of timber's presence in the compartment space and how it affected the external fire spread were, to some extent, established. Exposed timber ceilings affected the trajectory of external flames and had a bigger impact to the building of origin; exposed timber back wall behaved closer to the baseline experiments but had a bigger impact on targets opposite the building of origin. A prediction model developed by Lee et al. was modified to take into account the present experiments, giving adequate predictions on the impact that timber presence has on the building of origin.

Understanding the hazards of timber-lined compartments will allow architects and engineers to deliver safer, more sustainable, and aesthetically pleasing buildings to the public.

Acknowledgements

First and foremost, I couldn't have been any luckier with a supervisor, coming into a new country and literally picking a golden needle out of a massive haystack. People that know me have been bored to death or even felt jealous (sorry!) about the things I have said about my supervisor; nevertheless, they are merely descriptions (not exaggerations!) of the actual events. Dr Angus Law has guided, supported, and taught me so much in the course of the past four years. Due to him I was able to work in two large scale experiments, attend so many conferences and a summer school around the globe, come in contact with his academic and professional network (which he was more than happy to share and introduce me to), grow as an engineer into the field of fire safety, and, I'd like to think, grow a bit as a professional too. For his presence and support in both my academic and personal life I warmly thank him for all that he did for me; it is hugely appreciated and I'll be forever grateful. Thank you Angus!

I would like to thank Dr Rory Hadden, both as my second supervisor and as a lab manager, for the conversations we had as I was designing, assessing the risks, and even whilst performing my experiments.

I would like to thank my examiners, Dr Colleen Wade and Dr Ricky Carvel, who contributed with their comments to shaping this thesis into a better document and the constructive discussion during the examination process.

I would like to thank Dr Alastair Bartlett for his guidance and help in the lab, discussion over our joint project, all the experimental efforts and analysis, and his support during my conference presentations.

I would like to thank deeply Michal Krajčovič for his help, assistance, and guidance in the lab, his friendship, and for getting me into the hobby of coffee making.

I would like to gratefully acknowledge the contributions of: Adam Glew for giving me his thermocouple tree to modify and not have to start from scratch

the making of *Tiresias*; Dr Eric Mueller for dedicating a full day on calibrating DPTs; and Dr Jamie Maclean for sharing his coding skills and guiding me through image analysis.

Thanks to Dr Angus Law, Dr Rory Hadden, Dr Jan Christian Thomas, Dr Eric Mueller, Michal Krajčovič, Chris Bateman, and Vasileios Koutsomarkos (a.k.a. *the BRE gang*) for all the good times, lessons around the lab (starting from what exactly is a thermocouple and how it looks), and for making 5 weeks in the BRE Burn Hall feel like a breeze. Thank you also for my birthday cake, the first one I had away from home. :)

I would like to thank my unofficial supervisor for my Australian trip, Dr Juan Hidalgo Medina, for inviting me to make the trip and contribute to their large scale timber compartment experiments. Thanks to all the Aussie Fire Group family there for making me feel at home right from the very first day. Thanks to Andrea for being a familiar face upon arrival. Special thanks to Ian for being my local guide, the person to show me around of Brisbane, invite me over for a Sunday roast (thanks Ian's dad), and for being a great mate in the land down under.

Thanks to all the people in the John Muir building that made a difference to my daily routine. All the fun conversations in the kitchen during lunch, *Cake Club*, *Ian Pope's Curry Club*, *Friday Pints*, and barbeques. Sorry for all my spam at your desks during my wee breaks. Thanks to Zak, Carlos, Eric (a.k.a. *The Wildfires*), Zafeiris, Mohamed, Martina, Valentina, Simon, Uli, Daniela, Jamie, Jens, Lesley, Zeynep.

Special thanks are given to the Edinburgh Fire Group, which funded many ventures that happened in the past four years. The philosophy and the work environment that has been cultivated throughout the years was of paramount importance to me and I found a new home from Day 1. I would also like to gratefully acknowledge the University of Edinburgh for providing the funds and support to my PhD studentship, and the facilities of our campus where everything PhD-related happened.

As I'm getting close to the end, people I lived with or around changed me in many ways. These were part of my "Greek gang" (as Angus and Rory would say). Vasilis, thanks for all the last three years of co-habitation. Taking care of me when I was too busy with work or sick, making South Oxford street a place to call home, and for all the impromptu nights at the Jazz Bar, Stramash, The Royal Oak, and Brass Monkey. Cheers to all that! Honourary "gang" member, and our guest for two months, David; thanks my dude for being there for two months, force us to get out of the house more and all the great times in our flat. The rest of the Greek "family": Ilias, my quarantine super-buddy, being there along with Vasilis, through thick and thin, till tsipouro do us part; thanks for our daily adventures, however big or small, your friendship, giving me a bed before I moved in to the new flat, and for all the great times. Thanks to Niki, who joined our little trio and brought interesting conversations to the table, became a close friend, and was a great person to be around on a daily basis. *"One does not simply walk into Mordor"*, nor does one do a PhD without some support from past or current doctoral candidates: to Dr Potheini, Giorgos Indiana, Dr Kostas, Dr Giorgos, Dr Giorgos Sam thanks for being there to talk to. Eleftheria, Mitsos, Eirini, Giorgos F, and Zoe, thanks for tagging along to wee city adventures, meals and drinks together, and for being great friends, whether you were around or through a phone screen. Last but most certainly not least, Aigli, *my mpataro*, thank you for picking me from the Haymarket bus stop on the night that I landed in this strange and wonderful place, all the accommodation during my first 25 days in Edinburgh, giving me your friendship and support, and for all the coffees we had at Kilimanjaro.

Though 3,471 km separated us, all my friends from Larisa (my hometown) were there for me with hours of phone calls, video chats, or during vacations. Massive thanks to all my friends: Thanos (sRs), Giorgos (alani), Giorgos Dal, Dimitris Z, Vaso, Sofia.

Nothing would be possible without my family. Thanks and deeply indebted to my mum Maria, my dad Manolis, and my brother Stelios! To the three of you, I dedicate this work. :* :D

This page intentionally left blank.

Related publications

The following journal and conference papers have been published over the course of this thesis. Where these are based on part or whole of a chapter of this thesis, this is indicated.

Journal paper

A. Law and *G. Kanellopoulos*, “The rise and fall of the UK’s spandrel panel,” Fire Saf. J., vol. 115, 2020, doi: 10.1016/j.firesaf.2020.103170.

Conference papers

A. I. Bartlett, *G. Kanellopoulos*, and A. Law, ‘Heat flux distribution on a facade from timber-lined compartments’, Royal Holloway College, London, UK, Jul. 2019.

G. Kanellopoulos, A. I. Bartlett, and A. Law, ‘Investigation into global equivalence ratio and external plumes from timber lined compartments’, Proceedings of the Ninth International Seminar on Fire and Explosion Hazards. Vol. 1: 468-477, Saint Petersburg, Russia, 2019, doi: 10.18720/SPBPU/2/k19-68.

This page intentionally left blank.

Nomenclature

Latin symbols

A	Area (m^2)
B	Burning factor ($m^{-0.5}$)
C	(TSC) Calibration factor (-)
c_p	Specific heat of gas (J/(kg·K))
f_{ex}	Excess fuel factor (-)
g	Gravitational acceleration (m/s^2)
H	Opening height (m)
H_v	Opening height (m)
$H"$	Height above the neutral plane (m)
I	Incident radiant heat flux (kW/m^2)
J	Buoyancy (N)
K	Coefficient of eddy viscosity (m^2)
K'	Coefficient of eddy diffusivity (m^2)
l_1	Lee et al. length scale (m)
M	Momentum (N)
$\dot{m}_a$	Mass inflow rate (kg/s)
$\dot{m}_f$	Mass loss rate (kg/s)
m	Mass (kg)
n	Yokoi's opening shape factor (-)
O	Opening factor

$\dot{Q}$	Heat release rate (kW)
Q	Convective heat output (W)
$\dot{q}$"	Heat flux (kW/m^2)
r	Stoichiometric ratio (-); Radial distance of the point of interest from the fuel source (m)
r_0	Radius of the circular orifice/opening (m); Equivalent radius for a rectangular pool fire/opening (m)
S	Area (m^2)
T	Temperature (°C, K)
v	Horizontal gas velocity (m/s); Compartment exit velocity (m/s)
v_0	Velocity at the orifice/opening (m/s)
W	Non-dimensional gas velocity (-); Opening width (m)
w	Vertical gas velocity (m/s)
x	Distance from the orifice that velocity v is estimated (m); Stand-off distance of the ejected gas from the heat source (m)
x_0	Horizontal distance inside the opening (m)
z	Vertical distance of the point of interest from the fuel source (m); flame height above the top of the opening (m)
Z	Net height above the top of the opening (m)
Z_f	Time-averaged mean flame height (m)

Greek symbols

α	Absorptivity (-)
γ	transient compensation factor (-)

ε	Surface emissivity (-)
Θ	Non-dimensional temperature (-)
$\Delta\theta$	Temperature difference of the point of interest from ambient (K)
θ_0	Ambient temperature (K)
ρ	Density (kg/m^3)
σ	Stefan-Boltzmann constant (W/(m^2·K^4))
φ_p	Global equivalence ratio (-)

Subscripts

af	Air-to-fuel
air	air
c	Combustion
CLT	Cross-laminated timber (CLT)/timber
cond	Conduction
conv	Convection
d	(TSC) Disc
ex	external
fa	Fuel-to-air
g	gas
in	Internal
inc	incident
mod	Modified
out	Exit (mass flow)

rad	Radiation
st,s	Stored (energy) in the solids
st,g	Stored (energy) in the gases
t	Total (internal area excluding openings)
tot	Total
TSC	Thin skin calorimeter (TSC)
w	opening
∞	Ambient

Abbreviations

GER	Global equivalence ratio
HFG	Heat flux gauge
HRR	Heat release rate
TSC	Thin skin calorimeter

Chapter 1 – Introduction

1.1 Background

1.1.1 **Wood as a building material**

Timber is one of the first materials that were used in building construction. It possesses properties that can be favourable for construction, as it is lightweight and can function in both tension and compression on its own. Wood also has drawbacks, in terms of performance in a fire, inherent weak spots in its structure (e.g. knots), and can suffer in comparison with more modern material such as concrete and steel.

1.1.1.1 The good

The building industry, for the last decade, has been consistently and persistently advocating for the use of timber in modern construction [1]. This is due to the fact that timber is no longer available in the form of a single piece of wood, cut to size. Engineered timber products are now widely available in construction [2]; this signified a rebirth for this old construction material. Engineered timber products are comprised of pieces of timber, all bound together with either chemical (i.e. glues) or mechanical (i.e. screws, bolts, etc.) means.

These new products eliminate some of the weaknesses associated with single cut timber; knots in the virgin wood are now part of a larger product, meaning that they are less of a problem; mechanical properties are now more modifiable, as the products are assembled in order to create the desired mechanical performance (long beams, thick timber floor slabs, etc.). Timber products also perform very well in terms of energy efficiency; as they are prefabricated and assembled on site, they offer an opportunity to minimize error from the desired dimensions, therefore creating a more air-tight building shell. Finally, as the base material, timber can be sustainably grown and sourced, which makes it extremely popular in an industry that attempts to make a turn towards more sustainable practices.

1.1.1.2 The bad

Timber possesses a very distinguishable property; that is, its combustible nature (i.e. timber burns). In comparison to steel and concrete, this material contributes to a fire; due to this, its behaviour needs to be understood and accounted for when it is included in the built environment.

In the past, large fires like those in Rome [3], London [4], and Chicago [5] forced people to exclude timber from the list of potential construction materials. Exclusion may have led to the desired fire safety outcome in the past. However, in a modern built environment, where combustible materials are ever-present (e.g. polymers), timber does not stand alone as a combustible construction material anymore. Furthermore, wood's favourable properties should be weighed, alongside the less favourable ones.

Modern day use of timber started with timber elements that were covered with one or several layers of plasterboard; this technique of enclosing the timber within layers of other materials is called encapsulation. Encapsulation within one or several layers of non-combustible materials can be proven successful to protecting the timber elements from thermal degradation and involvement in the fire.

1.1.1.3 The unquantified

The engineering profession is constantly challenged by materials and architects' desired goals. In this sense, timber presents another sort of challenge. Timber's behaviour in a fire needs to be understood qualitatively and quantitatively. Research so far made progress in areas such as internal fire dynamics [6]–[9], bonding failures [6], [8], [9], and structural performance [10]–[12].

Despite the aforementioned work by several researchers, less focus was given to external fire spread and how this is affected by the presence of timber. The most recent project that included this as a studied hazard was from Gorska [9].

1.1.2 External fire spread

Fire, as a hazard, can present several challenges in the built environment. One of these is the external spread from a burning room to all external surroundings (i.e. neighbouring buildings, building of origin). External fire spread was taken into account after large conflagrations [3]–[5]; cities needed to recuperate after these events, and counter-measures were enforced to control or mitigate this fire hazard.

From a research aspect, this fire hazard has been thoroughly studied by various researchers, with multiple focus points into the drivers of the phenomenon and its impact. However, most of the research output was concerned with buildings or model compartments with non-combustible linings (e.g. concrete, masonry, steel, plasterboard, etc.). There has been little focus into the effect of combustible linings on external fire spread.

1.2 Objectives of the thesis

The present research aims to:

- undertake a state-of-the-art review on external fire spread and timber-lined compartments;
- establish whether or not timber changes the fire dynamics in a compartment fire;
- develop a system that can capture the behaviour of external plumes;
- test whether classic and modern plume theory models adequately predict the external plume behaviour;
- update and/or inform models with a new dataset on timber-lined compartment fires.

1.3 Summary of Chapters

The thesis consists of eight chapters; a summary for each chapter follows.

1.3.1 **Chapter 2 – Literature review**

This chapter is concerned with three key tasks. Firstly, it is to present the context and the drivers which led into this research project. Following that, a review of the UK regulatory system regarding external fire spread is performed; research that led to this regulatory approach is examined. The physical aspect of external fire spread is also examined; the role of burning timber in the compartment space, as this has been recorded so far by other researchers is presented.

1.3.2 **Chapter 3 – Methodology**

The methodology used in each experimental programmes is presented and described in full. The thorough description is given for: (1) the guiding principles which led to the development of the methodology; (2) the prototyping process, which included the fuel source, the ventilation conditions, the fuel load, and the resulting compartment design; (3) the experimental design of the experiments undertaken in support of this research.

1.3.3 **Chapter 4 – Excess fuel**

The Phase 1 experimental campaign consisted of four experiments, with a repeat for each one. The campaign aimed to identify key differences when timber linings were exposed in the compartment space. The global equivalence ratio was tried as a predictive variable for identifying potential external flaming.

1.3.4 **Chapter 5 – Creating a baseline**

After identifying exposed timber in the compartment as a driver for changing the hazard of external fire spread, a more refined and robust setup was developed. The Phase 2 (and 3) experimental setup was able to capture the needed measurements in order to proceed with characterisation of the external plume. The Phase 2 experiments aimed to provide a baseline of inert compartment behaviour for comparison with the following experimental programme where timber linings were exposed.

1.3.5 **Chapter 6 – Timber linings**

Key characteristics of Phase 3 experiments, regarding plume behaviour, were recorded in this chapter. This programme demonstrated the noticeable differences of inert versus exposed timber compartment fires. Deviations of the exposed timber with regards to calorimetry, incident heat fluxes at the surroundings, plume temperature profiles, and velocities at the compartment opening are presented in the chapter.

1.3.6 **Chapter 7 – Analysis**

Analysis of all three datasets from the current thesis is presented in this chapter. All plume related correlations were tested, in order to identify whether these are applicable in the case of exposed timber in compartment fires. A plume temperature model was identified; a heat flux model, with modifications to fit the current datasets, was re-established for timber-lined compartments.

1.3.7 **Chapter 8 – Conclusions and future work**

Conclusions of the findings of the thesis work are presented. Suggestions for future work and potentially interesting approaches are made.

This page intentionally left blank.

Chapter 2 – Literature review

The literature review is divided into three sections:

- Context – a brief overview of the use of timber in the construction sector is provided;
- Regulation of fire spread hazards from timber buildings – a review of the background the regulation of fire spread hazards and the studies that led to this approach (with a particular focus on UK regulatory systems);
- Physical processes governing external fire spread hazards from buildings.

2.1 Context

Trees are cut down to harvest wood as a product to be used in various applications (e.g. building material, furniture, etc.). Wood can be processed into smaller pieces – either of smaller cross section or smaller length. At this stage, the wood products can be referred to as timber or lumber depending on the level of process it has undergone; the former is used for less processed material and the latter for more processed products.

A distinction needs to be made between products that can be used for building construction and products that are used for furniture, etc. This work is considering only products that belong to the first category.

Pieces of timber, lumber or sawn products can be combined together to form a single structural element. This is achieved through adhesives to bind the strands, fibres, particles, veneers or boards of wood. Other methods of fixation, such as fixing using pins, are also possible. This aim is the same in both cases; to form composite materials. Materials with these characteristics are called engineered timber.

Engineered timber is applied as a construction material in various ways. It is found as a material for frames of low-rise dwellings [13]. It is also used as part of the load bearing system – in the form of a beam or column [14]. Finally,

engineered timber is also designed and applied as the primary load bearing construction material for modern mid- and high-rise buildings – in the form of beams; columns; floor slabs; masonry [10], [15].

Engineered timber products can be found in various applications. Each product has certain properties; these properties define its application – some kinds of engineered timber can have similar applications. Table 2.1 lists all the different engineered timber products [16].

Cross laminated timber (CLT) is an engineered timber product that is used in construction as a structural element; it is referred to by some as "super-plywood" [2]. It can be used as stand-alone material for the structural frame or as part of a composite system with steel and/or concrete elements. CLT members are used both in vertical orientation (i.e. walls) and horizontal orientation (i.e. floors/ceilings).

CLT is comprised of an odd number of layers (i.e. 3, 5, 7, etc.) as shown in Figure 2.1. CLT is formed based on the following process:

- Planks of timber are placed side by side to form the first layer (lamella); the orientation of the grain is parallel to the length of the element;
- Glue is applied on top;
- The second layer of planks is placed on top of the first; the grain forms a 90^{o} angle with the first lamella;
- The process is repeated until the last layer; this layer has the same orientation as the first one.
- Hydraulic presses are compressing together the members from the two ends to aid and ensure the binding of the lamellae with the glue.

CLT behaves as a composite material; the composite action is achieved due to the glue used to combine the different layer into one material. Due to the fact that lamellae orientation differs by layer (0^{o} for the odd-numbered and 90^{o} for the even-numbered lamellae), the end product (CLT) has a structural capacity in both orientations.

Table 2.1: List of engineered timber products, application, composition, and binding method.

Name of engineered timber product	Application	Composition	Binding method
Oriented strand board (OSB) [17]	Subflooring, single-layer flooring, wall and roof sheathing, structural insulated panels, webs for wood I-ioists	Cross-oriented wood strands	Adhesive (heat cured)
Laminated veneer lumber (LVL) [18]	Rafters, headers, beams, joists, studs, columns, and I-joist flange material	Wood veneers, strands or flakes of wood	Moisture resistant adhesive
Glue laminated timber (Glulam) [19]	Vaulted ceilings, simple purlins, ridge beams, floor and large cantilevered beams, large flat roof systems, complex arches.	Wood laminations – grains parallel to length of member	Moisture resistant adhesive
Cross laminated timber (CLT) [20]	Horizontal flooring/ceiling, load-bearing wall	Wood laminations – laminated in 90^{o} angle difference; outer layer grain parallel to the length of member	Moisture resistant adhesive
Plywood [21]	Cladding, doors, framing, flooring, joinery, shear wall, portal frames, panelling	Cross-laminated veneers	Adhesive (under heat and pressure)

Figure 2.1. Side view of CLT slabs with 3 (top) and 5 layers (bottom) [17].

Like steel and concrete, CLT can be used to form elements of superstructure of buildings. However, unlike steel and concrete, the primary material that comprises CLT is combustible.

Applications of CLT are case dependent; there are several different typologies of construction. For example:

- Pure CLT – where CLT forms all the principal structural elements. This form is most common in residential buildings where the CLT structural naturally forms a ‘honeycomb’ space of rooms and apartments;
- Timber Hybrid – where CLT slabs are used with glulam columns and beams. This form is commonly used in structures where a longer span is desirable such as educational buildings; and
- Hybrid – where CLT slabs are supported by a concrete or steel frame.

The degree to which the timber structure is exposed or ‘expressed’ within the finished building depends on the use of a plasterboard finish on the surface of the structure.

Examples of these different forms are as follows.

Pure CLT

Forte Living in Melbourne, Australia is an example of an internally fully encapsulated structure [18]. Floors, walls (except the featured exposed CLT

one), and ceiling were covered with plasterboard. A hardwood floor was fixed in all living areas; and the floor slabs were lined with two layers of plasterboard. One layer of plasterboard was applied also on the façade of the building.

A similar case to Forte Living is the Stadhaus in Hackney, London. The living areas are completely covered with plasterboard. Suspended ceilings and floating floors were installed; these installations enhanced the soundproofing of the rooms.

Dalston Works, in Hackney, is also an example. The joints of walls and ceiling are made from aerated concrete. The cladding system was built with a cavity and suspended bricks on the exterior. From drawings provided [19] it appears that the ceilings are protected with layers of plasterboard; nevertheless, the floor is lined with an engineered timber layer.

Timber Hybrid

Brock Commons (Canada) is a relatively new addition to the tall, engineered timber buildings. Strictly speaking, the two concrete staircases would force one to include the building into the category of hybrid buildings; however, the Glulam columns connected to the CLT floors put this building in the category of Timber Hybrids [20].

Hybrid

The Cube (Hackney, London) is a hybrid building; it incorporates CLT into a steel frame/concrete core construction [21]. The façade has exposed timber surfaces; the interior appears to have encapsulated walls and exposed timber floor [22].

The Wyoming Airport terminal incorporates all three building materials; timber; steel; and concrete [23]. Timber is used for columns, girders and ceiling; steel is used as a support system for the timber girders; the floors are comprised of concrete.

2.1.1 **The concept of "Tall Wood"**

The use of CLT in such different forms has been brought about in an attempt by contemporary architectural practice to address housing and sustainability problems simultaneously – whilst maintaining a high aesthetics level.

Michael Green presented this idea in 2013 [24], and in 2016 his idea was already realised as the "T3" building in Minneapolis, Minnesota [25]. Since Michael Green gave his talk, Tall Wood (or Tall Timber, or mass timber) has proliferated. In 2019, a report by Arup identified that there were hundreds of timber structures in the UK (shown in Figure 2.2), starting from zero in 2000, with governments around the globe making plans to allow tall timber construction [26]. By 2018 there were too many such structures to allow an audit (e.g. a recent publication identified 100 structures only in central London [27]).

In parallel and/or inspired by Green's idea several other projects developed. A few examples are Forte Living, The Cube, Dalston Works, The Treet (Norway), Brock Commons [28] (shown in Figure 2.3 - Figure 2.5). In Brisbane, AU, K5 is a new addition to tall timber buildings [29].

Of particular interest with respect to the promotion of timber buildings is the London Borough of Hackney – which ran a campaign to promote timber construction [30]. Due to this action, various buildings have been erected in this neighbourhood, using timber as the main structural component.

Figure 2.3 - Figure 2.5 show the internal arrangements of several of these buildings. It is notable that in some cases the structural timber is not visible, while in other cases some (or all) of the timber is exposed. Figure 2.5 shows Brock Commons during construction.

Figure 2.2. Map of the UK indicating locations where CLT case studies are applicable [27].

(a) (b)

Figure 2.3. (a) Room inside The Cube [31]; (b) Room inside Dalston Works [15].

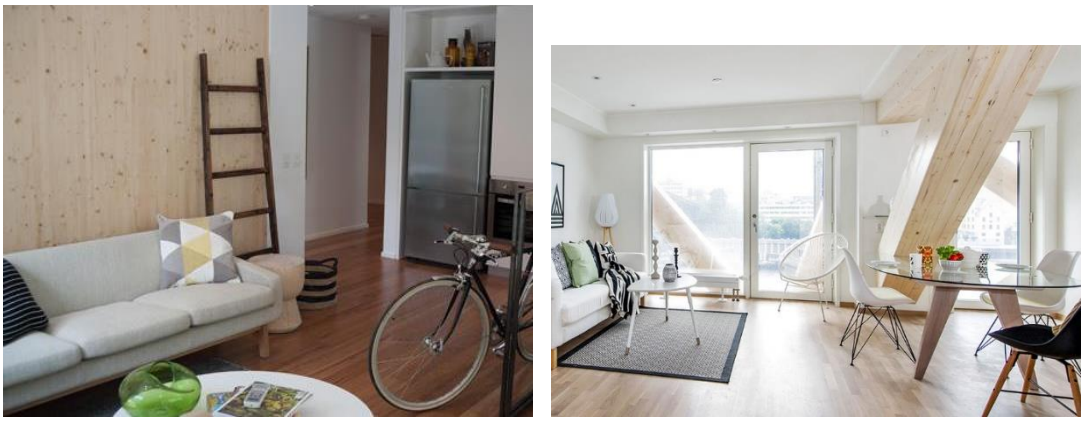

(a) (b)

Figure 2.4. (a) Room inside Forte Living [18]; (b) Room inside The Treet [32].

Figure 2.5. The interior of Brock Commons under construction [33].

2.2 Regulation of Fire Hazards

As previously demonstrated, timber has already been used in different occasions to create structures – from low-, to mid-, and high-rise buildings. Timber is a combustible material and therefore presents different fire hazards to other structural materials such as steel or concrete. It has the potential to become involved (at least partially) during an enclosure fire.

Mass timber elements are typically held together by adhesive. This is used to glue together the pieces of timber into one structural element. The adhesive can be affected at elevated temperatures (approximately 135-150 °C for melamine-urea formaldehyde as shown in the work of Wiesner et al. [12]), leading to change in structural behaviour – or, in certain cases, also delamination. This effect of temperature on the adhesive's performance is dependent on the type of adhesive used. Wiesner et al. presented different testing methods used worldwide for the assessment of the adhesive performance [11]. In parallel to this work, Wiesner and co-workers presented the shear failure changes of CLT at different temperatures; a shift of failure, from the second lamellae to the glue line, as testing temperature increased was recorded [12]. The temperature which affects the glue line is dependent on the adhesive.

A fire of long duration can lead to breach of compartmentation by compromising the integrity of doors, windows, or walls of the compartment and/or joints of elements. This can lead to external fire spread on the building, originating from the burning compartment.

During a fire, timber will pyrolyse, emitting flammable gases in (or in some cases even out of) the compartment. As a consequence of this release, there is a strong feedback loop between the structural material, and the fire dynamics.

The fire dynamics within the compartment has been the subject of several studies [34]–[38]. The focus of these studies was on the behaviour of compartment fires in general; apart from the first two, the rest of the

aforementioned studies were additionally focused on the effect of the timber presence in the compartment space. For the latter set of studies, the auto-extinction of timber was of primary interest. Hadden et al. [36] described a series of large-scale experiments conducted to investigate the effect of timber presence and orientation in the compartment space. Bartlett et al. [37] worked on the same dataset examining the factors affecting auto-extinction. Emberley et al. [38] conducted a similar large-scale experiment, complimented by bench-scale experiments; the experiment was designed so that exposed timber would achieve burnout after the imposed fuel load (wood cribs) was consumed.

Excess pyrolysate in the compartment increases the overall potential-to-burn gases. If all the flammable gases cannot be consumed inside the enclosure, they will be ejected out of the openings of the compartment and burn on the exterior of the compartment. Considering CLT products, if the first layer delaminates and falls off, this increases further the available fuel in the room.

Unburnt fuel exiting the compartment openings could change the intensity of convective and radiative heating; it can also affect the duration of external burning. External flaming and smoke can heat up the building's cladding (or external surface in general) and/or ignite the contents of rooms with a view to the external plume. The hazard of external fire spread – due to radiative heating mainly – is also present for adjacent/neighbouring buildings exposed to the openings of the compartment of fire origin.

The introduction of timber within the fire compartment therefore suggests that the fire spread hazard may be changed compared to conventional construction. This raises several critical questions: 1) what are the physical processes that arise from the introduction of timber into the compartment; 2) how do these affect the hazard associated with conventional building materials; 3) given the regulatory context do these changes have any material impact on the level of safety delivered by existing methods for design.

To formulate an answer to these questions, the regulatory background is first reviewed. Many of the experimental and testing programmes, which led to the

present understanding of the physical processes that control fire spread, emerge from the regulatory review.

2.2.1 **External fire spread**

In the event of a compartment fire, a building that has an opening on an external wall has the potential for external fire spread.

- If the compartment's openings are sufficiently large to provide enough oxygen to consume all the combustible gases inside, the burning will happen inside, and a hot smoke plume will vent out of the opening. This is termed as over-ventilated compartment fire (shown in Figure 2.6 (a)).
- If the compartment's openings are too small or the pyrolysis rate is higher than the combustion rate, unburnt combustible gases will exit the compartment through the opening. In this case, the external plume consists of both flames and smoke. This is termed as under-ventilated compartment fire (shown in Figure 2.6 (b)).

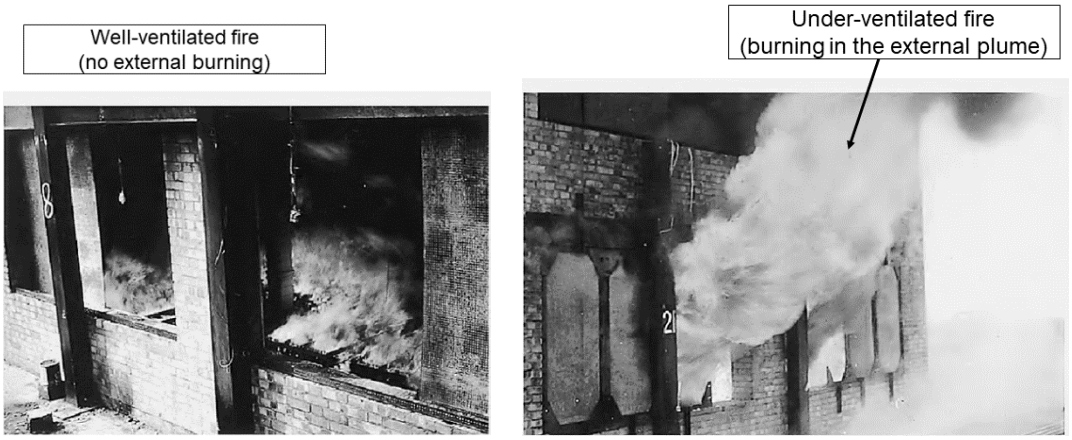

Figure 2.6. (a) Well-ventilated compartment fire (no burning on the exterior of the opening); (b) Under-ventilated compartment fire (combustible gases burning outside the opening). (modified picture [39])

External fire spread can occur due to convective and radiative heating from the external plume onto the building of fire origin. Flaming in the plume creates a higher incident heat flux (especially through impinging of flames onto

materials) on the façade; this raises the level of the potential hazard for vertical fire spread onto the building of origin.

In addition, the openings of a burning compartment and the external plume, spilling out of the burning compartment, are responsible for the irradiance to adjacent buildings. The heat flux provided by the opening and plume can lead to ignition of materials in adjacent buildings; this is the source of horizontal fire spread from the building of origin.

There are therefore two categories of external fire spread: horizontal fire spread (i.e. building-to-building); and vertical fire spread (floor-to-floor). This terminology will be adopted for the remainder of this thesis.

One of the following scenarios can occur in a compartment fire.

- The compartment remains sealed; the heat losses through walls/ceiling are higher than the produced heat, leading to lower burning rates, reducing the produced pyrolysate and eventually auto-extinction;
- There is a link of the compartment with the interior of the building through an opening; flame and smoke are spread towards the interior. This can lead to an internal fire spread within a building, or a "travelling fire" [40];
- The compartment remains sealed; the heat losses are lower than the generated heat. This leads to more pyrolysate production and awaiting to be mixed with fresh air through an opening, when that occurs (voluntarily or involuntarily). This can lead to a backdraught [41];
- There is an opening of the compartment to the exterior of the building; there is a fresh-air supply into the compartment. Smoke (and potentially flames) emerge from the opening and preheat surrounding materials; ignition can occur if the flammability conditions for the surrounding materials are reached.

The final two sub-categories can lead to external fire spread.

2.2.2 **Building-to-building fire spread from a historical perspective**

External fire spread from buildings is not a newly found concept or occurring phenomenon. On the contrary, as noted in the introduction, some significant historic fires happened due to external fire spread from building-to-building.

In 64 A.D. the Great Fire of Rome occurred. The fire started from the shops in the Circus Maximus and spread through the city; by the end of the great fire, 10 out of 14 districts of Rome burnt down [42]. Structures in this area of Rome were built in a rush, meaning no urban planning – a reason for narrow spaces between buildings [43]. The tight space between buildings, in addition to the dry summer weather (leading to dried building material and contents), promoted the spread between buildings throughout Rome.

The Great Fire of London spread rapidly in the autumn of 1666; according to sources [44], it lasted for almost 5 days; a total of 13,200 houses, 87 churches were in ruin after the fire. It is mentioned that the buildings of the area of the initial fire incident were made from timber; complimenting the timber presence, the proximity between estates aided the spread from building-to-building. There was also an abundance of fuel in the buildings. This fuel was in the form of: structural timber frame; pitch and thatched roofs on the exterior; contents in the buildings like oil and rope.

The Great Chicago Fire broke in October of 1871; it burnt for 3 days and claimed more than 17,000 buildings [5]. The fire started and spread from the building of origin (the O'Leary estate) north and east, to the city center area. The legend blames Mrs. O'Leary's cow for triggering this devastating event (Figure 2.7). Structures in the neighbourhood were built from timber, stone and brick. Unbuilt land and the lake (alongside the rain) played an integral role in stopping the fire spread from the southern to the northern part of Chicago [45].

Figure 2.7. The famous depiction of Mrs. O'Leary and her cow as the reason for the Great Chicago Fire [46].

One can say that a sense of "fire safety engineering" was developed due to these devastating events. Examining the example of Rome, a paradigm shift occurred in the building construction process. People started to build more with bricks instead of timber; less narrow arrangement was followed in the newly built buildings [3].

In London, active fire-fighting measures were present ever since the incident. The city was divided into sections for fire-fighting assistance; a number of buckets was available for each section; fire places were safety-inspected twice a year [4]. The greatest achievement for the city was the founding of a fire brigade, 14 years after the incident [4] privately funded by insurance companies. It was in 1833 that the London Fire Engine Establishment was formed. This was 9 years after the first organised municipal fire brigade was established; it was the Edinburgh Fire Engine Establishment, in Edinburgh, Scotland. James Braidwood served as a superintendent in the London Fire Engine Establishment due to his years of experience in the Edinburgh fire brigade [47].

Finally, as for the aftermath of the Great Chicago Fire, the building code that followed at the time demanded the presence on non-combustibles (e.g. brick, stone, marble, limestone) [48]. In addition to this, the Chicago Fire Academy was built in the place where the incident began – the O'Leary estate [48].

It is evident from these events that external fire spread, at its most extreme, can result in devastating urban conflagrations. The authorities in each case learned from these events and implemented regulations to mitigate the hazard. Passive (materials used on the buildings) and active (fire brigade force/training facilities/fire strategy) measures of fire safety were established as a response to these events. These measures, while effective, are evidence of an approach to construction known as '*design by disaster'* [49].

2.2.3 **Studies on horizontal fire spread**

Although urban conflagrations had led to an advance in human understanding about measures to prevent building-to-building fire spread, it was not until World War II that this became the subject of more systematic fire scientific study. Following WWII, work in this area continued (although in the interests of building safety, rather than urban destruction). Key researchers in this area at this time were: Law [50]; Kawagoe [51]; Ashton and Malhotra [52]; Webster and Raftery [53]; and McGuire [54].

These researchers established many of the physical processes associated with fire spread. Their work also led to the creation of various regulatory approaches, which are the focus of this section. This section will therefore focus on what was done, and what was concluded from a regulatory perspective – rather than presenting the physical processes.

2.2.3.1 The St. Lawrence Burns

In 1958 the village of Auntsville was amongst the ones selected for the St. Lawrence Power Project, a project to flood a large area for the creation of a hydro-electric plant [55]. Given the opportunity, the Division of Building Research of the National Research Council of Canada suggested and finally was granted approval to run fire related experiments on selected buildings.

Part of the purpose of these experiments was to gain understanding on building-to-building fire spread [54].

Different building types were available; combustible and non-combustible linings were applicable on the different buildings; the same applied for the cladding materials; measurement of irradiance from the burning building openings was done by radiometers (Figure 2.8 is an example of the experiments).

In the process of these experiments, the experimental methodology was optimised. Parts of the building that could ignite prematurely were managed accordingly.

Lessons learnt from this project were:

- the effect of wind passing through the building on changing the fire spread hazard;
- the effect of the presence of combustible materials, as linings and as cladding, on the external flaming and the external heat flux from the burning building;
- measurement techniques to obtain radiant heat flux data (Figure 2.9), and correlation of the measured values between the devices at the opening, using the concept of the configuration factors [56];
- development of the buildings that were used in the experimentation in order to minimise introduced errors/uncertainties from the original structure (i.e. removing materials from the building such as balconies, porches, etc.);

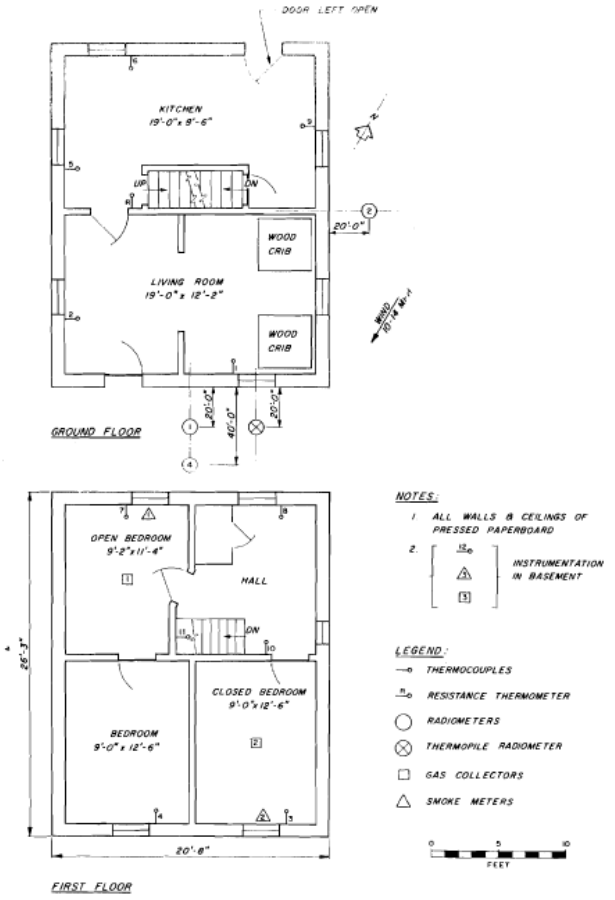

Figure 2.8. Building No. 5 – Two-storey wood frame building with clapboard cladding. The position of the radiometers and a plan view of the experiment are shown (figure modified from [54]).

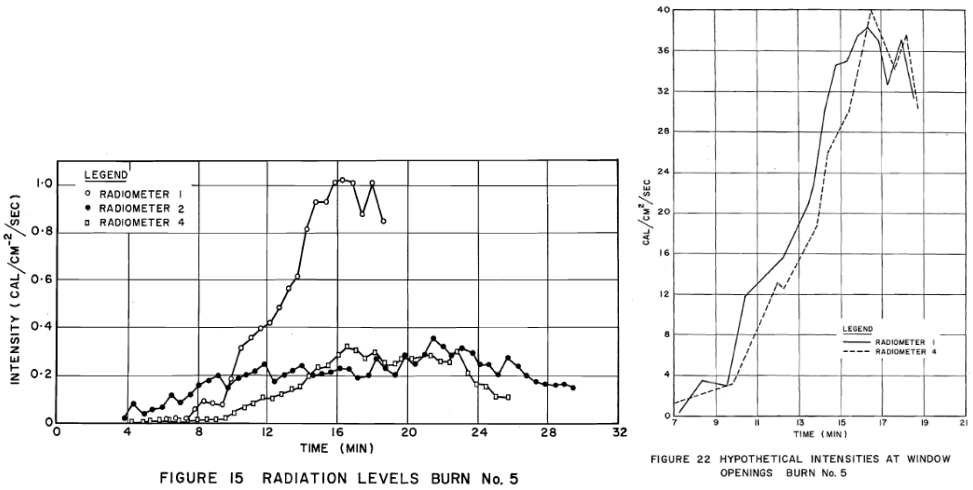

Figure 2.9. A comparison between measured values of the radiometers in different positions and the hypothetical value of the flame surface radiation for burn No. 5 (modified figures from [54]).

The aforementioned experiments – with measurements and observations – helped to enhance the understanding of the requirements for spatial separation.

2.2.3.2 Webster and Raftery

C.T. Webster and Monica Raftery published a report on a series of multi-scale experimentation [53]. This was part of a programme to study the burning rate of wood cribs and other variables' changes in a burning compartment.

Three different cubic boxes were used in these experiments (1, 2, and 3 feet a side, respectively). Direct radiation measurements were performed above the compartment opening and opposite the opening; the height of the former and the distance of the latter from the opening varied [53].

Webster and Raftery report peak radiation intensities over the opening approximately simultaneously to the peak external flame height. Opposite the compartment, radiation measurements appeared to increase in a linear fashion with the mass loss rate. Additionally, the box size seemed to have an effect on the time that the peak radiant intensity occurred, alongside the mass burning rate.

Although wood cribs in an enclosure showed little sensitivity to scale changes, the authors reported significant effects of scale to the radiation values, making it difficult to extrapolate large scale response from small scale data [53].

2.2.3.3 Kawagoe

Kawagoe's experimental programme [51] was pioneering at the time it was conducted. Previous work in fire safety in Japan, before the WWII, included only two studies; the fire test in Dojunkai apartment house by Tokyo University, and the Premium House sponsored by Osaka City. The study aimed to develop a way to estimate the fire duration based on the fire load and the compartment ventilation opening's geometry.

Experiments were conducted in various different scales; nevertheless, radiation measurements were reported only in some of the cases.

The key observations were that the irradiance peaked at the time that temperatures peaked. However, radiation presented a longer growth and a shorter decay period compared with the temperatures measured. Peak measured irradiance values ranged with scale, which comes in support of Webster and Raftery's observation [53].

A qualitative assessment was carried out for the stage of the fire; paints on the walls were used, with a colour change of the paint indicating fire had reached/passed that point of the building (or the adjacent building).

Kawagoe's work contributed to relate the ventilation conditions to the fire duration with his observations that $\dot{m}_b \approx 0.5 A_w \sqrt{H}$.

2.2.3.4 Margaret Law

Margaret Law was a fire scientist at the Fire Research Station since 1952, a position she held for over 20 years. In 1963, she wrote Technical Paper No. 5 for the heat transfer by radiation from fires and building separation requirements [48]. In her report, she attempted to shed some light into the necessities for building design requirements and how these could be presented to designers. Her criterion was that the proposed guidelines should have been "equation free" [57, p. 1]; any reference made for building separation distances should have been made with respect to the relevant boundary and not a building beyond the boundary.

In her pioneering work, after presenting the limitation criteria for the proposed methodology (e.g. minimum intensity of incident heat flux for piloted ignition), she proceeded to introduce the theoretical background for this methodology (i.e. heat transfer by radiation). The aforementioned works [51]–[53] were integrated in Law's meta-analysis, as presented in Figure 2.10.

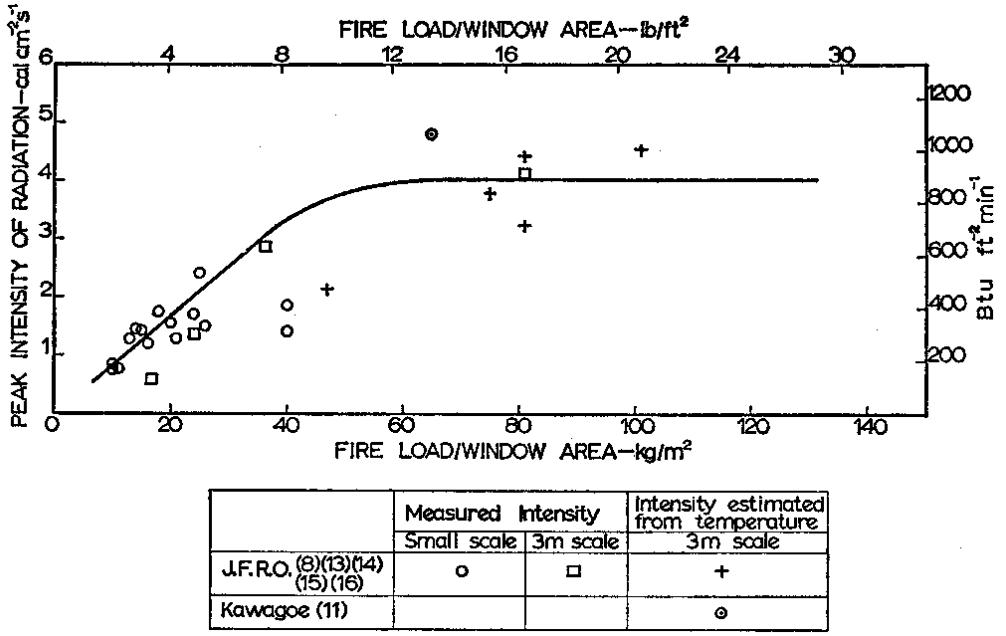

Figure 2.10. Correlation of peak radiative intensity and fire load (modified Fig. 2 from [50]).

Margaret Law introduced to the civil and fire safety engineering community a simple method – the enclosing rectangle method – to estimate separation distances for normal and low intensity fires, simply by using a diagram; this method is applicable of different opening scenarios and orientations of the buildings.

In order to use the enclosing rectangle method, the temperature of the radiator, i.e. the burning compartment, was needed. Law had to correlate the temperature of the opening (the radiator) with some variable change for the compartment.

Radiative power can be expressed as a function of the temperature of the radiating body as follows:

$$I = \varepsilon \sigma T^4 \qquad (1)$$

where I is the radiative heat flux [kW/m^2]; ε is the emissivity [-]; σ is the Stefan-Boltzmann constant and equal to $5.670367 \cdot 10^{-8}$ [W/(m^2·K^4)]; T is the absolute temperature of the radiator [K].

To determine an appropriate temperature for that radiating body, Law observed that changes of the ventilation factor A√H resulted in different peak temperatures (Figure 2.11).

Nevertheless, the ventilation factor was not the only variable affecting the peak temperature of the radiating body. Observation of Figure 2.10 showed that the available fire load was also relevant to the maximum potential temperature for the room; specifically, the ratio of available fire load to the ventilation factor. Threshold values for both the ventilation factor (5 $m^{5/2}$) and the fire load (25 kg/m^2) were derived; values lower than these thresholds delivered lower peak radiative intensity (Figure 2.10).

Temperature – although dominant – is not the only factor to affect the radiant heat flux; the emissivity of the radiating surface is also required in the calculation. Law explicitly stated that this method entailed a lot of simplifications since the engineers applying it could not be fire safety engineers, but civil or mechanical engineers.

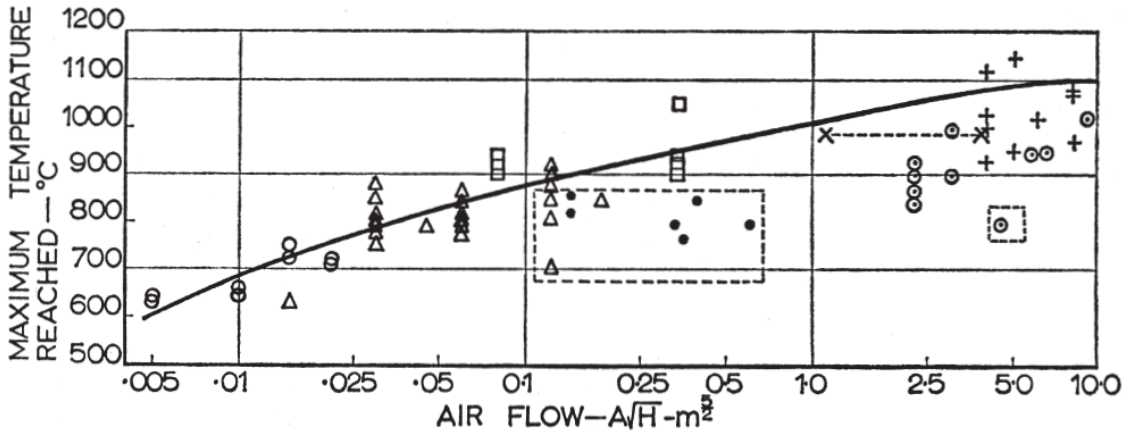

Points within the broken lines are those where the fire load is less than 25 kg/m² (5lb/ft²)

	Scale I floor area 0·09m²	Scale II floor area 0·49m²	Scale III floor area 1m²	Large-scale floor area 9m²
J.F.R.O. (7)(8)(10)	o	△	□	+
Swedish test (9)				x------x
Kawagoe (11)(12)			•	⊙

Figure 2.11. Correlation of the maximum temperature in a compartment to the ventilation factor A√H (modified Fig. 1 from [50])

A few key rules have to be set first to capture all aspects of this method.

1. The fire is developed and considered to be contained within the bounds of one compartment (comprised of one or multiple spaces). The compartment constitutes the radiating body;
2. The surface of the radiating body depends on the total area of the openings of one compartment;
3. Physical holes on the external wall (e.g. windows, balcony doors, etc.), parts of the external wall with lower fire resistance, and combustible parts of the external wall are considered as openings. This is due to the fact that these can potentially contribute to horizontal fire spread through radiation, once they ignite;
4. The source of maximum potential hazard is considered the compartment with the largest opening area.

Law understood that this method, considering a compartment of any size fully involved in the fire, was an over-estimation; however, she disregarded the contribution of the flames. A proposed work-around, without changing the whole method, was to assign an effective window area to account for the potential external flaming.

2.2.4 **The regulatory aspect of Law's work**

The modern day regulatory system in England and Wales (expressed as guidance through the Approved Documents in England) incorporates bits of the theoretical and actual concepts developed by Margaret Law in [50] in the Approved Documents B, vol. 1, 2 ([58], [59] respectively). This is evident by the use of the notional boundary, and the "enclosing rectangle" method, which are found in the regulatory text.

The notional boundary method was adopted in the guideline; it is the imaginary line used instead of a distance between buildings to define the separation between them. For a calculated separation distance, the length is halved to get the minimum allowed distance from the notional boundary. A building can

be built at a distance equal or greater to that; otherwise, a workaround to a distance smaller than the one from the notional boundary entails modifications in the design to minimise the amount of unprotected areas of the building towards that boundary.

A fire in a compartment radiates heat to its surroundings. The enclosing rectangle method assumes that heat is emitted only through the opening, disregarding the contribution of the external plume. The underestimation of the plume's contribution was considered to be covered by the overestimation of the contribution of the opening. This allowed to use the opening's geometry as a simplified way to estimate heat fluxes on targets around the compartment of fire origin.

Additionally, Chitty based his recent work for the BRE, entitled *External fire spread: Building separation and boundary distances* [60], on Law's method. The work of Chitty was informed primarily by Law's source material for [50]; he suggested additional methods (i.e., the aggregate notional area or protractor method) to calculate the requirements for the separation distance, expanding on Law's method. Chitty provided some cases studies to demonstrate the application of the method.

2.2.5 **Studies on vertical fire spread**

Listing the first studies on vertical fire spread, one has to first differentiate between two different cases: floor-to-floor fire spread through openings and vertical flame spread on the cladding materials.

2.2.5.1 Floor-to-floor fire spread

As described above, horizontal fire spread is a phenomenon that drew the public eye since the time of the Roman Empire. However, it was not until the proliferation of taller construction that vertical fire spread was systematically studied.

The Fire Grading of Buildings report, from 1946 [61], established provisions for floor-to-floor fire spread – though these were not deemed strictly necessary to be applied to all buildings. These provisions entailed a wall over a window

(from lintel to sill), with a fire resistance equal to the one demanded for the rest of the external walls.

In 1956 Ashton, in an attempt to investigate the contribution of spandrel panels and balconies to the prevention of fire spread, described an experimental series design in Fire Research Note 279 [62]. Following up on his previous work, Ashton and Malhotra, as members of the Fire Research Station at BRE, conducted a series of small and large scale experiments to assess the level of hazard (and the proposed countermeasures from the regulation in 1960 [52]) utilising the building previously described in [62]. Their study aimed to determine whether the regulations were realistically considering the hazard of external fire spread from burning rooms, or they were in need of an update, towards relaxation of proposed actions.

The experimental programme in Fire Research Note 436 [52] involved large scale compartment fire experiments (Figure 2.12). In addition to the design plans of the used rig, footage of the experiments conducted with it are available online [63].

Although radiative heat transfer was a source of energy transfer to the elements of the mock building, no direct measurements were made; instead, temperature data were recorded. A variety of fire loads, window sizes, spandrel panel and balcony presence were examined [52].

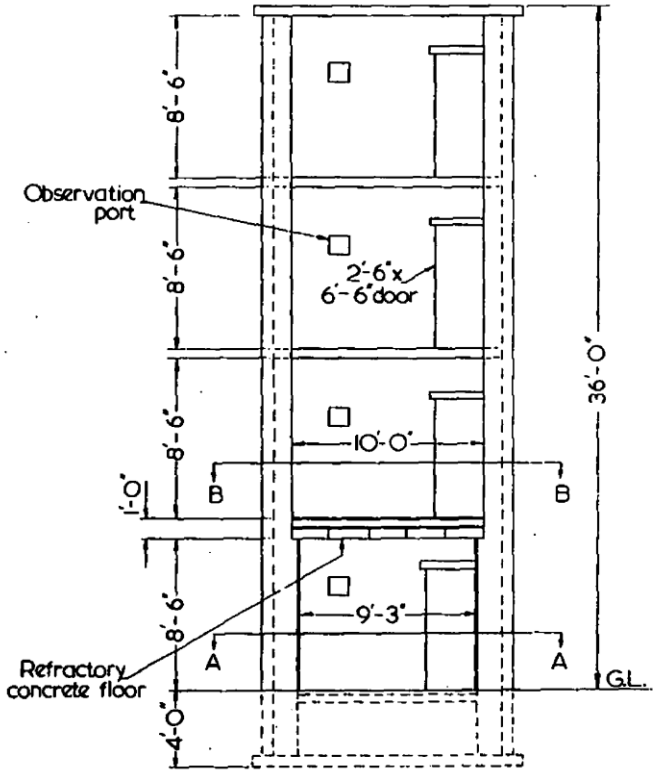

Figure 2.12. Elevation of the experimental setup (modified from [52]); the dimensions are in feet/inches.

Key observations of the research are listed below.

- The height of external flaming was proportional to the mass burning rate in well-ventilated compartment fires;
- For under-ventilated compartments, the ventilation opening dimensions were considered to be the driving factor for the burning rate;
- The potential of glazing failure due to flaming externally seemed to increase with longer duration;
- Non-combustible materials sustained comparable damage whether used as cladding or lining;
- Combustible cladding materials (i.e. timber) of significant thickness presented resistance to re-ignition, after the formation of a thick char layer;
- Dimensions of spandrel panels and balconies were proven ineffective to deflect flames away from the building.

In conclusion of Ashton and Malhotra's work, they noted that the distance of windows between two floors, based on the laws of 1960, was not sufficient to prevent fire spread. Additionally, spandrel panel and balcony's dimensions were not proven adequate to prevent fire spread. Finally, the use of non-combustible or timber cladding (thickness not less than ½ in.=12.7 mm) was thought to have a negligible effect in external fire spread; material other than timber needed to be assessed separately to draw a conclusion. Due to these, they proposed a relaxation on the regulatory requirements, as elements that were supposed to be effective against fire spread, were proven inadequate. A recent study discussed this specific topic [64].

Working in the same organisation with Ashton and Malhotra, Webster and Raftery included measurements of irradiance on the external wall over an opening for their experimental series, complementing previous work with their dataset [53].

Yokoi was driven by requirements in Japan for improved understanding of the burning of television towers and external fire spread from room fires. He contributed with his study of upward hot currents, informing on the trajectory of the ejected gases from compartment openings [65].

The National Research Council of Canada conducted a project entitled *"Fire spread via exterior walls of buildings"* [66]. It was in this study that Yung and Oleszkiewicz acquired a qualitative understanding of vertical spread from burning in the plume. Additionally, they were able to record the flame behaviour when applying a horizontal obstruction (i.e. balcony) and vertical wall extensions (e.g. shadings, building protrusions); the former provided a deflection of the flame whereas the latter channeled the flame to a higher level, due to lack of needed oxygen to burn the volatiles.

2.2.5.2 Vertical fire spread on cladding

Modern building materials, such as polymers, gave the opportunity to achieve new forms of the exterior or higher insulation to protect the interior from weather conditions; that came with a price – new hazards of fire spread for the

external wall arose. An alternate hazard is the spreading of fire on these cladding materials and/or material of the external wall assembly.

Since fire spread on the cladding materials is a relatively newly established hazard, research on the subject tends to originate from more recent work.

The 1988 NRC project entailed more than just floor-to-floor fire spread; Yung and Oleszkiewicz were also concerned with combustible material included on the façade [66]. As a preliminary result, the research concluded that combustible materials with some form of protection like aluminium siding with gypsum plasterboard provide a delay on the flame propagation upwards.

Building on this work, Oleszkiewicz realised that *"the hazard is extremely high for very tall buildings because a wall fire may extend beyond the reach of fire services"* [67]. He explored flame propagation onto the combustible cladding. Certain combustible materials could support infinite vertical fire spread. Reduced scale tests on flame spread on façades were questioned through this work; only full-scale tests were deemed appropriate to assess acceptability of cladding assemblies.

In Lund, Julia Ondrus performed a series of experiments with different types of thermal insulation on the cladding [68]. She attempted to assess a relative level of performance between different external insulation systems. Her deduction was that layering of materials on the wall exterior and geometrical characteristics were more important than the ignitability of each separate component. She too, as did Oleszkiewicz, concluded for the importance to use pass/fail criteria only on full-scale tests for the system as installed on the building.

2.3 A physics-based approach to external fire spread

The external fire spread from a compartment fire can be examined from two scopes. The first would be to consider the compartment; this would mean the energy and mass balance. The second scope would be to consider the external plume; that is, its behaviour and factors that affect it.

2.3.1 **The energy and mass balance of the compartment fire**

To understand the energy and mass balance of a compartment fire we first have to consider everything that happens in the control volume of the compartment.

2.3.1.1 The energy balance

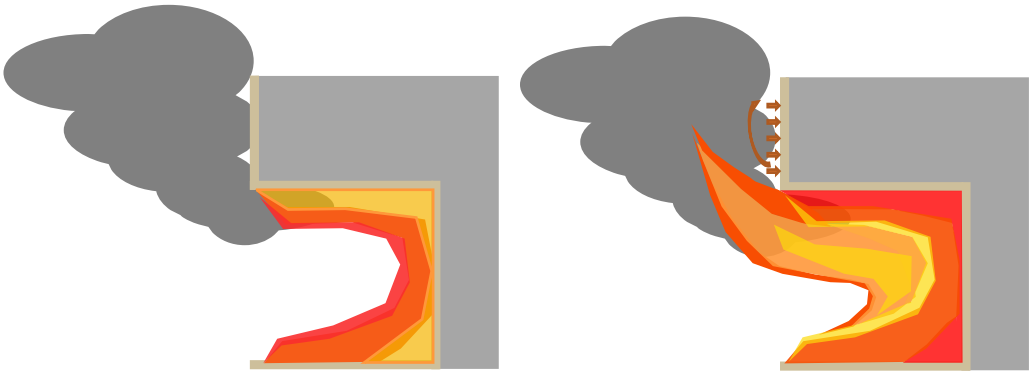

Figure 2.13. Sketches of: (a) well-ventilated; and (b) under-ventilated compartments.

Materials are ignited in a compartment; materials pyrolyse to flammable gases. The pyrolysis gases burn; from the burning process energy is released to the surroundings in the form of heat and light. If the incident heat flux on the burning or the surrounding materials is sufficient, it promotes the pyrolysis process, which leads to more volatiles. The volatiles, in turn, can oxidise and create further heat and light; all these create a feedback loop that aids the fire development.

Once we have the chemical energy released in the form of heat from the materials, one has to consider the energy losses from the combustion process to the surroundings. Heat losses can come in three forms: conduction; convection; and radiation.

The flames emit radiation to the surrounding walls of the compartment, the fuel bed, and through the openings; the compartment walls radiate towards the

flame as well. Heat is transferred, through radiation, from the "hotter" to the "colder" radiating surface.

As for the convective component, the fluid mechanics of the compartment fire need to be investigated. Fresh air enters the compartment space through openings; the air is entrained in the fire plume envelope, providing a convective cooling to the plume. The hot gases, through buoyancy and pressure, induce momentum and exit the compartment through the openings, providing further heat losses to the internal burning.

Finally, the conductive component needs to be considered. Conduction through the floor – in direct contact with the fuel load – promotes a small portion of losses. More significant conductive losses happen through the walls and ceiling; at this point it is important to note that these elements are convectively heated from the moving flames and hot gases in the compartment.

Moving beyond the classic heat transfer mechanisms, stored energy must also be considered. This is stored in the elements comprising the compartment boundaries (i.e. walls, floor, and ceiling); moreover, energy can also be stored in the gases from the combustion process. Nevertheless, the amount of energy that can be stored in the gas mass is notably lower than the energy stored in the solid elements of the compartment and usually disregarded from the calculations.

In equation form, the aforementioned parameters would be represented as follows:

$$\dot{Q}_c = \dot{Q}_{cond} + \dot{Q}_{conv} + \dot{Q}_{rad} + \dot{Q}_{st,s} + \dot{Q}_{st,g} \quad (2)$$

where $\dot{Q}_c$ is the heat release rate due to combustion of the fuel [kW]; $\dot{Q}_{cond}$ are the conduction losses through the compartment boundaries [kW]; $\dot{Q}_{conv}$ are the convective losses through openings [kW]; $\dot{Q}_{rad}$ are the radiative losses [kW]; and $\dot{Q}_{st,s}$ and $\dot{Q}_{st,g}$ are the expressions of stored energy in the solids and gases of the compartment fire respectively [kW].

In 1972, the research outcome of a round-robin series of compartment fires across laboratories in different countries was published. This experimental programme was proposed by D.I. Lawson, director at the time of the Fire Research Station, and the laboratories were part of the Conseil International du Batiment (CIB). Variables such as compartment shape, scale, ventilation openings, fire load density, and wind were considered. As part of the findings, Thomas and Heselden defined the opening factor O for a compartment as follows [69]:

$$O = \frac{A_t}{A_w\sqrt{H}} \tag{3}$$

where A_t [m^2] is the internal area of the compartment excluding the floor (as this is where the fuel is assumed to be, and thus an area of heat generation, not losses) and any openings, A_w [m^2] is the area of the openings, and H [m] is the opening height. The opening factor is a representation of the energy balance in the compartment control volume between the heat losses through conduction into the solid boundaries of the compartment (represented by A_t), and the heat losses by convection and radiation through the compartment openings (represented by $A_w\sqrt{H}$).

2.3.1.2 The mass balance

In the most basic concept, the mass balance refers to mass of material entering and mass of materials exiting the compartment space.

Starting from the latter, the materials exiting the compartment space will be products of combustion, or non-reacting by-products. Exiting materials can be found in the following categories:

- Carbon dioxide, as a product of complete combustion;
- Water in the form of steam, additionally as a product of combustion;
- Carbon monoxide in the case the combustion process in the compartment space is incomplete;
- Unburnt oxygen;
- Nitrogen;

- Carbon particles (soot), again as a product of incomplete combustion;
- Fuel that did not react inside the compartment;
- Other particles, which were part of the materials in the compartment, and can (or cannot) react with oxygen in the presence of heat.

Butcher et al. demonstrated that external flaming, and thus potentially mass transfer, is affected by the fuel load, but also the fuel location in the compartment [70]. In their experiments, fuel that was placed on the ceiling exhibited external flaming; this was particularly interesting, since experiments with similar and/or higher fuel load placed on the compartment floor did not present external flaming.

Based on the information presented so far, it becomes apparent that quantifying the mass of unburnt fuel exiting the compartment (if this is the case) is of interest, when studying the external fire spread. Researchers in the past, in an attempt to quantify the exiting fuel, formulated two terms: (1) the excess fuel factor; and (2) the global equivalence ratio. These two concepts are explained in the following text.

2.3.1.2.1 The excess fuel factor

The excess fuel factor was introduced as a concept of quantifying how much unburnt fuel exits a compartment during a fire [71]. It provides a way to differentiate among various compartment fires. Theoretically it could provide insight into the level of potential external fire spread hazard. The equation for the excess fuel factor is shown below.

$$f_{ex} = 1 - \frac{\dot{m}_a}{r_{af}} \cdot \frac{1}{\dot{m}_f} \quad (4)$$

where f_{ex} is the excess fuel factor [-]; $\dot{m}_a$ is the rate of air inflow in the compartment [kg/s]; r_{af} is the stoichiometric air-to-fuel ratio [-] for the type of fuel (or fuels) present; and $\dot{m}_f$ is the mass loss rate of the fuel [kg/s]. The stoichiometric ratio is determined based on the material burning and how much oxygen is required to burn everything, without excess oxygen remaining after

the combustion process. In this sense, the material chemistry determines the required oxygen, and effectively the stoichiometric ratio.

The excess fuel factor indicates when the compartment is under-ventilated; under-ventilated conditions mean that any fuel produced in excess will have to burn outside the compartment area. To understand meaning of different values of the term, negative values (with a maximum of -1) indicate well-ventilated conditions; zero value indicates stoichiometric burning; positive values (with a maximum of 1) indicate under-ventilated conditions.

2.3.1.2.2 The global equivalence ratio

A similar term to the concept of the excess fuel factor is the global equivalence ratio (GER) [72]:

$$\varphi_p = \frac{\dot{m}_f}{\dot{m}_a r_{fa}} \quad (5)$$

where φ_p is the global equivalence ratio [-]; and r_{fa} is the stoichiometric fuel-to-air ratio [-] for the type of fuel (or fuels) present (this is the inverse term of r_{af}).

A zero-value GER indicates that no burning is taking place; a GER of unity indicates stoichiometric burning conditions (all fuel is consumed in the compartment); a GER above one indicates that some fuel must exit the compartment to be able to oxidise. It should be noted that, while excess fuel factor and GER indicate the degree to which fuel *may* burn within the compartment, it does not follow that the fuel *does* burn within the compartment. Only in a perfectly well-mixed reactor would it be reasonable to assume that at GER of 1.0 would result in no external flaming. In reality, either flame extensions of the internal fire plume or slow mixing times, and mass transport of fuel will lead to external flaming from a compartment for values of GER less than 1.0.

It has been exhibited in a previous publication of this project [73], if no measurements of combustion efficiency are made, complete combustion cannot be assured that have happened during an experiment (or a real fire

scenario); in fact, it is considered unlikely that stoichiometric conditions will be applicable during a compartment fire. This introduces a maximum error of +1 to the GER value by the assumption of stoichiometric burning. This means that, potentially, no fuel is consumed inside the compartment, which can be confirmed or disproved with visual observation (i.e., if there are flames inside the compartment, fuel is being consumed within, meaning the introduced error is less than +1). Due to this fact, GER (and excess fuel factor) can serve as a useful first approximation of the *potential* for external flaming – but not necessarily as a predictor for external flaming.

Asimakopoulou et al. used the GER in their work as an identifier of under-ventilated condition in their compartment experiments [74]. The fact that the excess fuel factor (as well as GER) serves as an indicator is illustrated by Drysdale [75, p. 405] where it is shown that there is some correlation between excess fuel exiting the compartment with the heat flux measured above the compartment.

2.3.2 **The external plume**

The theoretical basis for the external plume was set by Yokoi in the 1960's [65]. Through his methodical research, correlations were formed for the temperatures of the external plume from a compartment fire. Both medium- and large-scale experiments were conducted; the former served as guidance for the formation of the correlations; the latter as a validation of the correlations. Where a derivation of unknown variables was not possible, he performed experiments to extract empirical values for his correlations.

Yokoi ran various experimental programmes; each of them served different purposes in developing an understanding for fire plumes. He approached the subject of fire and smoke plumes both as an upward (vertical) current and as an ejected (horizontal and vertical) current.

2.3.2.1 The rising plume

As a first approach, the origins of the rising plume were: 1) a point heat source (wick alcohol lamps) and; 2) an infinite line heat source during his initial

approach. For these two different heat sources, he derived the equations for temperature and upward velocity as functions of the convective heat release rate (convective heat output).

Yokoi used the following general equations:

Equation of Motion

$$w\frac{\partial w}{\partial z}+v\frac{\partial w}{\partial r}=\frac{g\Delta\theta}{\theta_0}+K(\frac{\partial^2 w}{\partial r^2}+\frac{1}{r}\frac{\partial w}{\partial r}) \quad (6)$$

Equation of Heat Continuity

$$w\frac{\partial \theta}{\partial z}+v\frac{\partial \theta}{\partial r}=\frac{g\Delta\theta}{\theta_0}+\frac{1}{r}\frac{\partial}{\partial r}(K'r\frac{\partial \theta}{\partial r}) \quad (7)$$

Equation of Continuity

$$\frac{1}{r}\frac{\partial}{\partial r}(rv)+\frac{\partial w}{\partial z}=0 \quad (8)$$

where w is the vertical velocity [m/s]; v is the horizontal velocity [m/s]; z is the vertical distance of the point of interest from the fuel source [m]; r is the radial distance of the point of interest from the fuel source [m]; $\Delta\theta$ is the temperature difference of the point of interest from ambient temperature [K]; θ_0 is the ambient temperature [K]; K is a coefficient of eddy viscosity (m^2); K' is a coefficient of eddy diffusivity (m^2).

These equations led to formulas of temperature and velocity for the case of a point and the case of an infinite line heat source (namely equations 1.114 and 1.115, and 1.125 and 1.126 respectively from [65], as shown in Figure 2.14).

(a)

$$\Delta\theta = 0.423\sqrt[3]{\frac{\theta_0 Q^2}{c_p{}^2\rho^2 g}}\,c^{-8/9}z^{-5/3}\left\{1+0.938\left(\frac{r}{zc^{2/3}}\right)^{3/2}+0.400\left(\frac{r}{zc^{2/3}}\right)^{3}+0.0940\left(\frac{r}{zc^{2/3}}\right)^{9/2}\right\}\exp\left\{-1.462\left(\frac{r}{zc^{2/3}}\right)^{3/2}\right\}, \quad \cdots\cdots\cdots(1.114)$$

$$w = 0.833\sqrt[3]{\frac{Qg}{\theta_0 c_p \rho}}\,c^{-4/9}z^{-1/3}\left\{1+0.917\left(\frac{r}{zc^{2/3}}\right)^{3/2}+0.399\left(\frac{r}{zc^{2/3}}\right)^{3}+0.1077\left(\frac{r}{zc^{2/3}}\right)^{9/2}\right\}\exp\left\{-1.462\left(\frac{r}{zc^{2/3}}\right)^{3/2}\right\}. \quad \cdots\cdots\cdots(1.115)$$

(b)

$$\Delta\theta = 0.663\sqrt[3]{\frac{\theta_0 Q_0{}^2}{c_p{}^2\rho^2 g}}\,c^{-4/9}z^{-1}\left\{1+0.529\left(\frac{y}{zc^{2/3}}\right)^{3/2}+0.0676\left(\frac{y}{zc^{2/3}}\right)^{3}-0.0323\left(\frac{y}{zc^{2/3}}\right)^{9/2}\right\}\exp\left\{-1.109\left(\frac{y}{zc^{2/3}}\right)^{3/2}\right\}, \quad \cdots\cdots\cdots(1.125)$$

$$w = 1.040\sqrt[3]{\frac{gQ_0}{c_p\rho\theta_0}}\,c^{-2/9}\left\{1+0.442\left(\frac{y}{zc^{2/3}}\right)^{3/2}+0.0474\left(\frac{y}{zc^{2/3}}\right)^{3}-0.00850\left(\frac{y}{zc^{2/3}}\right)^{9/2}\right\}\exp\left\{-1.109\left(\frac{y}{zc^{2/3}}\right)^{3/2}\right\}. \quad \cdots\cdots\cdots(1.126)$$

Figure 2.14. Equations for (a) point and (b) line heat source from Yokoi [76].

For Figure 2.14, w is the velocity at the centreline of the plume [m/s]; $\Delta\theta$ is the temperature difference (plume temperature minus ambient temperature) across the plume centreline [K]; Q is the convective heat output [W]; θ_0 is the ambient temperature [K]; c_p is the specific heat of the hot gas [J/(kg·K)]; ρ is the hot gas density [kg/m^3]; g is the gravitational acceleration [m/s^2]. The 'r' variable in the equations of Figure 2.14 (a) represents the radius from the point heat source; the 'y' variable corresponds to distance from the line burner (in Figure 2.14 (b)).

When the convective heat quantity (i.e. $\dot{Q}_{conv}$) of the source is given, the aforementioned equations can produce temperature and velocity results at any point of the rising plume.

Following the work on the rising plume (a phenomenon concerning buoyancy), the momentum component of an ejected (spill) plume was considered by Yokoi. A set of 60 experiments was performed. The setup was a box with two

openings in the same direction; one of them served as an inlet where air was blown in by a fan; on the other one orifices of circular and rectangular shapes were installed; the size of the orifice varied between experiments. The initial velocity at the outlet was another variable.

2.3.2.1.1 Circular orifices

Yokoi considered that a relationship should exist between the ratio of the velocity at any point away from the outlet to the velocity at the outlet of the box, and the ratio of the distance from the outlet to the radius of the orifice. It was found that up to a distance equal to ten times the orifice radius, the velocity was equal to the velocity of the outlet; beyond that point, the velocity has a relationship with the distance from the orifice $\frac{v}{v_0} = \frac{10r_0}{x}$, where v is the velocity at distance x [m/s]; v_0 is the velocity at the orifice [m/s]; r_0 is the radius of the circular orifice [m]; x is the distance from the orifice that velocity v is measured/calculated [m]. The proportional relationship of velocity to distance on the second region is the same as for the turbulent jet ejected from a point source.

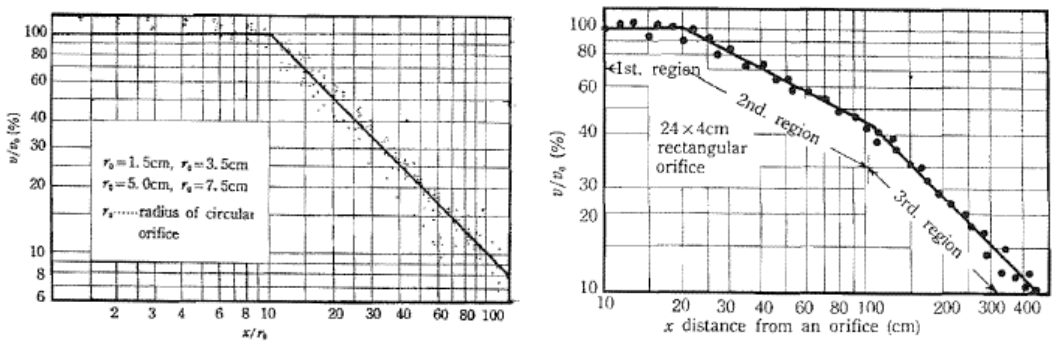

(a) (b)

Figure 2.15. (a) Velocity distribution from a circular orifice; (b) Velocity distribution from a rectangular orifice (both figures from [65]).

This very distinct "jump" from one state to the next is shown in Figure 2.15 (a).

2.3.2.1.2 Rectangular orifice

In the case of the rectangular orifices, three regions appeared to form as the distance from the orifice grew larger. The 1st and 3rd regions seem to follow the same rules as in the case of the circular orifice; the 2nd region has a proportionality of velocity reduction to distance from the orifice similar to a turbulent jet spreading from an infinite line source. The proportionality of the point source jet is the most stable one, hence the 3rd region has the same correlation.

An equivalent radius is proposed; essentially, an equivalent disc area is calculated, with an adjustment or shape factor (n) accounting for the rectangular opening's slenderness (see Table 2.1 of [65]); this factor was empirically formulated from observations of rectangular orifices. Using the equivalent radius of a circular orifice r_0, the following equations were formed.

$$\begin{aligned} x &\leq \frac{8.85 r_0}{\sqrt{n}} && : v = v_0 \\ \frac{8.85 r_0}{\sqrt{n}} \leq x &\leq 11.3 r_0 \sqrt{n} && : v = \frac{2.98 v_0}{\sqrt[4]{n}} \sqrt{\frac{r_0}{x}} \\ x &\geq 11.3 r_0 \sqrt{n} && : v = \frac{10 v_0 r_0}{x} \end{aligned} \tag{9}$$

Through the understanding of the rising plume from an unobstructed fire Yokoi aimed to develop the relationships for the ejected plume from a compartment fire. Following the work of the velocity distribution from circular and rectangular orifices, he performed experiments to empirically fill gaps that he could not derive for the temperature distribution above a circular burning pan. Once correlations were formed for the circular pan, an extension for rectangular pans, based on the law of similarity, was developed.

Yokoi did a dimensional analysis for the case of the rising plumes. There is a relationship between velocity and temperature difference with a power of the heat release rate. To formulate something useful, a non-dimensional velocity (W) and temperature (Θ) were introduced (equations shown below respectively).

$$W = \frac{w r_0^{1/3}}{\sqrt[3]{\frac{Qg}{c_p \rho \theta_0}}} \quad (10)$$

$$\Theta = \frac{\Delta\theta r_0^{5/3}}{\sqrt[3]{\frac{Q^2 \theta_0}{c_p^2 \rho^2 g}}} \quad (11)$$

where w is the velocity at the centreline of the plume [m/s]; $\Delta\theta$ is the temperature difference (plume temperature minus ambient temperature) across the plume centreline [K]; r_0 radius of the orifice (or the equivalent radius in the case of rectangular orifice) [m]; Q is the convective heat output [W]; θ_0 is the ambient temperature [K]; c_p is the specific heat of the hot gas [J/(kg·K)]; ρ is the hot gas density [kg/m^3]; g is the gravitational acceleration [m/s^2].

Two different types of heat source surfaces were used:

- a continuous heat surface (a pan of alcohol);
- a discontinuous heat source (wicks forming concentric circles).

The horizontal temperature distribution over height was measured and plotted as shown in Figure 2.16.

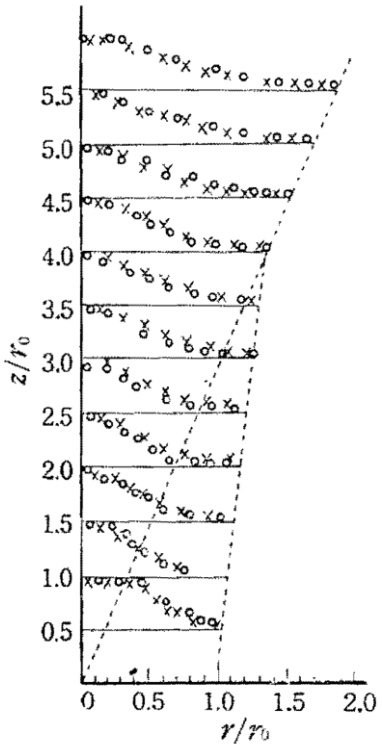

Figure 2.16. Horizontal distribution of temperature above circular heat source (reproduced from the original Figure 3.2 in [65]).

There are two domains/types as to the horizontal distribution of temperatures from a rising plume; these are separated around $z/r_0 = 2.5$. For heights below that, the rising plume does not spread widely; for heights above that, the plume spreads as if it originated from a point heat source, with the centre positioned in the centre of the circular source.

A similar approach can be applied to the case of a rectangular heat source. The circular heat source differs from the rectangular in the sense that both sides of the rectangle affect the plume behaviour; the shortest side will create the first boundary; the longer side will create a second boundary; beyond the second boundary, the behaviour is similar to that of the rising plume from a circular source.

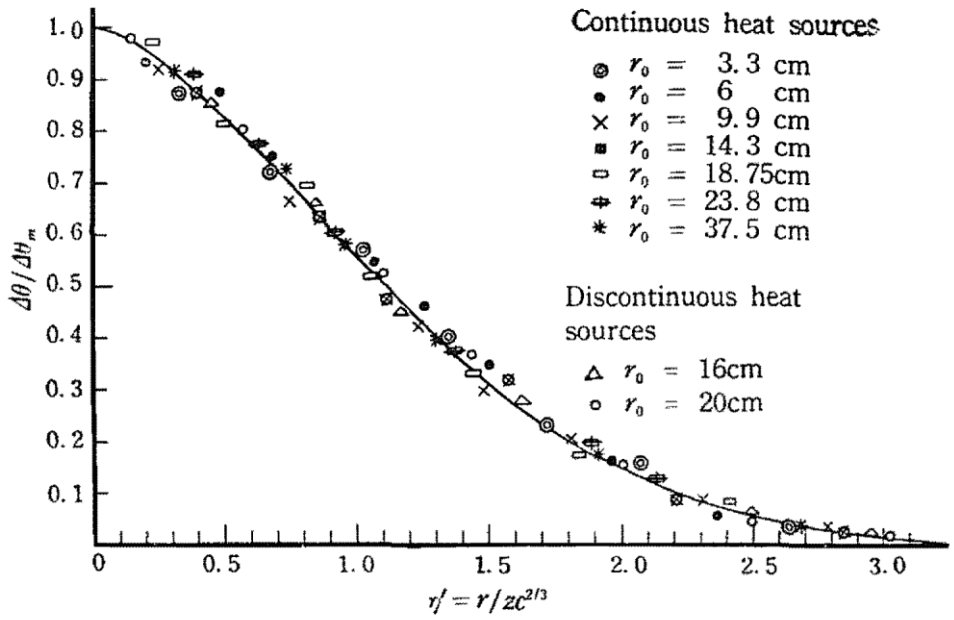

Figure 2.17. Horizontal temperature distribution of the upward currents from circular hear sources in the domain far from the sources (reproduced from the original Figure 3.5 in [65]).

Figure 2.17 supported the claim that temperature distribution at the domain far from the heat source behaves similar to the plume from a point heat source. Although experiments were not performed to support the same claim for velocities, Yokoi suggested velocity distribution follows a similar pattern as the temperature distribution.

Plotting the peak non-dimensional temperature over the normalized heights two distinct linear relationships are formed.

The independence of the patterns of temperature and velocity from the heat release rate of the heat source was proposed in the dimensional analysis; a dependency and a trend of the larger HRR to yield higher numbers was found through processing.

2.3.2.2 The ejected plume

As far as the spill plume is concerned, gas trajectory and gas temperature are going to be the factors of prime interest. Starting with full-scale experiments,

the compartments had one or multiple openings, depending on the experiment; the number and dimensions of the opening showed to have influenced the calculation of the neutral plane. Thermocouple trees were installed on the exterior to record the temperature distribution of the hot gases.

Some of the experiments had flaming in the external plume (internal flame extensions); this showed later to not present an issue with the correlations. However, it needs to be mentioned that the relationships developed by Yokoi were meant from hot gases and not external plumes with flames.

Key observations of the full-scale experimentation were as follows:

- Plume adherence to the wall depends on the ratio of height to width; a more slender opening will lead to a more detached plume and vice versa.
- The temperature distribution of hot gases (central axis) is comparable to upward currents from finite dimensions heat source.

In order to better understand the phenomena, small-scale experiments were conducted. Equations for the trajectory of the ejected gases were formulated. The generalised equation of gas trajectory is independent of the temperature of the gas; the equation is shown below.

$$\frac{z}{H''} = \frac{0.1047[\left(\frac{x}{H''} + \frac{x_0}{H''}\right)^{3/2} - (\frac{x_0}{H''})^{3/2}]^2}{\frac{x_0}{H''}} \quad (12)$$

where H'' is the height above the neutral plane (see Figure 2.18 (a)) [m]; z is the height of the ejected gas from the heat source [m]; x is the stand-off distance of the ejected gas from the heat source [m]; and x_0 is the horizontal distance inside the opening (as the line source of the jet) [m].

a. No façade above the opening.
b. Façade above the opening; n=1
c. Façade above the opening; n=1.5
d. Façade above the opening; n=2
e. Façade above the opening; n=2.5
f. Façade above the opening; n=3
g. Façade above the opening; n=3.4
h. Façade above the opening; n=6.4

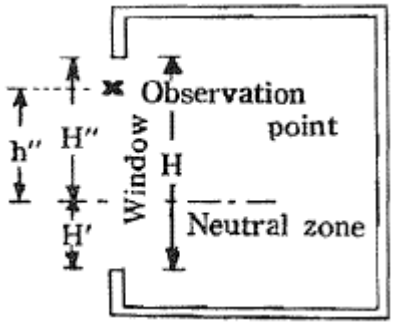

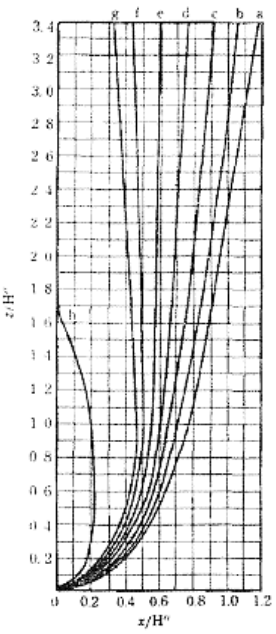

(a) (b)

Figure 2.18. (a) Yokoi's model compartment cross section (original figure 7.2 from [65]); (b) Trajectories of gases exiting various rectangular windows (original figure 7.4 from [65]).

Since x_0 was an unknown, Yokoi ran an experimental programme with various opening dimensions and ratios; he calculated the trajectory heights and widths; solving the aforementioned equation, he used the results to calculate x_0 or more precisely ${x_0}/{H''}$. The position of the maximum temperature at each row of thermocouples was used as an indication of the position of the plume trajectory.

Trajectories for compartments with a façade over the opening and for compartments with no façade over the opening were plotted in Figure 2.18 (b). Depending on the ratio n ($= \frac{W}{2H}$, where W and H are the width and the height of the opening respectively), and whether there is a façade over the opening, a different curve is appropriate to be used.

Yokoi plotted the curves for ejected gas trajectory. Yokoi developed an analytical solution for the case where there is no wall/façade above the

opening; this analytical solution is subject to corrections where there is a façade above the opening. For short and wide openings, the correction factor has a higher value than in the case of more slender (tall and narrow) openings.

A temperature distribution method was proposed, when the HRR (similar to the rising plume) and the dimensions of the opening are available. Yokoi assumed symmetry of the plume; time-averaged temperatures were used, similar to the rest of his work.

In medium scale experiments, the temperature distribution was found to be governed by the ratio *n* of the opening. The opening shape defines the temperature distribution regardless of the internal convective HRR at the opening.

In an attempt to use the upward currents equations on the ejected plume from a compartment fire, Yokoi presented the key differences:

- The heat source is on the vertical instead of the horizontal position. However, initially, the plume's direction, from a compartment fire, matches the direction of the plume from an unobstructed burner (plume rises perpendicular to the plane of the burner). In a compartment fire that happens due to the momentum of the gases exiting the compartment. Following that, buoyancy forces gases to rise parallel to the plane of the burner.
- The velocities from a compartment fire ejected plume are not uniform; approximately 2/3 of the upper layer of the opening serve as an exit; the rest of the opening serves as a fresh air (oxygen) supply.
- In cases where the space above the opening is blocked by a wall (façade), the external plume rises in the semi-infinite space, unlike the rising plume from an unobstructed burner.

Using the correlations for the upward currents, there are three distinct lines (as illustrated in Figure 2.19):

- the first line has a small deviation from the vertical direction;
- the second line is at approximately 45 degrees.
- the third line is at an angle approximately equal to $\tan^{-1}(3/5)$.

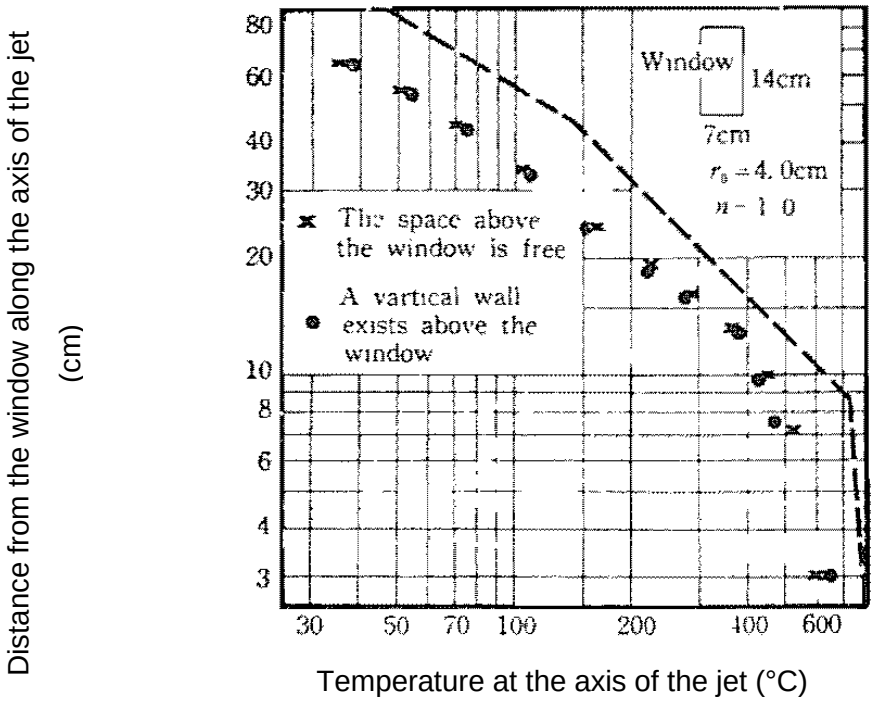

Figure 2.19. Temperature distribution along the axis of the ejected jet.

Transition from the first to the second domain happens at approximately $\frac{1.25H}{2}$; the transition from the second to the third domain happens at approximately $11.75 \cdot r_0 \cdot \sqrt{n}$, as r_0 and n are defined below.

The value of r_0 is the equivalent radius of a free burning, circular pool fire. The value is calculated based on the same area that the pool fire and the opening of the compartment would have. Despite Yokoi's assumption that approximately 2/3 of the opening are part of the outflow, the velocities close to the neutral plane are relatively low; Yokoi proposed that only half the height of the opening should be considered for the calculation of the equivalent pool fire radius, hence the following equation.

$$r_0 = \sqrt{\frac{H \cdot W}{2\pi}} \tag{13}$$

where H and W are the height and the width of the compartment opening respectively [m].

$$n = \frac{W}{2H} \tag{14}$$

The ratio n can help to differentiate openings of the same area that have a different shape.

For compartments that have multiple openings with different dimensions, the height H that will be used needs to be modified accordingly, in order to calculate the equivalent radius and the opening ratio.

From the model scale experiments Yokoi found that for wider and shorter openings the gas temperature is higher, and the trajectory of the plume is leaning towards the façade. Although half of the energy of the plume is not dissipated to the surrounding space due to the presence of the façade, the temperature is not twice as high as it would be for a free rising plume. Convective losses into and heat stored in the wall decrease the total energy of the ejected plume. For this reason, the type of material of the façade/wall could impact the temperature profile of the plume.

2.3.2.3 The Thomas and Law correlations

Not long after Yokoi's thorough research on the rising and ejected plumes, Thomas published a joint project with Webster and Raftery on the buoyant diffusion flames [77]. In this work, among other experiments, they performed compartment fires. A linear regression model can be derived through the presented data; this is a correlation of the normalised flame height of the ejected plume to the internal heat release rate – similar to Yokoi's correlations.

Following this work, Thomas proceeded with a solo venture. He performed an analysis of the linear model from his previous collaborative work [77] and Yokoi's correlations [65]. Assuming a flame tip temperature of 500 °C, Thomas

was able to compare the regression model to Yokoi's dataset (after some modifications) [78]. Although the research had merits, the adapted regression model to Yokoi's method was not able to predict Yokoi's calculated dimensionless temperatures in a similar manner.

About a decade later, Thomas and Law made a review of the studies available at that time (1972) that focused on the external plumes [79]. Notably, all the data in their meta-analysis regarded compartments with no obstacle above them. They developed a relationship for the plume's non-dimensional temperature (based on previous work [77]) and the external flame height. The resulting model was deemed acceptable to be used in other researcher's datasets to describe them; therefore, Thomas and Law proposed this model for predicting the temperatures of the external plume.

Law proceeded some years after this collaborative effort (1978) to develop her own model, predicting temperatures on exposed steel on the exterior of the buildings [80]. The aims were to prove that: (a) external steel does not experience the same severity of heat fluxes as do steel elements in a compartment fire (this was the design approach and the testing criteria of that era); and (b) have a reliable model that can be used for design purposes on external steel components in structures. She used the formulation they developed with Thomas, making some alterations to fit the dataset better.

2.3.2.4 The current approaches on the external plume

2.3.2.4.1 Frank et al.

The more recent BRANZ Study Report by Frank et al. summarises many projects that examined vertical fire spread onto the façade of the building of origin [81]. Equations which were developed for all examined projects are presented in Table 2.2.

Table 2.2. Summary of flame height correlations (original Table 1 from [81])

Authors	Key parameters and correlation	Experiment range
Thomas and Law (1972)	$z = 18.6\left(\frac{R}{W_o}\right)^{2/3} - H_0$ $R = 0.09WH^{3/2}$ (ventilation limited)	$9 < \eta < 45$ $0.5 < \frac{W}{D} < 2$
Law (1978)	$z = 12.8\left(\frac{R}{W_o}\right)^{2/3} - H_0$ $R = (0.18)A_o\sqrt{H_o}\left(\frac{W}{D}\right)^{1/2}(1 - e^{-0.036\eta})$ $\eta = \frac{A_T}{A_o\sqrt{H_o}}$	$9 < \eta < 45$ $0.5 < \frac{W}{D} < 2$
Quintiere and Cleary (1994)	$z = 0.0321\left(\frac{\dot{Q}}{\sqrt{\frac{2A_o}{\pi}}}\right)^{2/3} - H_o$	Based on Yokoi's experiments $(\Theta < 0.48)$
Ohmiya et al. (2000) Note that z is relative to the plume centreline, not the top of the opening.	$z = 0.65\dot{Q}^{*2/3}_{W_o}W_o + 0.04\dot{Q}^2_{ex}W_o$ $\dot{Q}_{ex} = c_pR_{fo}\Delta T + \dot{Q} - \dot{Q}_{v,crit}$ $\dot{Q}_{v,crit} = 150A_o\sqrt{H_o}\left(\frac{A_T}{A_o\sqrt{H_o}}\right)^{2/5}$ $\dot{Q}^*_{W_o} = \frac{\dot{Q}_{ex}}{\rho_0 c_p T_0\sqrt{g}W_o^{2/3}}$	$1.5 < \dot{Q}^*_{W_o} < 11$ $0.25 < \frac{W_o}{H_o} < 2$
Delichatsios et al. (Y. Lee et al., 2008)	For $\dot{Q}^*_{\ell_1} < 1.3, z = 3.03(\ell_1)\dot{Q}^{*2/3}_{\ell_1} - 0.6H_o$ For $\dot{Q}^*_{\ell_1} \geq 1.3, Z_f = 3.45(\ell_1)\dot{Q}^{*2/5}_{\ell_1} - 0.6H_o$ $\dot{Q}^*_{\ell_1} = \frac{\dot{Q}_{ex}}{\rho_\infty c_p T_\infty\sqrt{g}(\ell_1)^{5/2}}$ $\ell_1 = \left(A_o\sqrt{H_o}\right)^{2/5}$	$0.3 < Q^*_{\ell_1} < 7$

For the table, R represents the mass burning rate, $\dot{Q}"_{\iota_1}$ is the normalized HRR from Lee et al. [82].

Following an extended literature review, Frank et al. carried out a series of experiments in a compartment with inert linings. The variables used were the location of the fuel source (front/back of the compartment), the type of fuel source (heptane pool fire, wood cribs), and opening shape, size, and location on the façade. The presence of an apron (imitating a balcony) was also

considered in the experimentation. Simulations were carried out using FDS, and comparisons of values derived from existing correlations with the computed FDS data were made.

2.3.2.4.2 Lee et al.

Since 2004, Lee et al. published a number of work, related to the external plume from compartment fires [82]–[84]. Through this work, contemporary understanding was incorporated into the classic plume theory. These experimental programmes aimed to remove ambiguity from the correlations for external heat fluxes, flame height outside an enclosure, and update equations for external plumes. A series of different experiments was conducted; depending on the experimental programme, different shapes of compartments were used. The fuel source was a gas burner in all cases. The location of the burner could be an examined variable, depending on the experimental programme. Inert materials were used to form the compartment boundaries.

The compartment and the façade above the opening were instrumented to capture characteristics of the plume (e.g., temperature profile inside the compartment and opening, heat fluxes on the façade). Cameras were used to record the shape of the plume and oxygen calorimetry was performed for the whole experimental setup.

Lee et al. proposed alterations in Yokoi's formula for non-dimensional temperatures of the external plume, to reflect the current understanding on entrainment [84], substituting the hot gas density for the ambient air density (ρ_0).

$$\Theta = \frac{\Delta\theta \tilde{l}_1^{\,5/3}}{\sqrt[3]{\frac{Q^2\theta_0}{{c_p}^2{\rho_0}^2 g}}} \qquad (15)$$

Lee et al. also proposed two new length scales (equations 16 and 17), as they were considered more compartment relevant, compared to Yokoi's equivalent circular orifice [82].

$$\tilde{l}_1 = \left(\frac{\rho_g}{\rho_0} A_w H\right)^{2/5} \quad (16)$$

$$\tilde{l}_2 \propto \left(\frac{\rho_g}{\rho_0} A_w H^2\right)^{1/4} \quad (17)$$

These length scales were considered by Lee et al. as a representation of an equivalent external burner outside the opening, representing the sides of the burner, as shown in Figure 2.20.

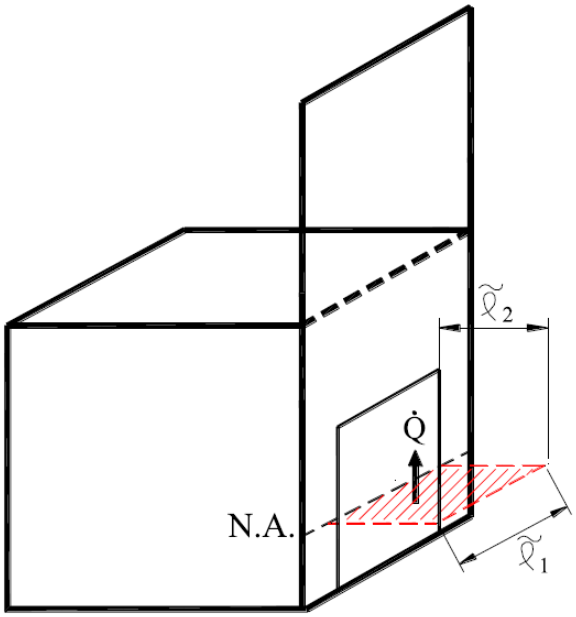

Figure 2.20. Sketch showing the length scales' physical representation proposed by Lee et al. (original figure from [84]).

Lee et al. developed also a heat flux model correlating the external heat release rate to the incident heat fluxes on the façade. The correlation is shown in Equation (18).

$$\frac{\dot{q}''_t \, Z_f e^{0.6(H/\tilde{l}_1)}}{\dot{Q}_{ex}/\tilde{l}_1} \propto \frac{Z}{Z_f} \quad (18)$$

where $\dot{q}''_t$ is the incident heat flux on the façade [kW/m^2]; Z_f is the average flame height [m]; $\dot{Q}_{ex}$ is the external HRR [kW]; Z is the height above the

opening of the measured incident heat flux on the façade [m]. The plotted data are shown in Figure 2.21.

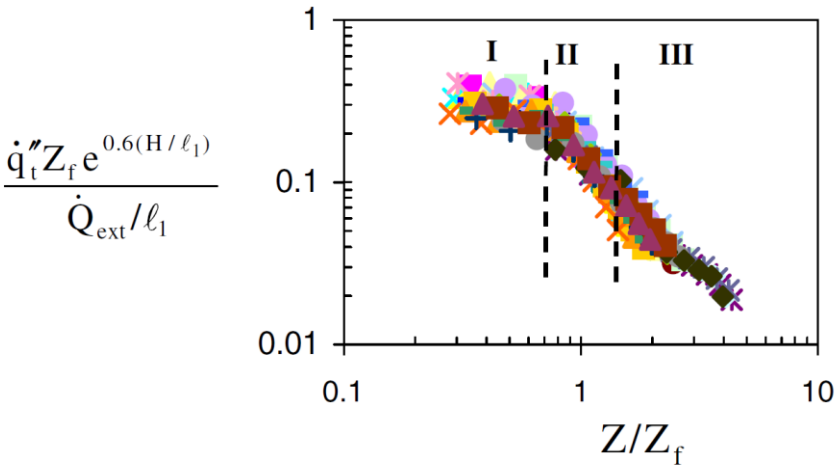

Figure 2.21. Normalised heat flux over normalised height above the opening (original figure from [82]).

2.3.2.4.3 Gorska

By far the most recent (2019) and relevant work is the thesis of Carmen Gorska. In her work, she investigated exposed timber compartments with respect to internal and external fire dynamics, and self-extinguishment (or auto-extinction) of the combustible linings [9]. Her experimental campaign consisted of medium-scale compartment fires; a large-scale proof of concept demonstration was performed as part of a collaborative work, as described in [38].

In the medium-scale experimentation, Gorska used a steel frame to mount CLT panels. The surfaces were encapsulated using plasterboard, when the surfaces needed to be inert; when combustible linings were needed, the CLT was left exposed. Photographs of the setup are shown in Figure 2.22.

Gorska used kerosene as the liquid for the pool fires, which were the fuel source for the compartment fires. The pan was connected externally, using a tube, to a tank of kerosene. The level of the pool inside the compartment matched the level of the tank outside; a floater system triggered a refill of the

tank to keep the pool at a prescribed height. This method gave control to the level of the pool fire and made possible to extend the steady state period for any desired time. A sketch of the system is shown in Figure 2.23.

(a) (b)

Figure 2.22. (a) Steel frame of Gorska's experimental setup; (b) Compartment assembly with instrumented façade (modified photographs from [9]).

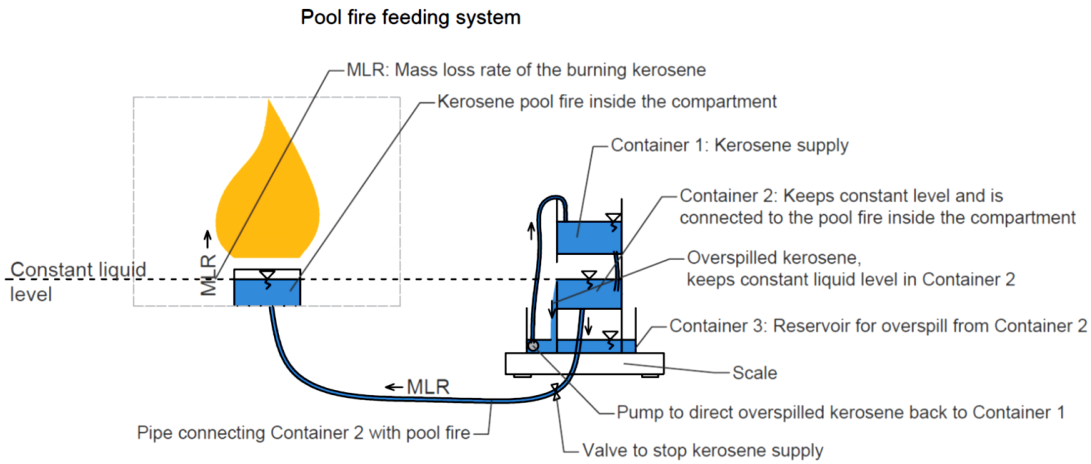

Figure 2.23. Pool fire and kerosene tank system schematics (modified plot from [9]).

Through these experimental programmes, a new approach for the compartment fire dynamics was developed. The classic compartment fire framework had introduced the opening factor (described in Section 2.3.1.1) with Gorska's proposition of a modified opening factor for exposed timber compartment fires; this is further analysed in Section 4.2.2. This proposition accounts for the burning timber linings as areas where heat is generated; due to this, the area is excluded from the calculation of the opening factor. Gorska's dataset fits over the classic compartment fire framework correlation of opening factor and compartment temperature, as depicted in Figure 2.24. Normalisation was applied based on the inert compartment's opening factor and temperature, respectively.

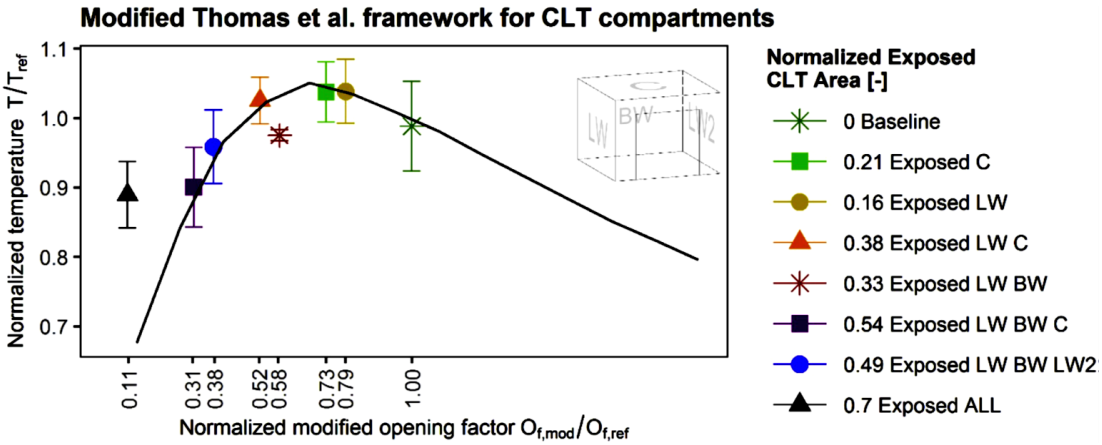

Figure 2.24. Opening factor versus compartment temperature (modified plot from [9]).

Gorska modified correlations from Lee et al. for heat fluxes on the façade from compartments with inert linings and was able to fit the modified models with her acquired data for timber lined compartments. As it is shown in Figure 2.25, the two experimental programmes have a distinct deviation in the continuous and intermittent flaming regions. Gorksa developed her modified correlations based on linear models for each region in this plot. Results of the modelling compared to experimental measurements show good agreement (Figure 2.26).

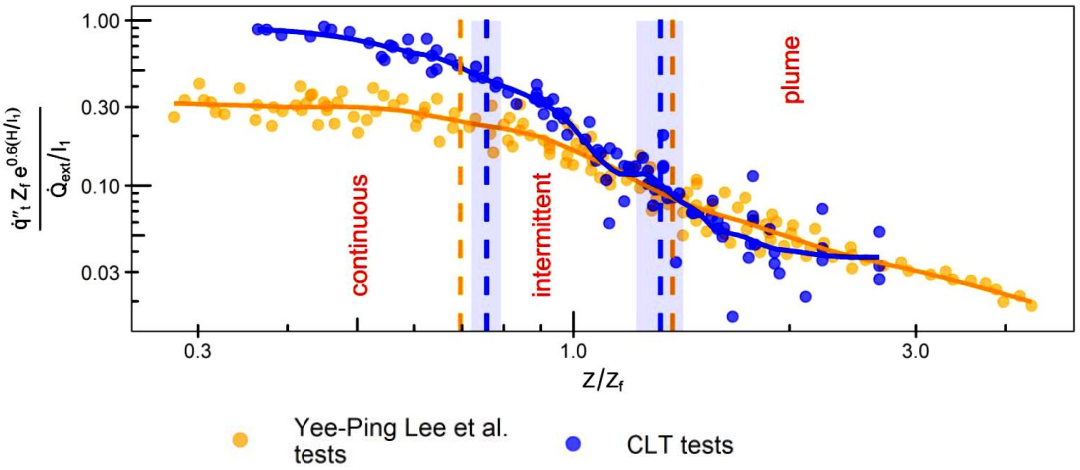

Figure 2.25. Comparison of Lee et al. (yellow) and Gorska (blue) datasets (modified plot from [9]).

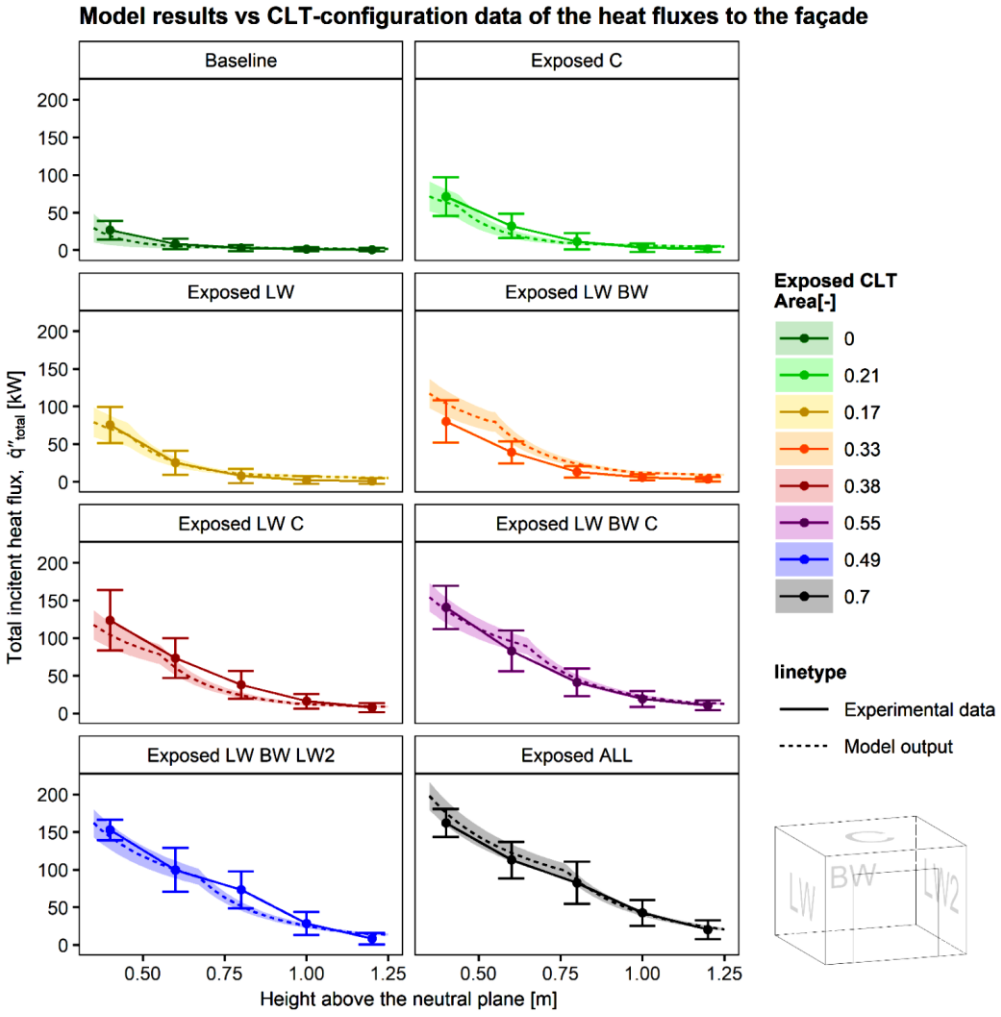

Figure 2.26. Model predictions and experimental measurements of heat fluxes on the façade (modified plot from [9]).

2.4 Where the current project fits in

In the previous sections a review of the current trend in modern constructions was clearly identified – that is tall timber construction. Mass timber offers advantages in terms of prefabrication, construction time, energy efficiency, and also aesthetics. Architects, the construction industry, and even local authorities are pushing for the approval and use of mass timber for mid- and high-rise buildings. However, timber has a main drawback; it burns.

A review of external fire spread was also performed in sections 2.2 and 2.3; this was done from a regulatory and physics perspective, respectively. A gap in the literature for the consideration and understanding of the external fire spread from timber-lined compartments was demonstrated.

This project will be focused in:

- Identification of the change in hazard when timber is exposed in the compartment;
- Identification of alteration in the external plume behaviour;
- Characterisation of the external plume, using techniques from the literature;
- Assessment of the fitness of current techniques for the description and prediction of the external plume behaviour;
- Identification of variables that drive the external fire spread phenomena when timber is exposed in the compartment space.

Chapter 3 – Methodology

The previous chapter has outlined the key physical concepts that are known to influence the hazard presented by the external plume. It has been shown that the presence of timber linings in a compartment fire can have an impact on the external plume. The physical drivers for this are, to some extent, known. For example, it has been shown that a higher mass loss within a ventilation controlled compartment will increase the excess fuel factor, and thus the heat released in the external plume.

The following chapters are concerned with elucidating the behaviour of the external plume. The objectives are to:

- Quantify the degree to which timber linings change the excess fuel factor;
- Quantify the degree to which such timber linings may affect the external fire spread hazard;
- Characterise the plume to allow more detailed interrogation of the underlying physical mechanisms.

In order to explore these parameters a series of experimental programmes were undertaken. This chapter is concerned with why and how the experimental programmes were designed and carried out. In particular, a detailed presentation of the experimental procedures followed and the equipment used to do so. The description of the experiments is split into two phases, there are substantial similarities between the two experimental phases – however, there are also notable differences in the instrumentation.

3.1 Guiding Principles

To investigate the relevant parameters a series of compartment fire experiments were undertaken. The literature has shown that there are two approaches to investigating compartment fires: full scale, and small-scale experimentation. The scale of full-scale experimentation means that the magnitude of the results obtained are “realistic” with regard to building fires –

however, their scale means that (without significant time and financial resources) repetition and systematic variation of parameters is impossible. Small to medium scale (i.e. of the order 0.5-1.0 m) has, therefore, been commonly employed by researchers to allow investigation of key parameters.

The use of medium-scale experiments introduces challenges in relation to how phenomena may be scaled. Some properties (e.g. opening factor, global equivalence ratio) could be scaled by solving a mass and/or energy balance on an element or control volume of the compartment/surrounding space. Other properties, such as the emissivity of flames, could be inherently connected to the size of the experiment.

3.2 Prototyping

3.2.1 **Fuel source**

Assessing the options for fuel load for the compartment fires, there are three popular options: (1) gas burners; (2) pool fires; (3) or wood cribs. These fuel types present pros and cons, regarding the first phase of the project.

Gas burners can generate enough heat to achieve burning of timber linings. It affords a great control of the fuel load burning inside the compartment space, as seen in previous work [85]. This control however, does not aid exploratory research because the experimentalist has to determine the burning rate *a priori*. This part of the work did not have a desired target of burning rate due to lack of evidence on what kind of HRR was needed. For this reason, it did not serve the desired purpose of the Phase 1 experiments.

Pool fires are often used for their more realistic thermal contribution to a compartment fire [74]. The soot yield is close to what can be recorded from conventional compartment contents, and the fire development curve is also comparable to a “real fire” (i.e. ignition, growth, flashover, full development, decay). However, unless one uses a very deep pan to have the liquid in or create a flow control system as described by Gorska [9], pool fires are relatively short in duration. Emberley et al. noticed that mass timber elements, when exposed to heat fluxes common for a compartment fire, needs approximately

10 minutes to enter a steady state (i.e. the burning rate reaches a plateau with minimum fluctuations) [86].

Wood cribs are a fuel that creates its own HRR curve (similar to the pool fires), dependent on the feedback and losses from its surroundings (although less sensitive to compartment feedback compared to pool fires). Furthermore, wood cribs can achieve a long burning duration; this has good potential of achieving steady state conditions for the timber linings of a CLT compartment. As it is well-known, wood cribs have been a fuel source used in research in the past [52], [87] up until the present day [86], [88]. These facts made wood cribs the ideal fuel source for the first experimental series.

3.2.2 **Ventilation**

The ventilation conditions within the compartment affect the burning behaviour both inside and outside the compartment. When more air is available, more flammable gases are available to react inside the compartment. Conversely, smaller openings offer less oxygen to react with the pyrolysis gases, potentially leading to unburnt fuel exiting the compartment and burning externally. In the case where fuel exits the compartment, the external burning becomes important to fire spread onto the building of origin; external burning also changes the assumptions made for fire spread on neighbouring buildings.

As noted by Yokoi, the shape of the external plume is dependent on the ratio of width to height of the opening [76]. A taller, more slender opening will produce a more projected external plume; on the contrary, a shorter, wider opening will result in a plume more adhered to the wall above the opening (or lean more towards the virtual, vertical plane above the opening, at the lack of wall above it).

The shape of the opening was designed according to the CIB experiments [69] (full-height slot). The choice of this shape meant that there would not be a sill or lintel. The lack of a sill eliminated the potential effect on the ventilation conditions of the full bed by induced vortices of air entrained in the compartment. Respectively, the absence of a lintel meant that the smoke

height was established by the compartment's geometry. This removed the need to decide on the 'right' height, as this would dictate the height of the retained smoke in the enclosure. The smoke height would have a direct effect on the fuel bed (for experiments where the fuel bed is influenced by heat feedback). Despite the fact that a full-height slot is not typical of classic architecture, more modern designs adopt a floor-to-ceiling opening for accessing the exterior of the building. The dimensions of the opening were chosen to produce an opening factor (for the case of inert compartments) approximately equal to the opening factor of previous work [88]–[90]; the opening for all compartment experiments in this thesis was the same. The resulting opening factor for an inert compartment was 19.7 $m^{-1/2}$. The opening factor provides a means of comparison across different scales. It is for this reason that a value approximately 20 $m^{-1/2}$ was selected. Most of the relevant timber compartment experiments (as listed in Bartlett's paper [90]) were conducted with approximately this value.

Based on the definition of the opening factor, Gorska identified that timber compartments present a change to the heat losses through conduction from their timber-lined boundaries [9]. The timber surface burns; the heat losses through that boundary approach zero while the surface contributes to the fire, due to heat generation – practically the area of timber should no longer be accounted for as part of A_t. Due to this fact, Gorska proposed the area of these surfaces is subtracted from total wall area A_t of the opening factor, resulting in lower values of O, as more timber gets exposed.

Law had already found a correlation of the ventilation conditions of the compartment and the peak temperature in the compartment [91], shown in Figure 3.1. This correlation demonstrated further scalable parameters that can be used for comparison of different compartment fires.

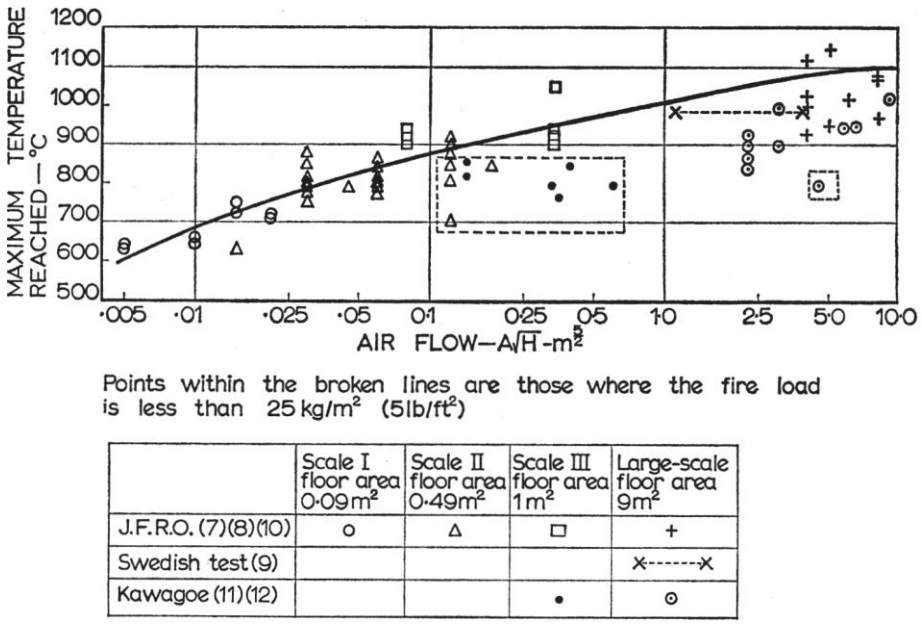

Figure 3.1. Peak temperature and air flow correlation (Fig. 1 from [91])

The objective of the first phase of experiments was to provide a means of comparison of the excess burning between the different experiments. To aid that comparison, the quantitative comparison of the fuel that cannot burn within the bounds of the compartment box was chosen. There are two methods to approach this, as it was already presented in the literature review chapter; (1) the excess fuel factor; (2) and the global equivalence ratio (GER).

Both concepts accomplish the objective of quantification of the unburnt fuel exiting a compartment. Nevertheless, the GER provides a more tangible understanding of the mass of fuel. A GER of 0.0 is interpreted as no burning taking place; a GER of 1.0 means that, in principle, there is sufficient oxygen within the compartment to allow all the fuel to burn inside the compartment volume; a GER of 2.0 means that, in principle, there is only sufficient oxygen entering the compartment to allow half of the fuel to burn inside the compartment – with the remainder burning externally. For this reason, the GER was selected as the comparative variable for this experimental series. However, as it was already mentioned in the review chapter, it must be recognised that GER is indicative of the potential location for fuel to burn inside

the compartment – in reality, with a GER of 1.0, it is likely that some fuel will burn externally.

The formulation for GER, as shown in the literature chapter, is represented by Equation (5). As seen from the equation, the mass loss rate of the compartment and the inflow rate of fresh air are needed. Appropriate equipment is needed to record/estimate the required variables. This is explained in full in section 3.3.

3.2.3 **Iteration of Fuel Load**

The first experimental series was initiated with the aim of quantifying the degree to which the presence of timber would increase the mass burning rate. As previously noted in the literature review, other authors have attempted this in both small and large scale [86], [88], [92].

However, in order to provide a useful baseline for this study, a series of compartment fires with non-combustible linings were needed. This provides a direct comparison, since the only change would be due to material properties, not geometry.

The experimental specification was optimized through iterations before the final arrangement was decided. During the first attempts the movable fuel load, the exposed CLT surfaces, the stick size of the wood cribs (thin cribs used 15 mm thick sticks, thick cribs used 38 mm thick sticks – section of sticks were square, spacing was equal to the thickness of a stick), and the opening shape were altered. Figure 3.2 shows the heat release rate (HRR) curves to demonstrate the difference in steady state burning conditions.

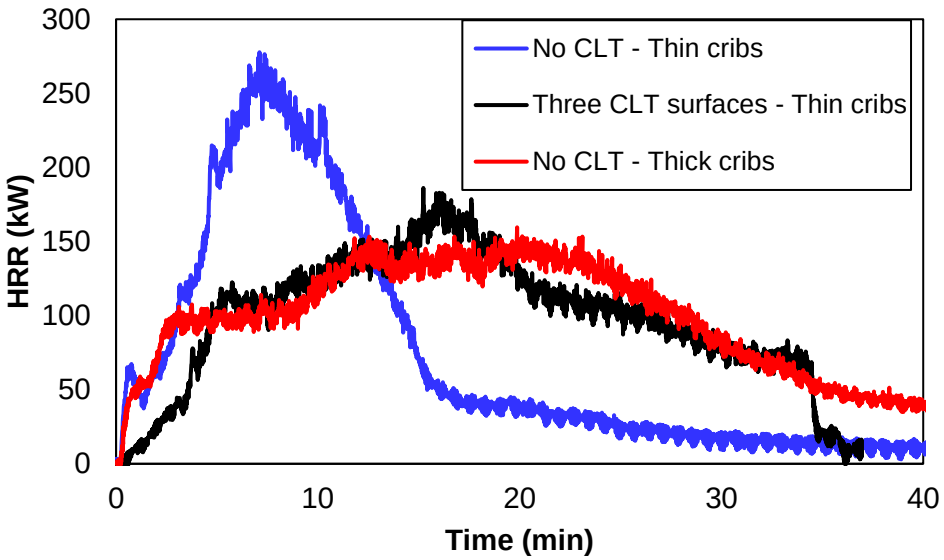

Figure 3.2. Heat release rate for different exploratory experiments.

The thin cribs resulted in short fires:

- For the case of three exposed CLT surfaces, the opening was very wide and short, and the fuel load not sufficient to surpass the critical burning rate of timber. Due to this fact, the exposed timber surfaces could not sustain burning after the movable fuel burnt out. In this experiment, a discernible steady state was not achieved. It is also noticeable that this HRR curve resembles the one from the experiment with no exposed CLT and the thicker stick wood crib (red line in Figure 3.2).
- For the experiment with no exposed surfaces (blue line in Figure 3.2), the crib's HRR peaked very quickly and the burning rate of the fuel did not achieve a noticeable steady state. The ventilation opening was taller and narrower in this case, which meant less smoke accumulation inside the compartment.

Conversely, the cribs with increased stick thickness resulted in a lower heat release rate; nevertheless, a steady state burning was recorded (approximately 10 minutes). It will be demonstrated on the following chapter (Chapter 4 – Phase 1) that the burning duration achieved by thicker sticks was sufficient to create quasi-steady burning conditions for all experimental setups.

3.2.4 **Compartment design**

The compartment design process was influenced by the work of previous authors. The aim was to keep the dimensions (and general length scale) approximately the same as previous work; this could make it easier to draw comparisons with other datasets. Some of the works that this project considered for the design are as follow:

- In the CIB round-robin experimental programme compartments of side less than 1 m were used in many cases [87] – the internal dimensions ratio varied.
- In the work of Gorska et al. the compartments were 0.5 m deep and 1 m wide [92].
- Bateman et al. [88] used almost cubic compartments, with the internal dimensions ranging from 575 to 700 mm.

Moreover, there were other key factors that affected the design process. These were:

- Having an opening factor (directly affected by the opening dimensions) similar to work of previous researchers. This provided a comparison across different length scales.
- Using a fuel source similar to previous researchers.

It was for these reasons that the final design was informed in the following manner.

Based on the aforementioned experimental programmes, the compartments in the current project were designed as cubes; cubes were used by Bateman et al. The internal cube had a side of 700 mm, an option closest to Bateman et al. and Bartlett's design. Bartlett's work was particularly useful for direct comparison, as his compartments were lined with CLT. However, it should be noted that his work focused on burnout whereas the present thesis aims to understand the potential changes in behaviour of external fire spread, regardless of burnout conditions that might (or might not) occur in the decay phase.

3.3 Experimental Design

3.3.1 **The wood crib experiments – Phase 1**

3.3.1.1 Design

The first experimental programme aimed to identify key differences between traditional compartments with non-combustible linings and timber compartments. A compartment (Figure 3.3) was constructed with internal dimensions of a 700 mm cube. The opening of the compartments was a 200 mm wide full height central slot.

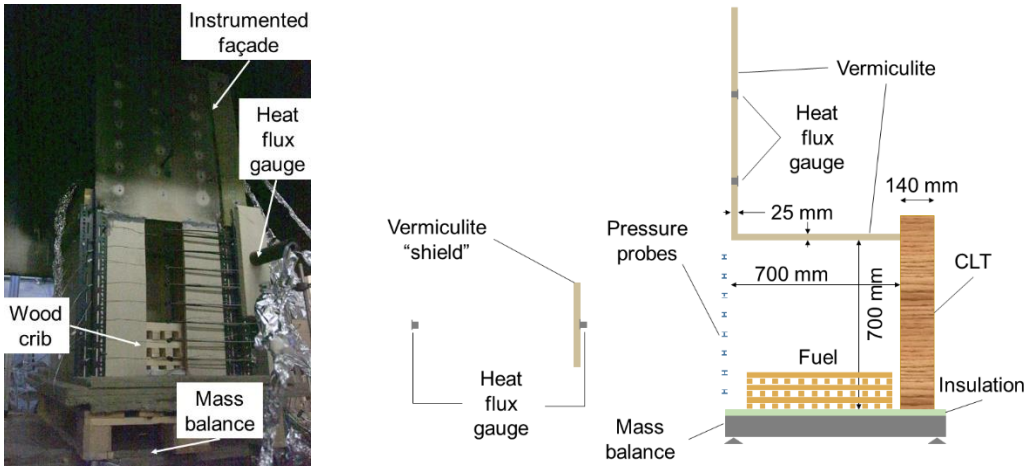

Figure 3.3. (a) The experimental setup with annotations for the equipment used. (b) Indicative compartment and instrumentation geometry.

3.3.1.2 Configurations

Four configurations of the compartment box were examined, with a repeat for each, to compare the repeatability for each configuration. The configurations were:

- no exposed CLT (i.e. completely inert compartment);
- exposed CLT back wall;
- exposed CLT ceiling;
- and exposed CLT back wall and ceiling.

3.3.1.3 Materials

The compartment was constructed using non-combustible and combustible linings. Where the former was applicable, 25 mm thick vermiculite boards were used (see Table 3.1); where the latter were applicable, CLT panels of 700x800 mm in size and 140 mm thickness (the outer lamella thickness was 34 mm). The compartment was supported using a pinned steel-profile external frame. Wood screws were used to connect the CLT slabs to the steel profiles (or other CLT elements, where applicable). The compartment's joints, inner and outer, were sealed with fire cement Mapei Mapeflex Firestop 1200˚C.

Table 3.1. Vermiculite board properties [93].

Thermal conductivity [W/(m*K)]		Density [kg/m^3]	Specific heat [kJ/(kg*K)]
200°C	0.18		
400°C	0.20	700-900	1.15
600°C	0.21		

3.3.1.4 Fuel load and heating source

The movable compartment fuel load was a six-layer wooden crib, of stick thickness 38 mm; the sticks had a square section and were spaced equally; the spacing was 38 mm; the wood crib was located at the centre of the compartment floor, occupying an area of 600x600 mm^2. Based on an assumed heat of combustion of 17.5 MJ/kg for timber, this gave a total fuel load of 315 MJ, or dividing by the 0.49 m^2 compartment floor area 643 MJ/m^2. Along with the CLT panels, the wood crib sticks were conditioned at 20°C and 50% relative humidity prior to experimentation.

3.3.1.5 Instrumentation

A façade was located above the compartment, on the same plane as the opening as shown in Figure 3.4. This was constructed from a 25 mm thick vermiculite board.

The following measurements were made:

- Mass loss (m_f) of the wood crib (and the timber linings where present) was measured by placing the entire compartment assembly on a mass balance.
- Mass flow rates of gases entering (air) and exiting (combustion products and unburnt fuel) the compartment were calculated using velocity data from bi-directional pressure probes [94]; the probe array was placed on the centreline of the opening, as shown in Figure 3.4 – with some variations between experiments to ensure improved data acquisition.
- The heat flux ($\dot{q}''$) on the façade above the compartment was measured using water-cooled Schmidt-Boelter heat flux gauges (HFGs) – these were placed at 240 and 600 mm above the top of the opening.
- An array of 21 thin skin calorimeters (TSCs) was installed on the façade, in addition to the HFGs, to allow calculation of the heat flux onto the façade. TSCs were arranged in three columns; the central column was aligned with the centreline of the opening; the additional two columns were placed at 225 mm at either side of the central column. Each TSC was co-located with a 1 mm diameter K-type inconel sheathed thermocouple to measure the gas phase temperature, as shown in Figure 3.4 (a).
- The heat flux ($\dot{q}''$) opposite the compartment was measured using HFGs – these were placed at 650 and 1300 mm from the compartment opening.
- Total convective heat release rate ($\dot{Q}$) was estimated using a furniture calorimeter; the method used was oxygen consumption calorimetry, due to the measurements of O_2, CO_2, CO provided by the furniture calorimeter.
- Video camera recorders for relative flame shape and size.
- A vermiculite “shield” was used to block the opening radiation to the gauge at 1300 mm, as shown in Figure 3.4 (b). The intent of this configuration was to distinguish the fraction of radiation originating from

the compartment's interior through the opening, and the fraction of radiation associated to the plume/external façade.

Measurement readings were made at 1 Hz for all instrumentation used.

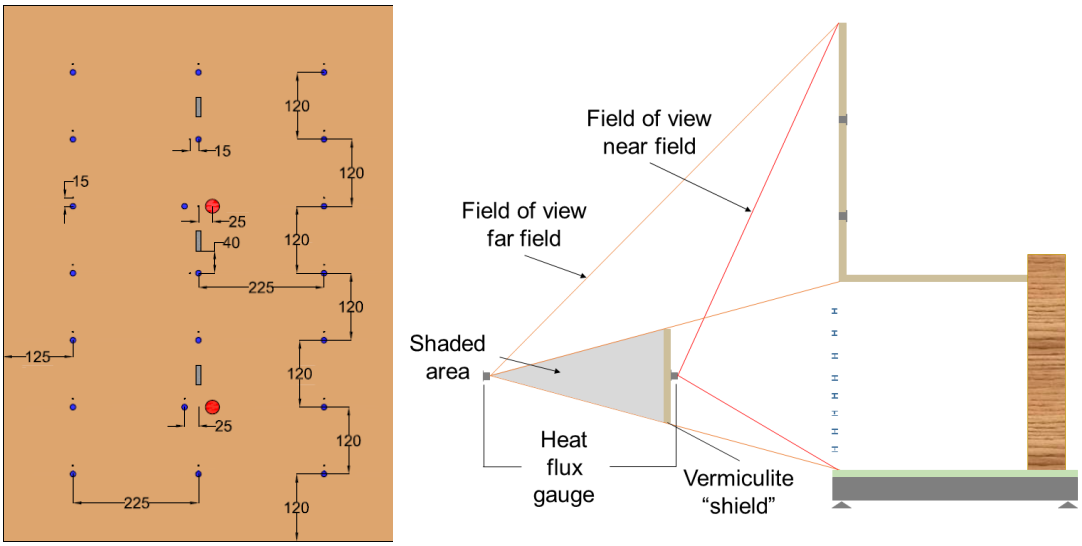

(a) (b)

Figure 3.4. (a) Pseudo-façade instrumentation: array of TSCs (blue circles) collocated with thermocouples (black dots); HFGs (red circles) were positioned alongside the TSCs for comparison purposes; pressure probes (gray rectangles) measured vertical gases pressure changes. (b) Field of view of the heat flux gauges opposite the compartment.

Heat flux gauges and thin skin calorimeters were used to quantify the incident heat flux on the façade above the burning compartment. At this stage, a brief explanation of the two different options to measure heat flux is given to establish the validity of choice of each.

3.3.1.5.1 The Heat Flux Gauge

Heat flux gauges (or heat flux meters) are instruments developed to register incident heat flux on their surface. A first approach to the instrument's design was presented by Gardon back in 1953 [95]. The gauge assembly (depicted in Figure 3.5) consists of:

- a thin constantan foil plate; the surface facing the thermal radiation is painted black, for maximum absorptivity;

- a block of copper attached to the sides of the constantan foil disc;
- a thin copper wire attached to the back face of the constantan disc;
- a second thin copper wire attached to the block of copper;
- a tube of water connected to the block of copper.

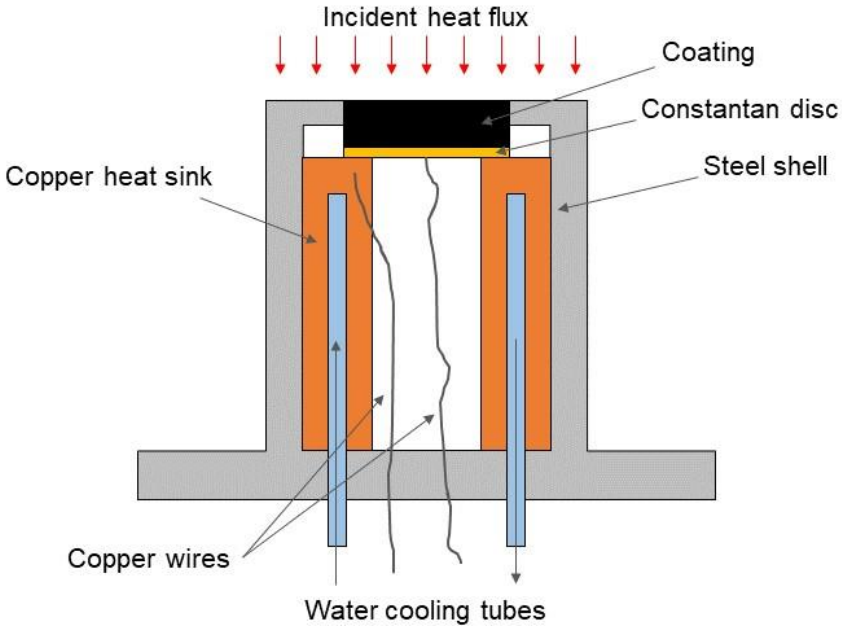

Figure 3.5. Sketch of a heat flux gauge.

The block of copper is constantly being water-cooled, i.e. the boundary temperature is constant. The circumference of the disc attached to the copper block (the "cold" boundary) is in a thermal quasi-steady state, due to water-cooling; the boundary of the disc exposed to thermal radiation (the "hot" boundary, which is represented by the middle part of the disc) is sensitive to changes. The incident heat flux on the disc changes the resistance of the disc; the recorded voltage change is related to the incident heat flux on the disc; the manufacturer of the gauge provides this recorded relationship of voltage to incident heat flux (which is a linear one); the higher the available heat flux range, the lower the resolution of the measurement.

Since 1953 of course, these instruments have been improved; in the case of fire safety engineering, the response of a gauge can vary, to better address

the needs of the measurement (from low measurements, in the order of 5 kW/m^2, to high heat fluxes, up to 200 kW/m^2) [96].

Although the heat flux gauge is an instrument of great accuracy, it is worth mentioning that some of the materials comprising the gauge are susceptible to extreme conditions. The coating of the disc can be damaged, leading to uncertainties of the absorbed radiation from the surface – and in this way the back-calculated imposed heat flux. Damage of the water-cooling system or improper cooling of the instrument leads to uncertainty of the boundary conditions (i.e. the "cold" boundary), since temperature can now vary, leading to a more significant uncertainty of the conductivity, and as a result, of the incident heat flux at the disc.

3.3.1.5.2 The Thin Skin Calorimeter

A detailed description of the thin skin calorimeter (TSC) was presented in the publication of Bartlett et al. [97]. However, to aid the reader's understanding of the merits/limitations and the energy balance of the instrument, a brief description in the current document is considered appropriate.

The TSC serves as a low-cost alternative to the Schmidt-Boelter or Gardon heat flux gauge mentioned previously [98]. Material procurement and manufacturing costs are relatively low; this means that more sensors can be utilised in the instrumentation of the façade, leading to higher data resolution.

Thin skin calorimeters in this project consisted of three parts:

- an insulation material. In the current study, this material was the vermiculite board of the façade;
- a metal disc. Inconel 600 metal was used in this experimental programme;
- type K thermocouple wires.

The thermocouple wires were welded separately at the surface of the disc, with a small gap in between. Laschutza showed in his thesis that a separation of the wires yielded more accurate results [99]. It was for this reason that the

thermocouple was not welded on the back of the disc; rather, the whole surface of the thin Inconel disc was used as the thermocouple "bead".

The energy balance of the TSC is shown in Figure 3.6. In equation form it is translated as:

$$\dot{q}''_{inc} = \dot{q}''_{st} + \dot{q}''_{cond} + \dot{q}''_{conv} + \dot{q}''_{rad} \quad (19)$$

where $\dot{q}''_{inc}$ is the incident heat flux on the TSC, $\dot{q}''_{st}$ is the stored energy in the Inconel disc, $\dot{q}''_{cond}$ are the conductive losses to the vermiculite insulation, $\dot{q}''_{conv}$ is the convective exchange term of the disc to the surrounding air, and $\dot{q}''_{rad}$ are the radiant losses of the disc to the surroundings.

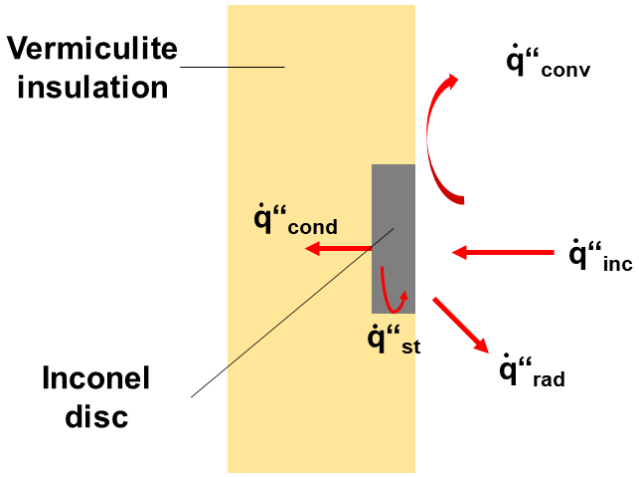

Figure 3.6. The energy balance of the thin skin calorimeter (adapted from the drawing of Hidalgo et al. [98])

As the calculation of the conductive losses to the vermiculite are not easy to quantify, Hidalgo et al. introduced the concept of a correction factor C [98]. This factor is a function of the temperature of the Inconel disc; the function can be calculated through the calibration process, as was presented by Hidalgo and co-workers [98].

Substituting each of the terms on the right-hand side, the formulation of the energy balance is the one presented below (from Bartlett et al. [97]).

$$\dot{q}''_{inc} = \frac{1}{\alpha_{disc}(1-C)}\left[\gamma \frac{m_d}{S_d} c_p \frac{dT_d}{dt} + h_c(T_d - T_{air}) + \varepsilon_{TSC}\sigma T_d^4\right] \quad (20)$$

where α_{disc} is the TSC absorptivity [-]; C is an experimentally obtained calibration factor accounting for conductive losses from the back of the disc [m^{-2}]; γ is a transient compensation factor [-]; m_d and S_d are the mass [kg] and surface area of the TSC [m^2] respectively; c_p is the specific heat capacity of the TSC [J/K/kg]; $\frac{dT_d}{dt}$ is the temperature change of the disc over time [K/s]; ε_{TSC} is the emissivity of the TSC [-]; σ is the Stefan-Boltzmann constant [W/m^2/K^4]; T_d and T_{air} are the temperatures of the TSC and air respectively [K]; and h_c is the convective heat transfer coefficient on the surface of the TSC [W/m^2/K].

The calibration factor function C used was:

$$C = -4.1723 \cdot 10^{-4} \cdot T_{TSC} + 0.5098 \quad (21)$$

where T_{TSC} is temperature of the TSC [°C]. This calibration factor function accurately predicts the incident heat flux within the range of 5 and 40 kW/m^2; the validation of results came from the comparison of the acquired incident heat flux measured by a heat flux gauge and a TSC. Material values used in the analysis process were presented in Table 3.2.

Table 3.2. Values used for the TSC analysis (from [97]).

Parameter	Value	Source
α_{disc}	0.8	Laschutza [99]
γ	0.8	Hidalgo et al. [98]
m_d/S_d	5.929 [kg/m^2]	Measured
c_p	404.76 + 0.4154T - 0.002T^2 [kJ/kg·K]	Inconel data sheet [100]
ε_{TSC}	0.8	Laschutza [99]

In order to provide a comparison of the TSC and a water-cooled heat flux gauge during a real fire scenario, both sensors were mounted next to each other at two different heights. The heat flux gauge is a sensor primarily used for radiant heat transfer measurements. The presence of convective phenomena could have been a source of deviation from the irradiance readings. Nevertheless, as it was shown by Bartlett et al. the convective component of the TSC's energy balance was significantly lower compared to the radiative component [97]. A direct comparison between the two heat flux measuring tools is illustrated in Figure 3.7.

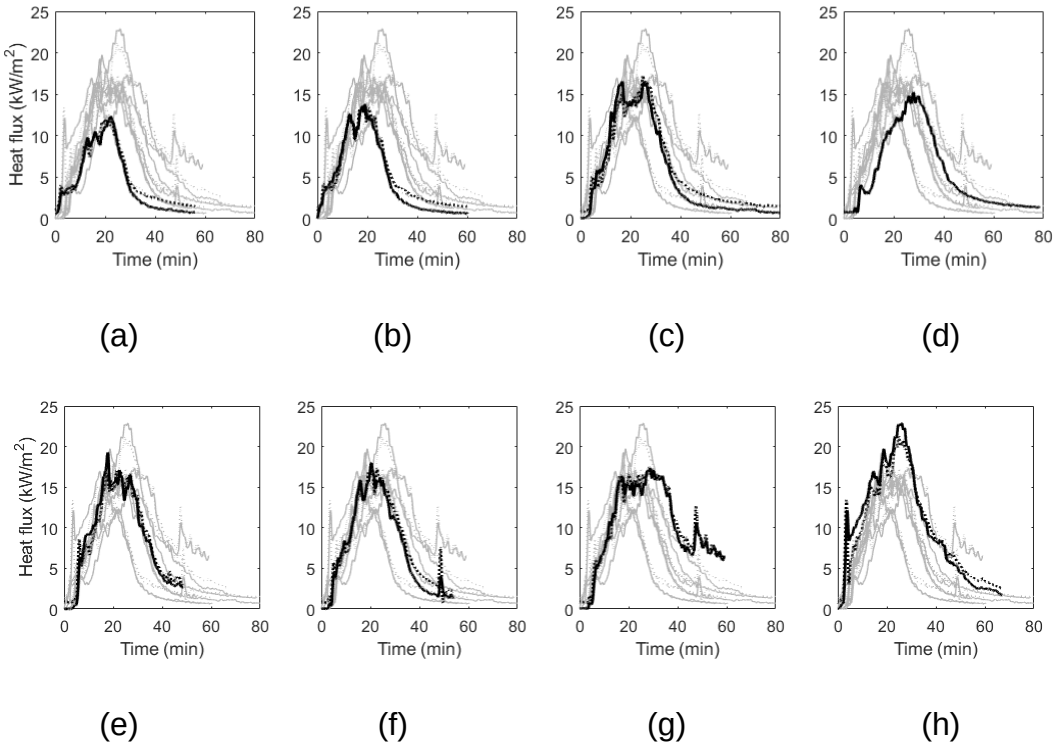

Figure 3.7. Average deviation of HFG (solid line) with co-located TSC (dotted line). (a-b) No CLT; (c-d) CLT back wall; (e-f) CLT ceiling; (g-h) CLT wall and ceiling.

3.3.1.6 Instrumentation errors

Each measurement made has inherent errors associated with the pieces of equipment used to acquire the measurement.

- The mass loss rate was calculated using data from a mass balance of ±2 g accuracy.
- The gas flow through the opening was estimated using pressure data at various heights in the centerline of the opening; the pressure transducers used have an accuracy of ±0.25 Pa; the pressure reading was converted to velocity using the Bernoulli equation.
- The heat release rate measurements have errors regarding the gas analyser accuracy limitations, and the calculation method used. The estimates for error from a furniture calorimeter can vary, from ± 7%, ±12% [101], and up to ±16% [102], depending on the literature source. The calorimeter was calibrated prior to each test, to eliminate uncertainties associated with the calibration procedure.
- The videos recorded were not calibrated (for instance with a checkerboard of known square size). For this reason, as other objects of known dimensions were used as a proxy for calibration, the resulting measurements served more as a qualitative comparison.
- The HFGs used have a sensitivity of ±0.008 mV/(kW/m^2).
- The TSCs used in this programme provided accurate readings for a range of heat fluxes of 5-40 kW/m^2; the mean error in this range was 0.36 kW/m^2 (in comparison to a heat flux gauge as shown in Figure 3.7).

3.3.2 **The propane burner experiments – Phase 2 and Phase 3**

While the timber cribs served the objective of Phase 1, the presence of the cribs affected the mass flow measurements at the opening; the heat release was also dependent on thermal feedback from the compartment and heat losses from the opening. For these reasons a more reliable (and controllable) fuel source that was not heat-feedback dependent was introduced – the propane burner. Designed after the propane burner used in Majdalani's thesis [85], a steady state heat source was established (Figure 3.8).

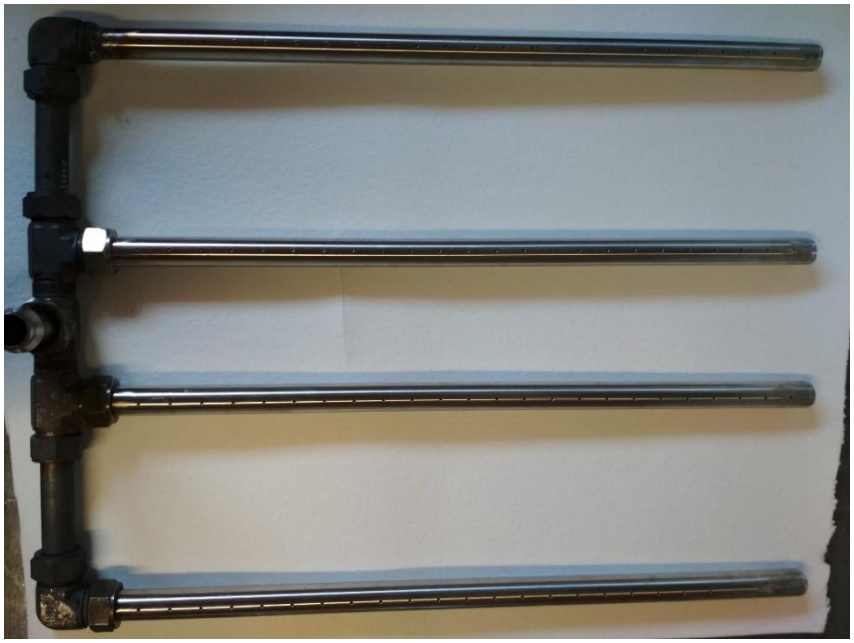

Figure 3.8. The propane burner used in Phase 2 and 3.

In the commissioning phase of the new system a maximum period of burning was established; this was the product of trial-and-error test runs of the propane burner. Temperature measurements at the opening demonstrate this point in Figure 3.9.

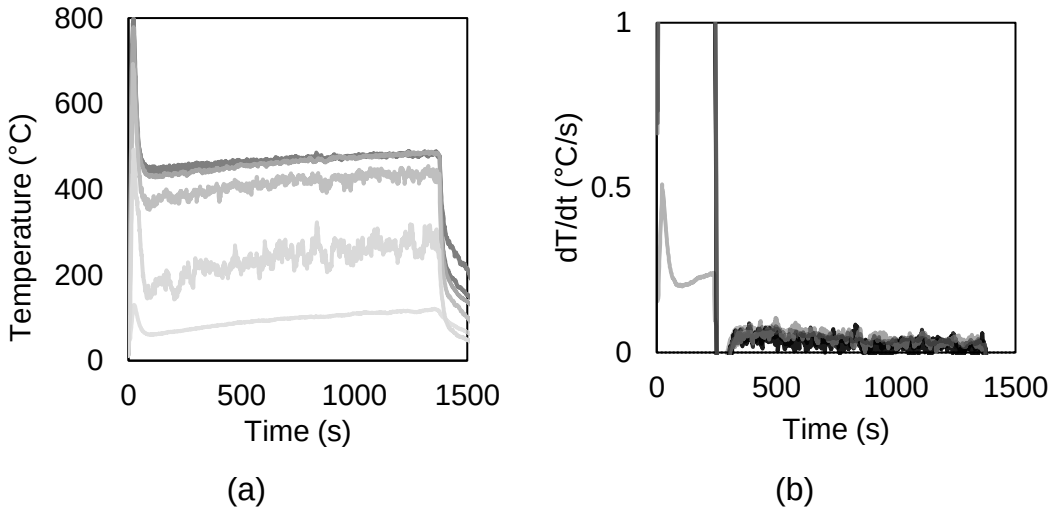

Figure 3.9. (a) Temperatures at the opening over time; (b) Temperature derivative over time. Temperature values approach a steady value after 1000 seconds from ignition in this experiment and derivative approaches near-zero value.

The parameters affecting the decision were: (1) necessary time to achieve quasi-steady state conditions (i.e. measurements fluctuating slightly and the gradient appearing almost horizontal); (2) structural integrity of the burner (providing longevity for the experimental programme).

Initially, the burner was fabricated from stainless steel, but the environment in the compartment was too aggressive for a burner to be used repeatedly. The burner that was therefore used for this experimental programme was fabricated from Inconel 600, providing greater resistance to the effects of temperature during experimentation. Holes were drilled to the tubes of the burner to allow gas to flow through; these were facing the floor of the compartment, producing jets flames towards the floor which, in turn, created diffused rising flames across the floor surface. The burner was wrapped in ceramic paper to offer some protection against radiation from the internal compartment linings.

During operation, it was observed that there was a build-up of soot within the holes of the pipes. The burner was therefore regularly cleaned between experiments to ensure that the holes remained unobstructed.

3.3.2.1 Design

Upon completion of Phase 1 experiments, difficulties regarding the compartment assembly arose. Namely, the construction of the compartment was insufficiently robust, and it required reconstruction after each experimentation. For this reason, a more modular setup was created that would allow the same compartment to be used for multiple experiments (Figure 3.10). This modular design allowed changes in parts of the wall and ceiling without having to reassemble the whole compartment each time (this was of interest for Phase 3 experiments, where timber linings were re-introduced).

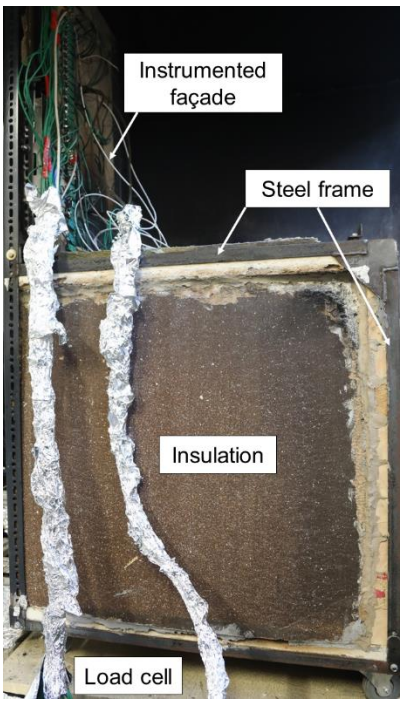

Figure 3.10. Side view of the new compartment frame and setup.

The insulation used as a compartment boundary was found to be very effective in maintaining its shape and providing a barrier between the compartment space and the outside environment. Internal dimensions were kept the same as Phase 1 for continuity and comparability of the results.

3.3.2.2 Configurations

Two repeats were run for all listed configurations, to provide a repeatability assessment. The configurations used in Phase 2 and 3 experimentations were:

- No exposed timber;
- Fully exposed timber ceiling;
- Fully exposed timber back wall;
- Half exposed timber ceiling (front – closest to the opening);
- Half exposed timber ceiling (back – closest to the wall);
- Half exposed timber back wall (top – closest to the ceiling);
- Half exposed timber back wall (bottom – closest to the floor).

3.3.2.3 Materials

A steel frame was constructed; the parts of the frame were held together by nuts and bolts. Furthermore, the boundary materials of the box were altered. The vermiculite boards, forming the compartment boundaries, appeared to be very brittle after each experiment; for this reason, they were replaced by 50 mm thick Superwool HT boards, cut to size. The insulation boards allowed multiple experiments to be conducted, with low maintenance needs. The inert compartment is shown in Figure 3.11. The façade from Phase 1 was used in Phases 2 and 3.

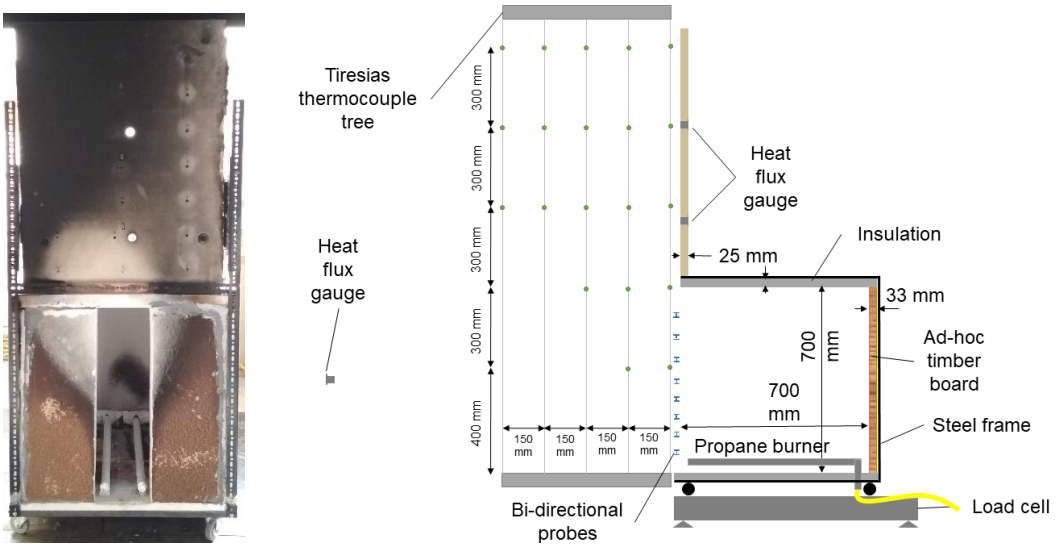

(a) (b)

Figure 3.11. (a) Compartment box – non-reacting insulation linings on a steel frame. Propane burner wrapped with ceramic paper at the bottom of the compartment. (b) Sketch of the compartment and instrumentation layout.

CLT panels were also replaced by ad-hoc panels of the same dimensions (shown in Figure 3.12) of pine boards (33 mm thick) screwed into a plywood board (9 mm thick); this allowed easy replacement of the boards that fitted within the steel frame. Due to the fact that experiments were performed only for steady state burning conditions, the needs for timber's thickness were satisfied by that of the ad-hoc boards. The same façade as in Phase 1 was installed on top of the steel frame.

(a) (b)

Figure 3.12. (a) Side view of the ad-hoc panel of plyboard and pine planks; (b) Front view of the ad-hoc timber panel.

3.3.2.4 Fuel load and heating source

Following the Phase 1 experiments, where wood cribs were used as a fuel source, inherent issues of this type of fuel were identified. The wood cribs affected the flow measurements at the opening, as they presented an obstacle located inside the compartment. For this reason, the fuel source was replaced with a propane burner, located at the floor of the compartment. Gas was flowing towards the floor to create a more diffused flame (compared to jets that would be a case, if the gas was ejected towards the ceiling).

As the importance of the mass loss rate was established by the Phase 1 experiments, measurements of Phase 2 and 3 experiments accounted for this need. Mass flow of propane was set to the desired levels; flow fluctuations were minimal (±0.005 g/s based on video recorded data); the propane burner, as a fuel source, led to good repeatability between experiments of the same configuration compared to the timber cribs. Where experiments included timber components, the whole compartment assembly was placed on top of a mass balance.

3.3.2.5 Instrumentation

Phase 1 experiments served the purpose of identifying key differences between inert and timber-lined compartments. Nevertheless, based on the available data, a complete external plume characterisation was not possible; either necessary data were not recorded or were recorded but would benefit from a higher accuracy data gathering. Phase 2 served that purpose.

The instrumented façade was used in Phase 2 and 3 as well, as it provided a comparison for the impact of burning in the external plume for the experiments conducted. Additionally, only one heat flux gauge was used opposite the compartment opening; this served as a general comparison of the far field radiation on the gauge.

In Section 3.3.1 video footage was used for flame shape and dimensions – however no calibration was used. In the propane experiments camera recorders were set as perpendicular to the plane of the external flaming as possible. Moreover, a checkerboard was used to provide the means of calibrating the footage and extracting higher fidelity results for flame dimensions.

Two out of the six bi-directional pressure probes used were coupled with more sensitive differential pressure transducers to provide a more accurate flow estimation. Despite the fact that flow measurements were of low accuracy, recorded values appeared to have relatively small errors, indicating a good repeatability between two experiments of the same configuration.

During the Phase 1 experiments a correlation arose of the excess fuel released from a compartment and the incident heat fluxes onto the surroundings of the compartment. This was previously supported showing a weak correlation between the two [75, p. 405]. However, in order to quantify the plume's contribution and characterise it, gas phase measurements were necessary.

3.3.2.5.1 "Tiresias" – the external thermocouple tree

An external thermocouple tree, herein referred to as *"Tiresias"*, was repurposed from a previous thesis project [103]. Modifications made to the

original thermocouple tree to aid image processing in the analysis section. *Tiresias* provided a temperature matrix for the external plume, similar to the work of Yokoi, Tang et al., and Asimakopoulou et al. [76], [104], [105]. A picture of *Tiresias* is shown in Figure 3.13 (a); the layout of the thermocouples on *Tiresias* is shown in Figure 3.13 (b) and (c). Glass fibre thermocouples of 1.4 mm diameter were made in the lab and attached to the external tree.

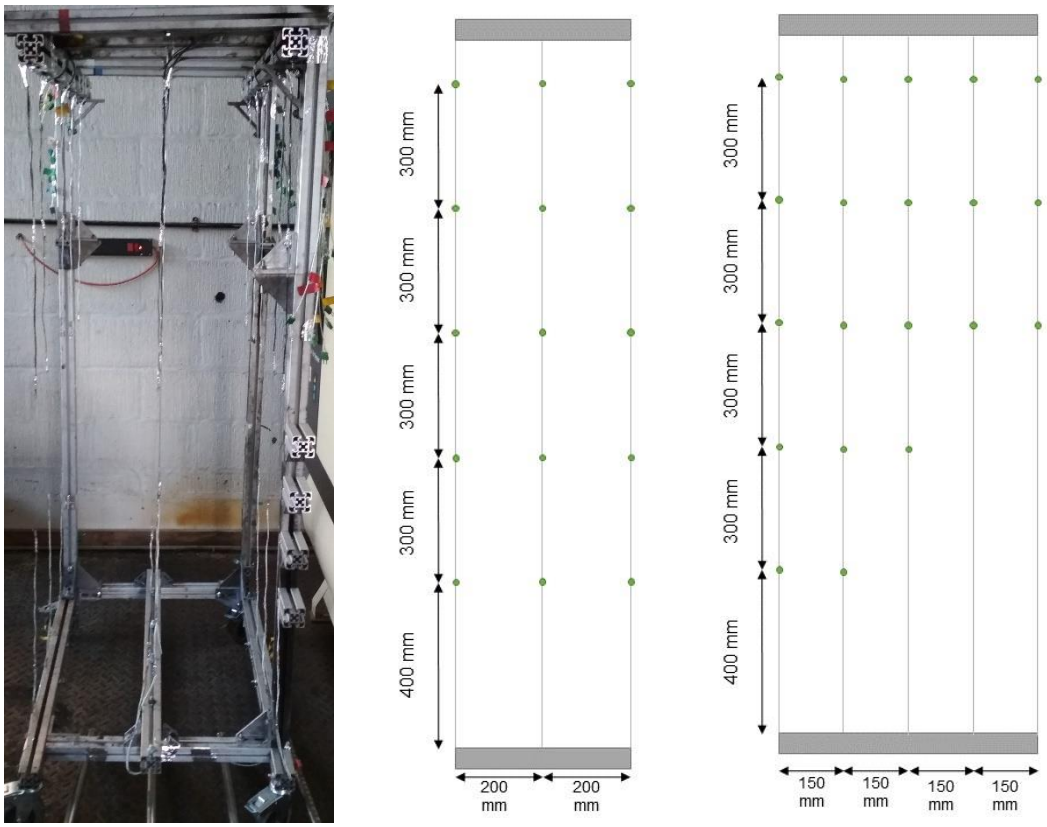

(a) (b) (c)

Figure 3.13. (a) Picture of Tiresias in its reformed shape; (b) Front view of the Tiresias; (c) Side view of Tiresias. Green dots on the sketches indicate the thermocouple location.

3.3.2.6 Instrumentation errors

The thermocouples used in Glew's thesis [103] were:

- 0.25 mm Inconel seethed industrial made thermocouples;
- 1.4 mm glass fibre, lab-made thermocouples.

A sensitivity analysis of the acquired data from Glew's thesis was performed. The deviation of the lab-made thermocouple from its thinner industrial-grade counterpart was, on average, 3% (or approximately 18 °C) [103]. This error is considered acceptable, given the advantages of manufacturing costs/replacement and robustness of the glass fibre thermocouples when exposed to naked flames.

Chapter 4 – Excess fuel

This chapter is concerned with the first experimental programme, hereafter referred to as Phase 1. This first programme of experiments was intended to identify how the presence of timber linings affected the mass loss rate of a compartment fire and whether the incident heat fluxes on the surroundings of the compartment's opening were affected by the presence of timber.

The methodology that was followed during Phase 1 is described in detail in Chapter 3. In short: a compartment box was created, and a wood crib ignited within it; different combinations of CLT and inert materials were used to line the box so that differences could be quantified; measurements were made of mass loss, heat release, flow and temperature in the opening, and heat flux opposite and above the box.

The novelty of this approach was that this phase of experiments brought together measurements of the internal fire behaviour (i.e. mass loss) with characterisation of the fire spread hazard from the external plume into a single experimental programme. Previous work on the external plume had been limited to “traditional” compartments with non-combustible linings [69], [76]; other previous work had used some combustible linings, but had not characterised the external plume [70]. Much of the previous work had also focused on extinction of timber [8], [86].

The latest available work (2019) on timber-lined boxes that recorded external fire spread characteristics only regarded visual observations and heat fluxes onto the façade [9]. Contemporaneously with the work that was undertaken for this thesis, Gorska was undertaking a doctoral dissertation on a similar topic. However, unfortunately, as this work was running almost in parallel and there were limited publications available to inform the development of the present study. Given the similarity between some of the experiments in Gorska’s thesis, and those undertaken within this work – some of the datapoints from Gorska’s thesis have been used to supplement the data gathered within this phase of experimental work.

4.1 Results

Key observations from the Phase 1 experiments are shown in Table 4.1.

Table 4.1. Significant observations for all experiments.

	No CLT		CLT back wall		CLT ceiling		CLT back wall and ceiling	
	1	2	1	2	1	2	1	2
Time to external flaming	1:31	1:23	0:49	1:24	1:10	1:38	1:33	1:35
Time to cease external flaming [a]	33:00	31:00	41:00	42:00	48:00	46:00	64:00	53:00
Peak HRR (kW)	150	169	168	176	189	182	199	195
Average HRR (kW) [b]	145	155	155	170	175	175	185	185
Peak heat flux near field (opposite opening)	12.4	13.3	14.7	12.4	14.5	13.0	12.7	11.9
Peak heat flux at 0.24 m above the opening	12.3	13.7	16.5	15.2	19.3	18.0	17.3	22.9

[a] estimated visually to the nearest minute
[b] during approximate steady state

All the experiments had similar times to initiation of external flaming. However, in the timber lined compartments the duration of external flaming was 10 to 15 minutes longer (for the case of one exposed surface) and up to 20 minutes or longer (in the case of the two exposed surfaces). The experiments with inert linings burned out when the fuel was consumed; manual extinction was applied to all experiments with exposed linings to protect the instrumentation; delamination of the first lamella occurred during one of the experiments with two exposed CLT linings and was manually extinguished while still flaming

externally; the delamination is reflected in data acquired for mass, HRR, heat fluxes, and flame heights.

The heat release rate was higher in the experiments with exposed CLT linings compared to the inert compartments, as was expected. Heat fluxes opposite the opening were comparable between the experiments, without a discernible difference (i.e. on average for each configuration there was a ±7% deviation from the baseline inert experiments); heat fluxes on the façade increased as more timber linings were included in the enclosure (on average deviations ranged from 22% to 55% from the baseline experiments).

During the experiments, the combustible contents of the compartment create different stages of the fire, starting from ignition until extinction (by decay or by manual means). These are depicted in Figure 4.1.

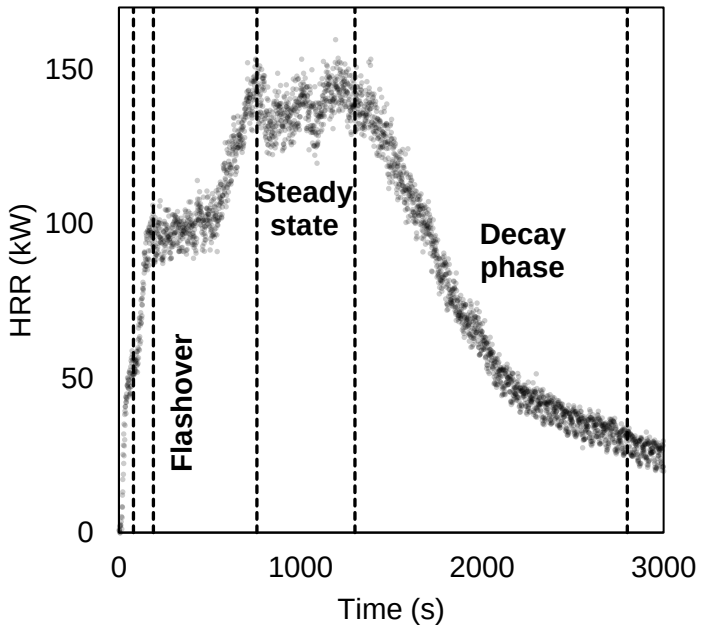

Figure 4.1. Stages of a compartment fire (inert configuration experiment).

The crib is ignited at 0 seconds; after the crib's ignition, the fire grows; following the growth period, the compartment undergoes a flashover (all combustible contents ignite). After flashover and a peak (here in HRR), the compartment is

at the fully developed stage; at this period, a quasi-steady state was considered the time during which the smoothed data plot was approximately horizontal (±5% fluctuations) for more than two minutes; this is an arbitrary decision from the author that was considered satisfactory for the present analysis. The average value of different measurements during the steady state period will be later referred to as 'average value'. After the steady state period, the movable fuel load (in this experimental programme wood cribs) is exhausted. If the rest of the combustibles also cease to burn, this leads to a decay phase, and eventually extinction (or burnout); if the combustibles continue to burn, this can lead to a feedback loop, and the fire can enter a secondary stage of steady state burning.

4.1.1 **Mass loss rate and Heat Release Rate**

Figure 4.2 (a) shows the calculated HRR, from calorimetry, over the course of the experiments; Figure 4.2 (b) shows the mass loss rate over time for all the experiments. Raw data were smoothed with a local regression function over a period of 120 seconds; data acquisition stopped close to burnout or when manual extinction was used.

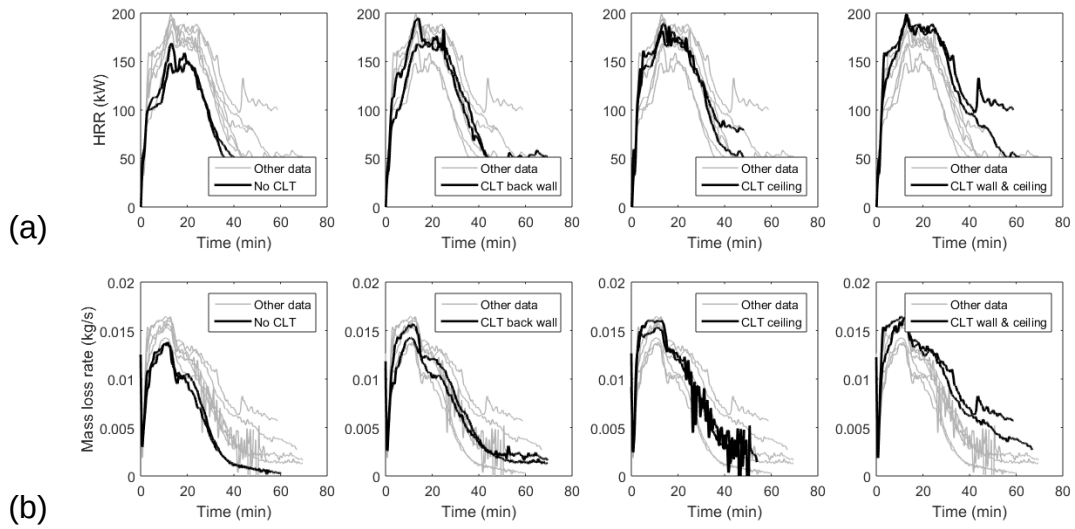

Figure 4.2. (a) Heat release rate over time for all the experimental configurations; (b) Mass loss rate over time for all the experimental configurations.

Table 4.2 and Table 4.3 present some comparison for the HRR and mass loss rate data, to reflect the repeatability between the two experiments of the same configuration.

Table 4.2. Mean and standard deviation of HRR between iterations of the same configuration.

	Average difference (kW)	Standard deviation (kW)	Average difference (%)	Standard deviation (%)
No CLT	9.5	7.8	10.4	8.51
CLT back wall	10.0	16.1	11.2	18.11
CLT ceiling	8.8	12.2	7.4	10.23
CLT back wall and ceiling	11.1	20.5	8.7	16.10

Table 4.3. Mean and standard deviation of mass loss rate between iterations of the same configuration.

	Average difference (g/s)	Standard deviation (g/s)	Average difference (%)	Standard deviation (%)
No CLT	0.2	0.6	3.6	10.8
CLT back wall	0.1	1.2	1.9	18.3
CLT ceiling	0.6	1.2	6.6	13.1
CLT back wall and ceiling	0.6	1.3	5.7	13.8

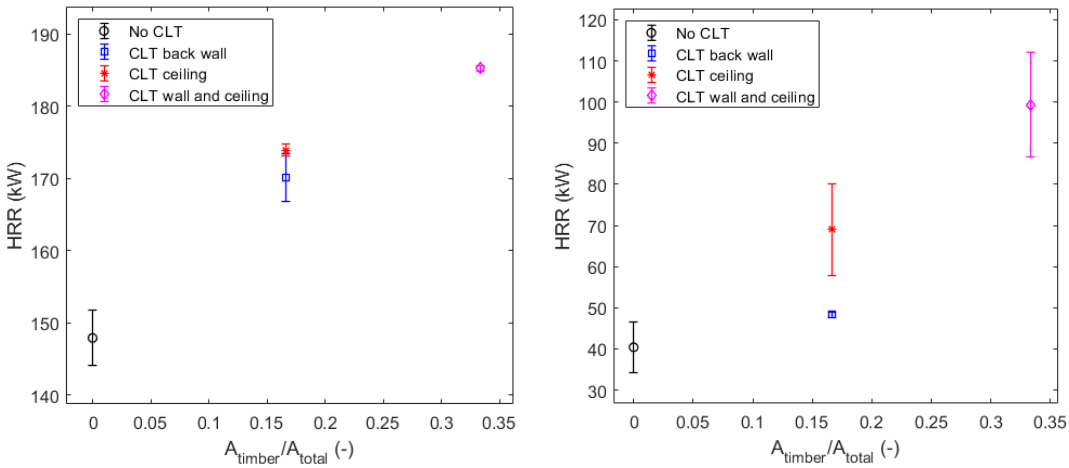

Figure 4.3. Averaged HRR at the (a) steady state and (b) decay phases for all configurations.

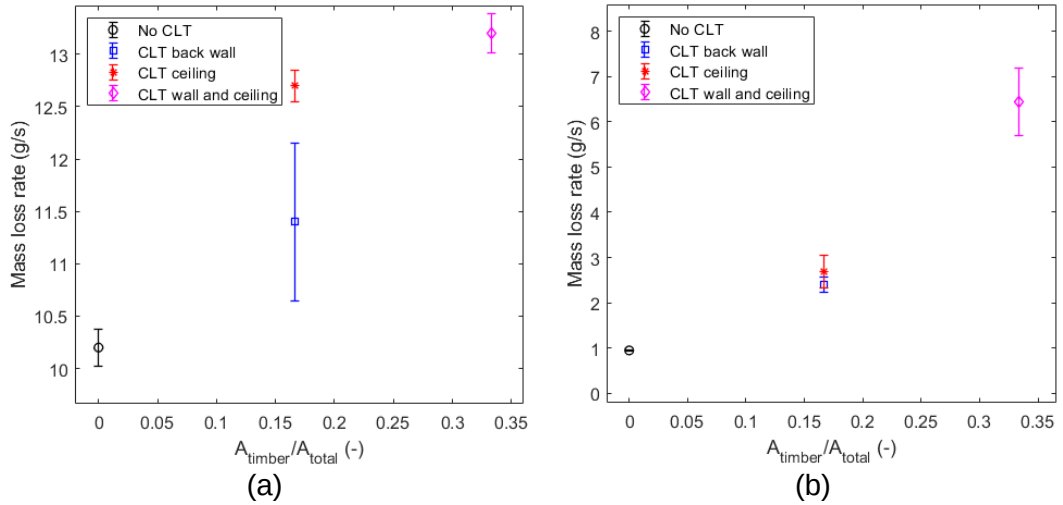

Figure 4.4. Averaged mass loss rate at the steady state and decay phases for all configurations.

It is evident from both sets of graphs that in the cases where timber was exposed, both the HRR and the mass loss rate were higher. In the case of exposed CLT wall and ceiling, HRR and mass loss rate were (unsurprisingly) higher over the rest of the configurations.

Figure 4.3 shows the average HRR for steady state and decay for all experiments. On average, there is approximately a 20% deviation in the case one exposed surface; in the case of two exposed surfaces the deviation went to 30%. In the quasi-steady state, the percentile difference is 12%, 23%, and 27% for the CLT back wall, CLT ceiling, and CLT wall and ceiling configurations respectively. However, in the decay phase these differences are approximately 30% for both cases of one exposed lining and 43% for two exposed linings.

Figure 4.4 shows mass loss rate data in a similar manner. For the mass loss rate, on average, there is approximately a 35% deviation in the case of one exposed surface, and for two exposed surfaces that was 40%. In the quasi-plateau, the percentile difference is 10%, 14%, and 17% for the exposed back wall, ceiling, and wall and ceiling configurations respectively. In the decay

phase these differences had a significant deviation, with approximately 45% for both cases of one exposed lining and 61% for two exposed linings.

4.1.2 External flame heights and incident heat fluxes

4.1.2.1 Detecting flame height

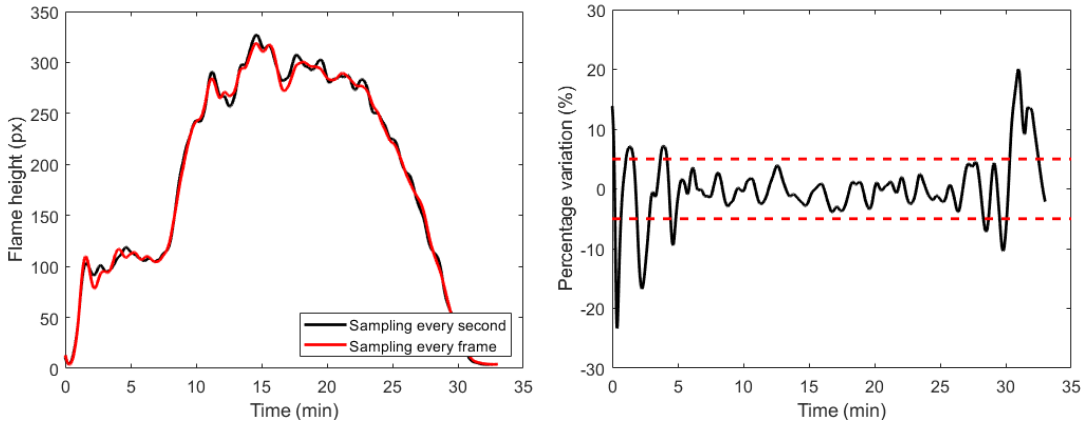

(a) (b)

Figure 4.5. (a) Smoothed data over 120 seconds for different sampling rates; (b) Percentage difference of the smoothed data between the two different sampling rates.

The video footage from all experiments was processed using a MATLAB script. Sampling rate was initially set at every frame, however, this was computationally expensive, so data was instead analysed at a rate of 1 Hz. It was found that once the data was smoothed (over 120 s, the same smoothing applied to all presented data herein) the average percentage variation between the two methods was 3%, as shown in Figure 4.5.

Once the sampling rate was established, video was processed by analysing the image. A brightness threshold was used to distinguish between flames and the rest of the elements in the image. This brightness threshold varied per experiment as where smaller flames were present more sensitivity was required; adjustments were also made in order to avoid misidentification of the reflective surfaces as flaming regions. The RGB image was transformed into binary (black and white pixels). The largest white region represented the

continuous external flaming; the pixel height was extracted from this region. The raw and engineered images are shown in Figure 4.6.

(a) (b)

Figure 4.6. (a) Raw video image; (b) Engineered binarised flaming region.

Objects with a known dimension within the field of view were used to provide a pixel-to-millimetres transformation ratio. While this approach yielded results, the potential inaccuracy was not quantifiable solely by these results, as there was no means of comparison. As it is shown in Chapter 5, where a camera calibration was done, when the camera is perpendicular to the plane of the flames, the standard deviation is approximately 0.5 mm among the different points of the image. If the camera is not perpendicular to the flames, the angle of shooting and also the lens' curvature can potentially affect the accuracy of the image.

Figure 4.7 illustrates the flame heights above the top of the opening, as were recorded using a video camera. Data gathered below the opening were disregarded in this analysis. The flame heights in each case are illustrated using a solid black line. It is observed that the experiments with exposed timber

linings had a higher flame height. During some experiments the top of the flame was obscured by the extraction hood (where it was lowered to prevent products of combustion from spilling into the lab); in these cases, data are omitted from the plot after this time.

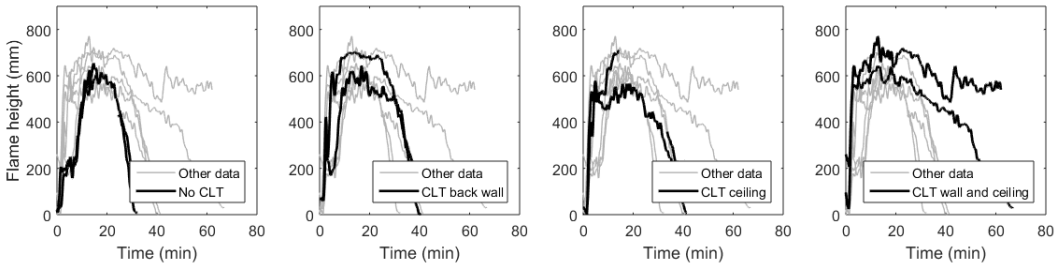

Figure 4.7. Flame heights over time for all configurations.

4.1.2.2 Incident heat fluxes from the external plume and opening

Heat fluxes measured by the heat flux gauges (HFGs) on the façade are shown in Figure 4.8. The compartments with no exposed timber had a lower incident heat flux on the façade, as heat fluxes were consistently lower than the case of one (20% and 30% for exposed back wall and ceiling respectively) or two exposed timber surfaces (on average 60% higher). In all exposed timber cases there was a longer burning time (especially in the case of the two exposed surfaces).

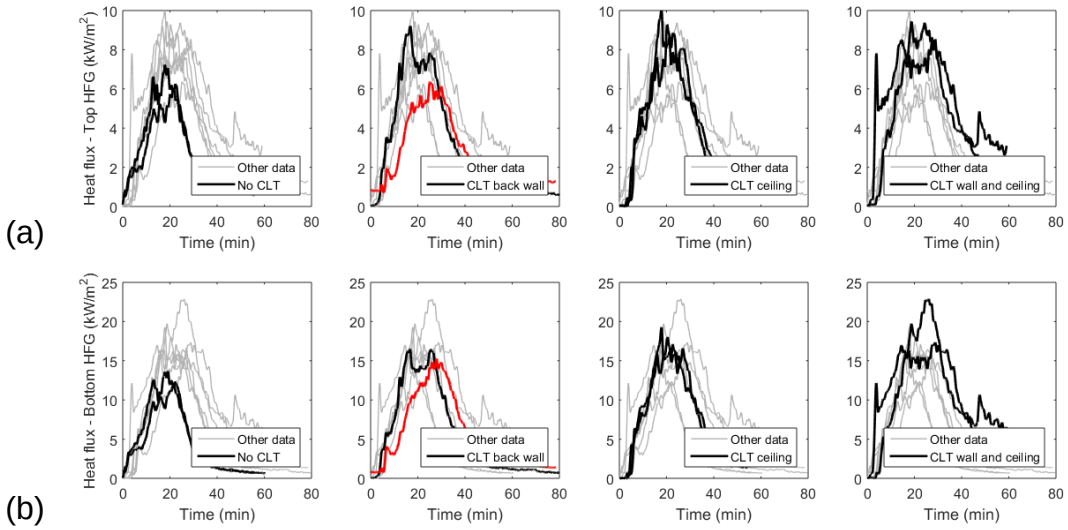

Figure 4.8. (a) Heat fluxes on the façade (1300 mm height from floor level); (b) Heat fluxes on the façade (940 mm height from floor level). Red lines indicate substituted data from the co-located TSC.

As shown in Chapter 3, thin skin calorimeters (TSCs) and HFGs have a good agreement, with a mean difference of 0.36 kW/m^2. Due to this fact, heat flux gauge data missing in one of the CLT back wall experiments, due to instrumentation failure, were substituted with the TSC data from the respective positions.

The methodology chapter demonstrated the value of TSC data and deviations noticed in comparison to a heat flux gauge. Utilising the TSCs, more measurements were possible onto the façade surface. Figure 4.9 illustrates the relationship of flame heights recorded above the top of the opening over the incident heat fluxes on the façade. The contour plot records the temporal evolution of heat fluxes over height. There is a clear correlation of the two, with an agreement of the flame height trends to the corresponding heat fluxes incident to the façade. A time lag is observed on the measured heat fluxes, as they tend to follow the flame height plots.

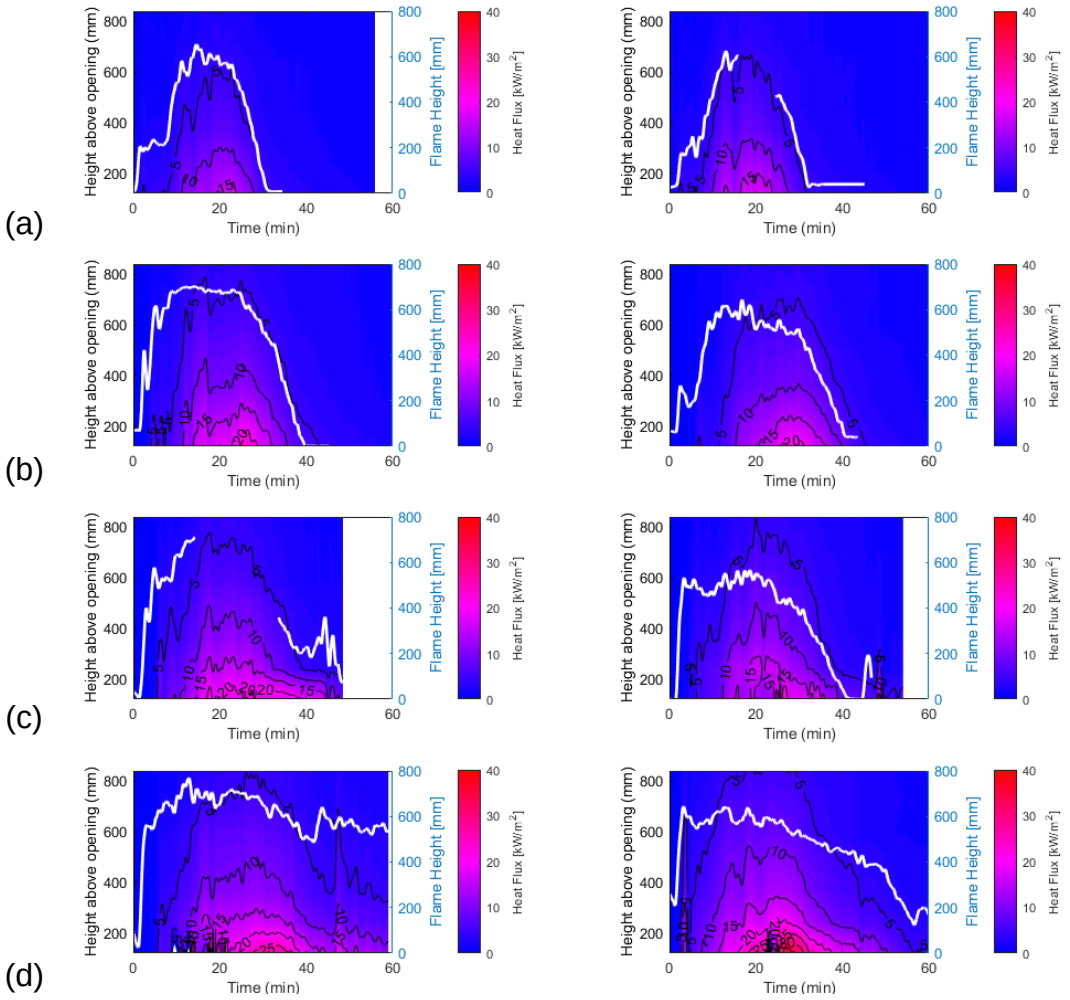

Figure 4.9. Contour map of heat fluxes over time and height: (a) No exposed CLT; (b) CLT back wall; (c) CLT ceiling; (d) CLT wall and ceiling. White lines indicate the recorded flame height over time.

Figure 4.10 illustrates the heat fluxes measured from the near-field HFG (at 650 mm distance opposite the opening) and the far-field HFG (at 1300 mm distance opposite the opening); both were at 350 mm height from floor level. In the case of one of the experiments of the simultaneously exposed back wall and ceiling the support of the near-field gauge (attached to the vermiculite shield) failed; results are reported up to that moment; data of the far-field gauge after that moment are presented in the analysis section, for comparison purposes.

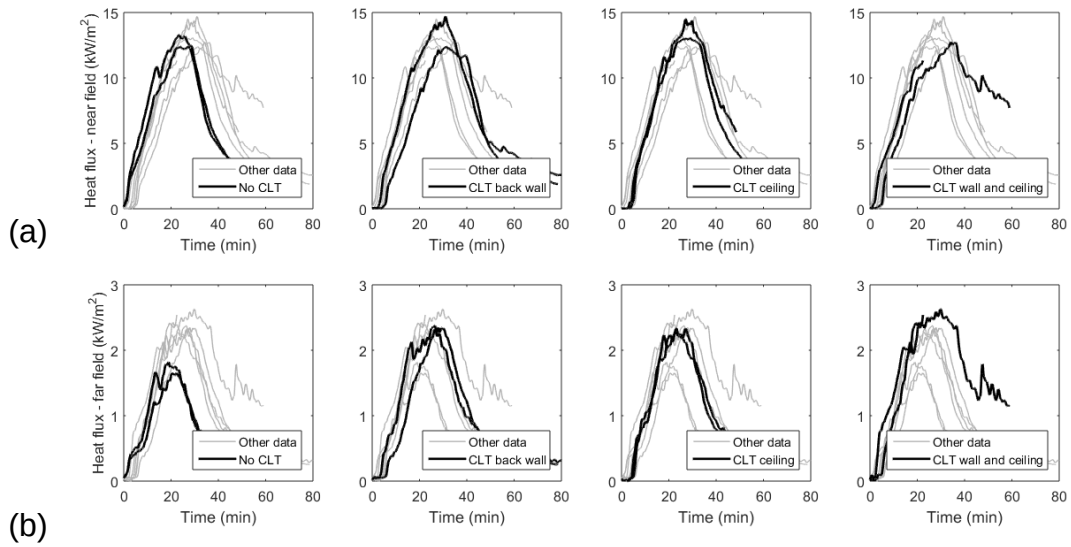

Figure 4.10. (a) Heat fluxes opposite the opening (at 650 mm distance); (b) Heat fluxes opposite the opening (at 1300 mm distance).

The near-field measurements appeared similar for both cases of exposed and non-exposed timber surfaces; at close range, the opening's radiation dominated, leading to a scenario similar to Law's suggestion for an enclosing rectangle [91]. This could be attributed to a configuration (view) factor towards the radiant heat source; this is primarily affected by the opening. The proximity and the angle of the external flaming to the HFG resulted in a configuration factor that did not favour heat transfer to the gauge in a manner that could affect the measurements significantly.

On the other hand, higher heat fluxes were recorded from the far-field HFG. This indicates that the presence of combustible linings in the compartment affected the external plume; the linings introduced more flammable gases on the exterior of the compartment, leading to higher irradiance. Additionally, it can be observed that the timber linings affected both gauges for longer, as the burning time was extended.

4.1.3 **Incident heat fluxes onto the façade and opposite**

Figure 4.11 shows the heat flux distribution on the façade, as it was measured by the TSCs, at the time when the maximum heat flux occurred. In comparison

to the peak heat fluxes measured for the inert compartment (18.8 kW/m^2), the data from the exposed timber configurations were as follows:

- for the case of exposed timber on the back wall the peak heat fluxes were 31% higher;
- the peak heat fluxes were 39% higher for the exposed ceiling configuration;
- for the two timber linings, the peak heat fluxes were 125% higher than the inert compartment configuration.

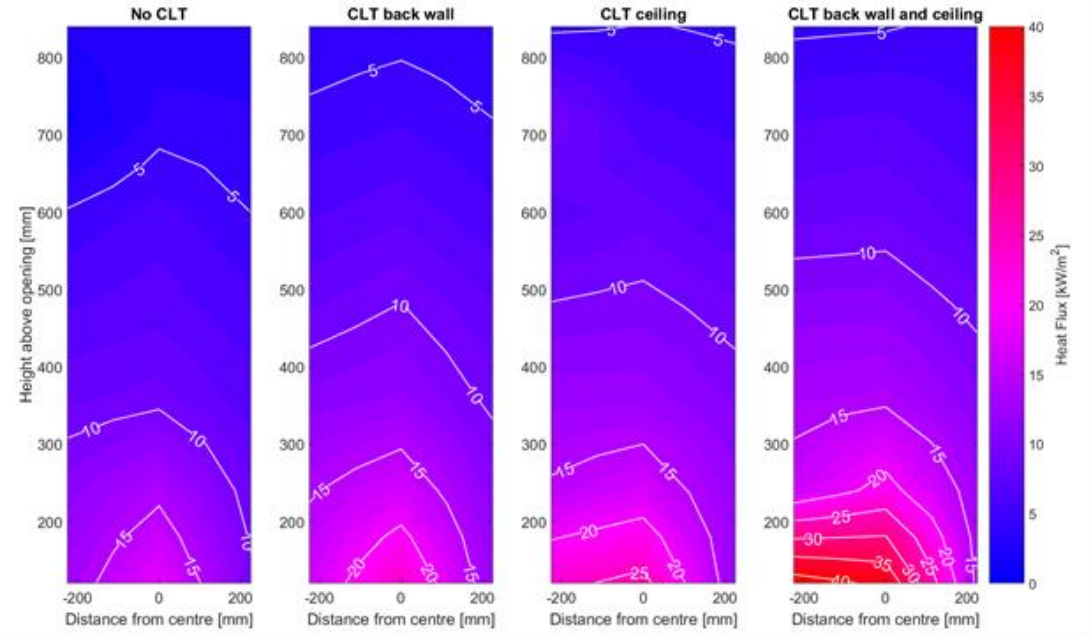

Figure 4.11. Heat flux distribution on the façade at the time of peak heat flux occurrence (figure from [97]).

For the case of the exposed CLT ceiling, the slightly higher percentage increase (compared to the exposed back wall surface) was attributed to a shorter mixing time – leading to more oxidation on the exterior. The two exposed surfaces had a higher heat flux, as all the additional fuel from the second exposed lining could only burn outside of the compartment; that was expected as the compartment was already oxygen-starved when peak values were manifested for the cases of one exposed and no exposed lining.

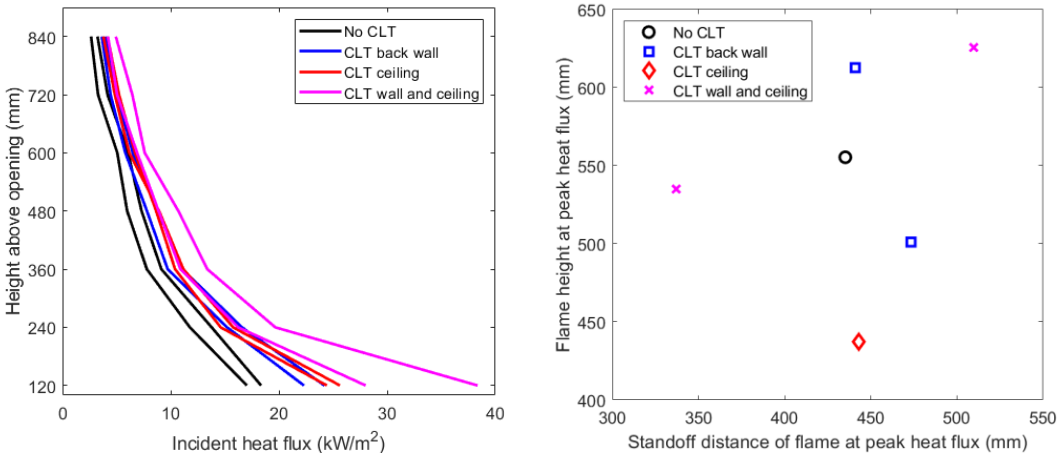

(a) (b)

Figure 4.12. (a) Heat fluxes over height at peak (from the centerline TSC data); (b) Flame standoff distance and height during peak heat flux.

As shown in Figure 4.12 (b), the external flaming coordinates have a direct effect on the incident heat fluxes on the façade. The heat fluxes mostly have the same trend between the same experimental configurations. A noticeable discrepancy is shown between the experiments with the two exposed CLT surfaces; this is explained due to the fact that the flame appeared to be closer to the façade, compared to the repeat experiment. As it was noted before in the current text, the flame dimensions serve more of a qualitative check in this work, as a camera calibration procedure was not performed. Where there were visual obstacles in the recording procedure, data are omitted; consequently, some repeats of the particular configurations are missing in Figure 4.12 (b).

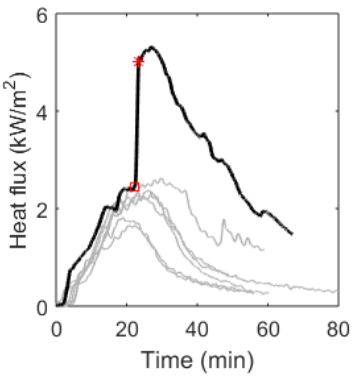

Figure 4.13. Heat flux measuments opposite the opening before and after the failure of the vermiculite shield for the two CLT surfaces configuration.

Due to failure of the vermiculite shield, a direct comparison of the heat flux from the plume and a total heat flux from both the opening and the plume was made possible. In Figure 4.13 the red square marks the heat flux before the failure (2.5 kW/m^2); the red star the heat flux almost directly after the failure (5.0 kW/m^2). This shows that, at the time of quasi-steady state burning, the incident heat flux originating from the opening could be assumed to be approximately 2.5 kW/m^2. Despite the fact that this is a single datapoint, it could provide some insight into the contribution of the opening comparatively to the plume; of course, only experimentation on this could provide further understanding on whether this was a single occurrence or a repeated observation.

4.2 Analysis of Phase 1

4.2.1 **Mass and Heat Release Rate**

The burning behaviour of the wood crib in the compartment fire is dependent on the heat feedback from the surroundings. The mass loss measurements were made for the compartment and fuel load as a whole (i.e. the movable fuel load was not weighed separately).

An assumption about the HRR can be made at steady state, in an attempt to decouple the contribution of the fuel load from the contribution of the compartment linings. At steady state, the inert compartment fire had an average HRR of 147.9 kW. Subtracting this from the steady state values of the timber configurations, generated values as shown in Figure 4.14; the data of the present work are presented alongside Gorska's data [9], as her project was strictly relevant with the current work.

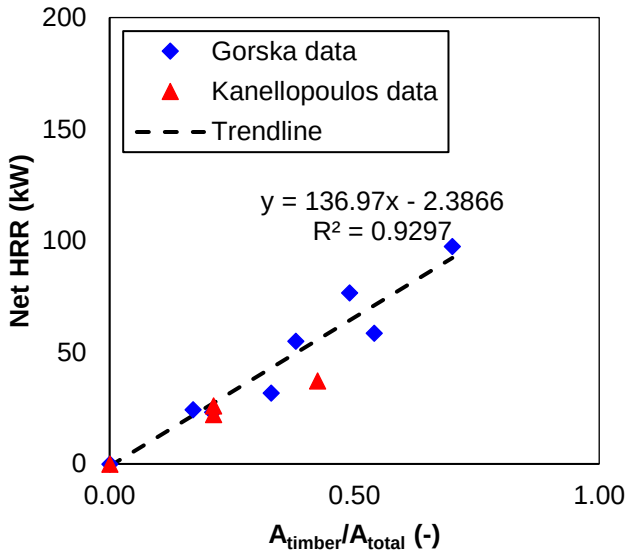

Figure 4.14. Net HRR of timber at steady state (excluding HRR of the fuel load) versus the ratio of the exposed area of timber in the compartment to the total internal area (excluding the floor and opening).

The two datasets create a strong correlation (R^2>0.9). Another way to correlate these two datasets is to compare the HRR per unit floor area (illustrated in Figure 4.15). This method yielded a strong correlation as well (R^2≈0.9), contributing to a more complete view on compartment fire dynamics as a whole (both internally and externally).

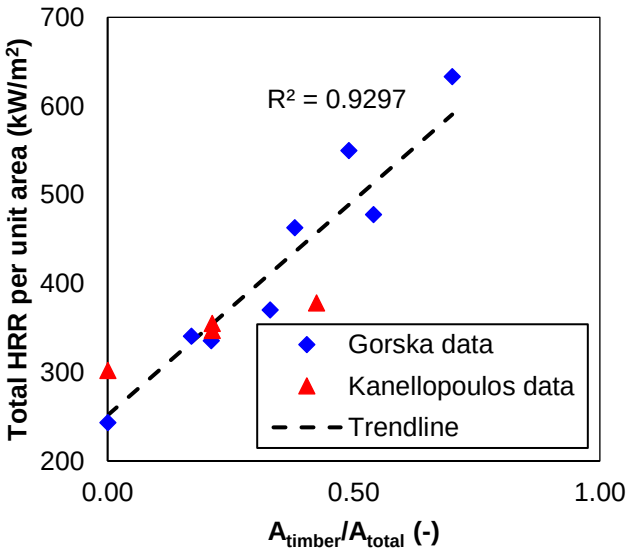

Figure 4.15. Total HRR per unit area at steady state versus the ratio of the exposed area of timber in the compartment to the total internal area (excluding the areas of floor and opening).

Notably, these two experimental campaigns used different fuel types and fuel loads; nevertheless, data hold a strong correlation, especially in the experiments where timber was exposed in the compartment space. Despite the fuel type difference, the percentage of exposed timber seems to be the variable that leads the phenomenon (once timber is exposed).

Based on indicative measurements at the compartment opening, it was possible to sample species concentrations (O_2, CO, CO_2) to estimate the internal heat release rate. These measurements are presented in Figure 4.16 for qualitative comparison only, due to their low fidelity. It seems that a more efficient combustion in the interior of the compartment can potentially be attributed to experiments with exposed timber. The indicative readings are presented to be higher for the timber configurations. Gorska suggested in her thesis an equation for the internal HRR ($\dot{Q}_{in}$), presented below.

$$\dot{Q}_{in} = 3000 \cdot 0.4 \cdot A_w \sqrt{H} \tag{22}$$

where A_w is the area of the opening [m^2]; and H is the height of the opening [m].

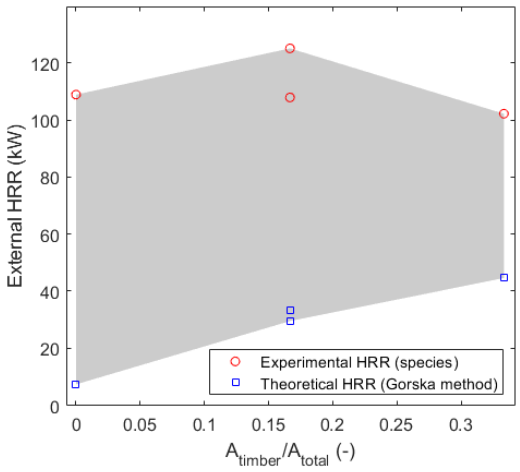

Figure 4.16. External HRR estimations for different percentages of exposed timber area (two different methods for estimation of the internal HRR).

The range between the two different methods is, admittedly, vast. In the analysis section of this chapter, there is an additional comparison of the potential global equivalence ratio values for each experimental setup.

4.2.2 **Classic compartment framework**

Since the ventilation factor remains unchanged, due to the fact that the opening was the same for all experimentations, higher temperatures were recorded for the configurations with exposed timber. Results are plotted in Figure 4.17. Law's correlation appears to underestimate the temperatures where timber was present in the compartment. The highest temperatures at the opening were recorded for experiments including exposed CLT at the back wall. This could be indicative of better mixing conditions leading to higher temperatures from a higher combustion efficiency.

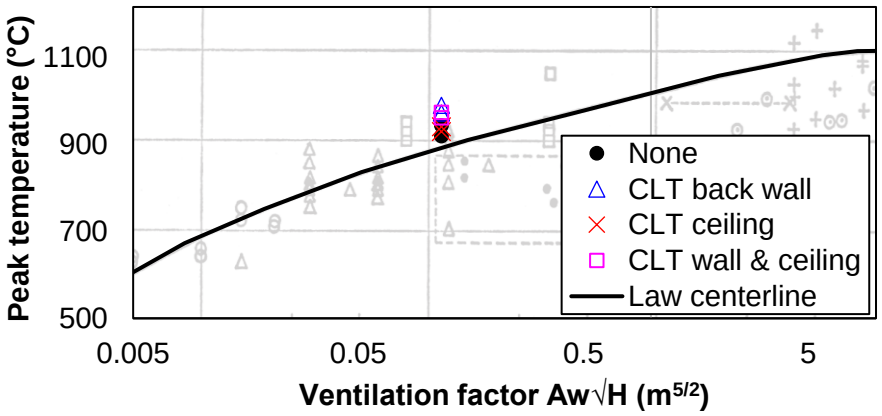

Figure 4.17. Peak temperature and ventilation factor (modified figure from [91]).

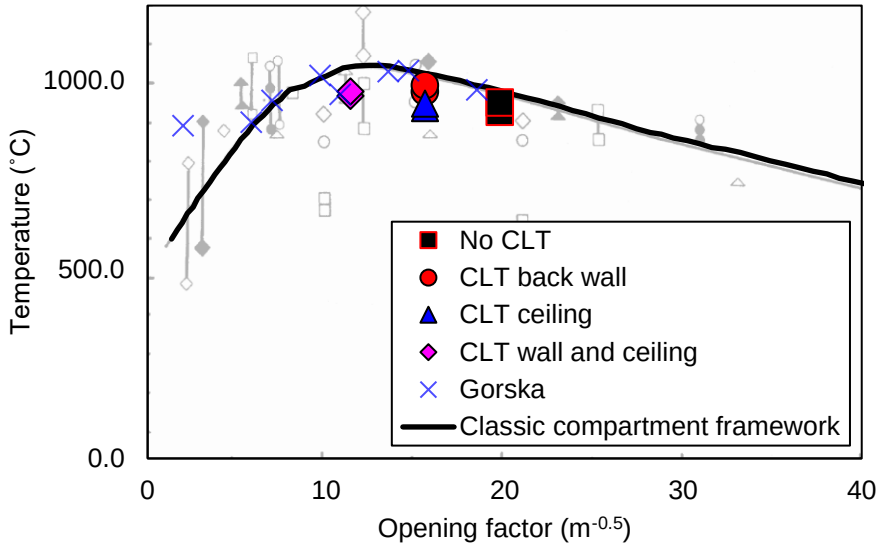

Figure 4.18. Averaged peak compartment temperature during steady state burning compared to the modified opening factor for the experimental configurations (modified plot from [69]).

Figure 4.18 illustrates the plot Thomas and Heselden presented in their work in 1972 [69]. The dataset created from the current work, as well as Gorska's data, are plotted in the figure. A modification of the opening factor, for the experiments containing CLT (combustible) surfaces was done according to Gorska's suggestion in her thesis [9]. The equation is:

$$O_{mod} = \frac{A_t - A_{CLT}}{A_w\sqrt{H}} \tag{23}$$

where A_{CLT} is the surface area of the CLT [m^2].

The timber surfaces are involved in the combustion process; heat is released from the surface, ergo there are heat gains, not losses, from the timber components of the compartment. Due to this fact, Gorska proposed the area of these surfaces is subtracted from total wall area A_t of the opening factor, resulting in lower values of O_{mod}, as more timber gets exposed. Gorska's method essentially aligns with the assumption used for the original method to

formulate the opening factor, by Thomas and Heselden. Due to this fact, it is adopted herein.

The data used in this figure are the highest temperatures recorded, at steady state, at the compartment opening (since internal temperatures were not recorded). The current dataset falls close to the proposed line by Thomas and Heselden, similar to the Gorska dataset (also plotted in Figure 4.18). This proves a good agreement with the classic compartment framework theory; using the curve Thomas and Heselden produced, with a modified opening factor appears to yield valid temperature predictions. The ventilation factor has the capability to capture only convective and radiative losses; where openings have the same shape, a differentiation is not possible. Conversely to the ventilation factor, the modified opening factor leads to better data correlation and prediction of compartment temperatures, as the conductive heat losses (not just convective and radiative) are also accounted for; due to this, observation of differences is possible.

A comparison of the HRR and mass loss rate at steady state and during the decay phase with the corresponding modified opening factor is shown in Figure 4.19. The decay phase was considered an arbitrary interval of 1200 seconds, from time t_1=1300 s to t_2=2500 s, as in all cases this was the time after the steady state. There appears to be a strong correlation of the modified opening factor with the total HRR and mass loss rate. This is expected since the burning rate is affected by the amount of heat losses of the system, and the surface area of combustible linings (turning the heat losses on these surfaces into heat gains for the control volume of the compartment).

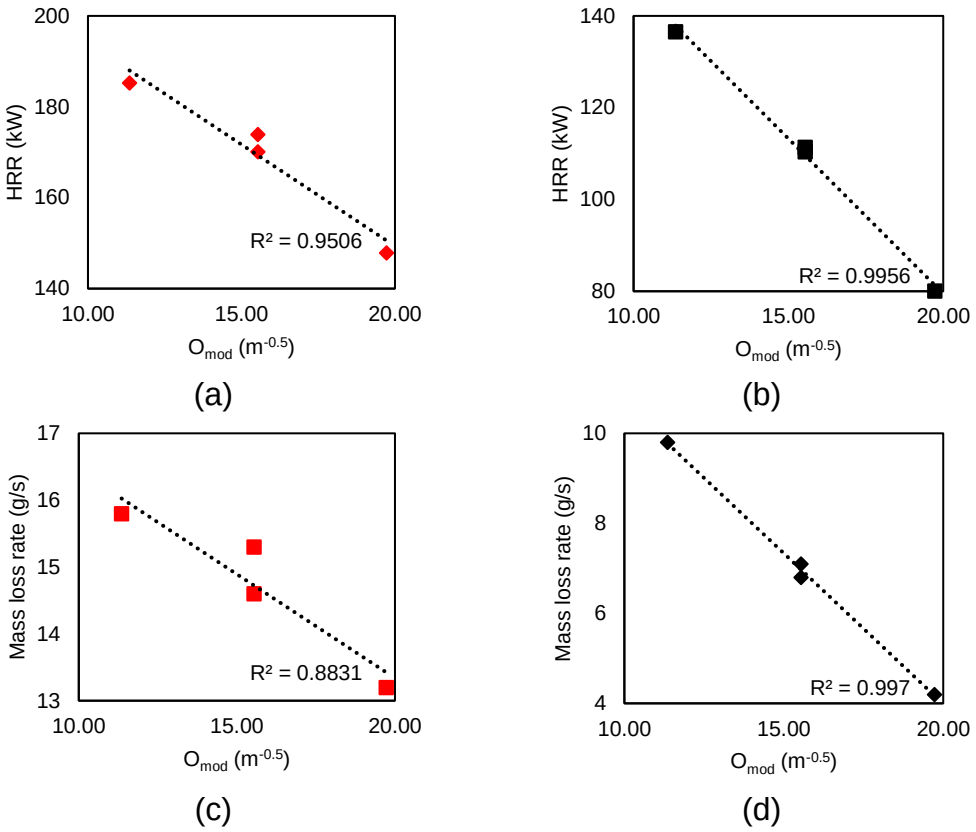

Figure 4.19. (a) HRR at steady state; (b) HRR at the decay phase; (c) Mass loss rate at steady state; (d) Mass loss rate at the decay phase. Opening factors modified using Gorska's equation.

4.2.3 **The GER and the "burning factor" in the compartment framework**

The calculation of the GER for the experiments requires measurements of the mass loss rate and mass inflow rate of fresh air into the compartment. It was found that the pressure probe data were unreliable with respect to the calculation of mass flow into the compartment. To allow calculation of the GER (from Equation 5), two different methods of estimating the mass inflow of air were used:

(a) the mass inflow rate was calculated from the formula $\dot{m}_a \approx 0.5 \cdot A\sqrt{H}$ from Kawagoe [106];

(b) a more complex approach proposed by Bartlett and Law [90] was also used (the assumptions used herein are similar to the ones Bartlett and Law made in their publication). The equation is:

$$\dot{m}_a = \frac{2.04 A_v \sqrt{H_v}}{\left[1 + \sqrt[3]{3.4\left(1 + \frac{\varphi}{r}\right)^2}\right]^{\frac{3}{2}}} \tag{24}$$

where A_v is the area of the opening [m^2]; H_v is the height of the opening [m]; φ is the global equivalence ratio [-]; r is the stoichiometric air-to-fuel ratio [-]. This is an iterative process; it was found that for the current dataset values converged after 10 iterations.

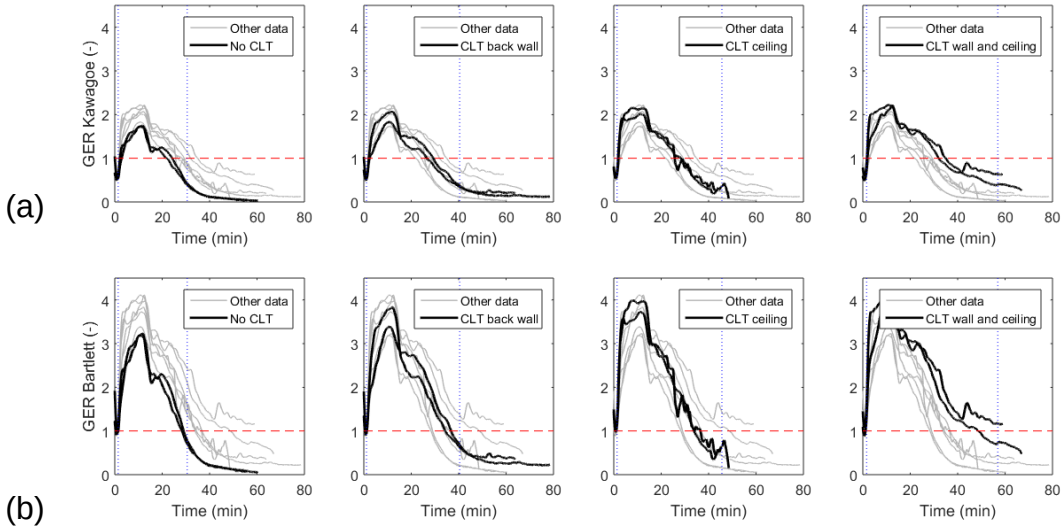

Figure 4.20. (a) Global equivalence ratio values calculated using the theoretical mass inflow rate from Kawagoe; (b) Global equivalence ratio calculated using the Bartlett method. Blue dotted lines indicate beginning and ending of visual external flaming from video data.

The results using the values of ventilation from Kawagoe are presented in Figure 4.20 (a). GER values appear to be higher for the cases of exposed CLT, therefore the potential time of burning outside the compartment was longer for

all exposed timber cases (as was also evident from the video processed data shown in Figure 4.7).

However, the results from the ventilation equation from Bartlett and Law in Figure 4.20 (b) led to data that better reflect what was observed from the video footage in terms of the times at which external flaming commenced and finished (data shown in Table 4.1). The blue dotted lines on both sets of graphs reflect the average time for onset and cessation of flaming. It appears the second method (shown in Figure 4.20 (b)) is a better predictor of the initiation/termination of external flaming. It is worth mentioning that GER values in Bartlett's method are almost twice the values of the Kawagoe method. This is primarily due to the fact that the Bartlett and Law method assumes less oxygen will become available in the compartment, leading to more external flaming.

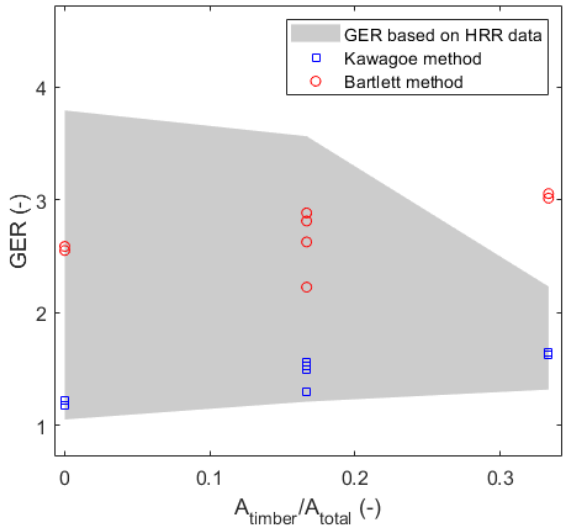

Figure 4.21. Comparison of GER values (steady state) using two methods with theoretical and experimental estimation of the ratio of total to internal HRR (grey envelope).

Both the measurements of species at the compartment opening and Gorska's suggested equation led to an estimation of the internal HRR. The ratio of total to internal HRR is the ratio of what was burnt in total to what was burnt inside the compartment; therefore, this is a ratio same as GER. This results in a

confidence interval of GER values (from measured and theoretical internal HRR) that the Kawagoe and Bartlett ventilation methods can be compared to. This comparison is illustrated in Figure 4.21.

The Kawagoe method appears to be at the lower bound of the (HRR produced) GER confidence interval. The Bartlett method is more centrally located with the range (apart from values for the two CLT surfaces configurations).

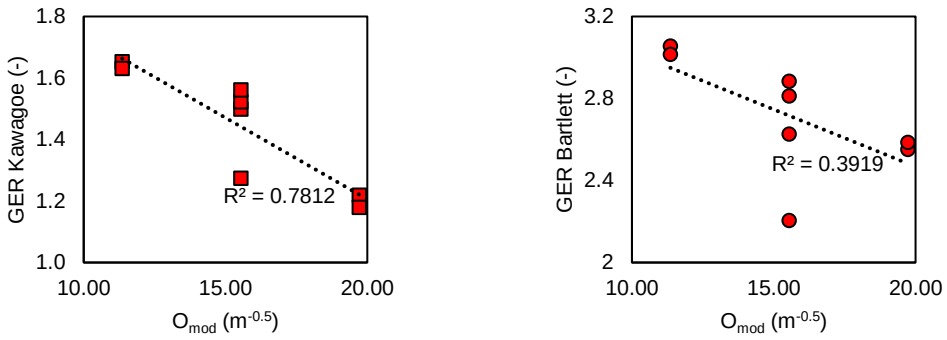

(a) (b)

Figure 4.22. GER at steady state correlated with the modified opening factor for (a) Kawagoe's ventilation method and (b) Bartlett's ventilation method.

Figure 4.22 illustrates the relationship of GER (applying the ventilation methods of Kawagoe and Bartlett) with the opening factor. The opening factor corresponds to heat losses. Since the GER is linked to the fuel production (through mass loss rate), a better correlation was expected. The data produced by the Kawagoe method appear to correlate better than the Bartlett method counterparts; despite this fact, no strong correlation was presented for both.

Bartlett and Law devised the burning factor as a method of correlating the GER to the properties of the compartment. The burning factor accounts for heat gains in a compartment fire with timber linings in comparison with the convective and radiative losses from the opening [90].

$$B = \frac{A_{CLT}}{A_w\sqrt{H}} \tag{25}$$

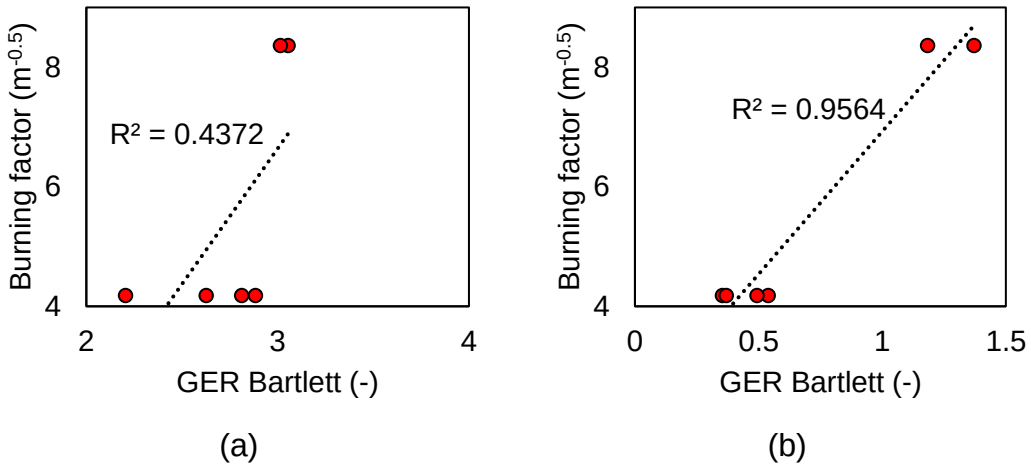

Figure 4.23. (a) GER at steady state using the Bartlett-Law burning factor; GER at the decay phase (after fuel burnout) using the Bartlett-Law burning factor.

As Bartlett and Law noted in their work, the burning factor correlates well using a linear correlation (R^2>0.9) with the GER during the decay phase; this is evident in Figure 4.23 (b) for the current dataset. As a decay phase was considered the phase when the fuel was mostly spent; this moment was arbitrarily chosen from the video data, since mass loss measurements were made of the compartment as a whole (not the fuel load separately to the compartment).

The burning factor appeared to not correlate well at the steady state period (following the peak), again supporting the unsuitability of the burning factor for such correlation; this was noted in the Bartlett and Law work [90]. This is indicative of the crib behavior dominating the overall compartment conditions.

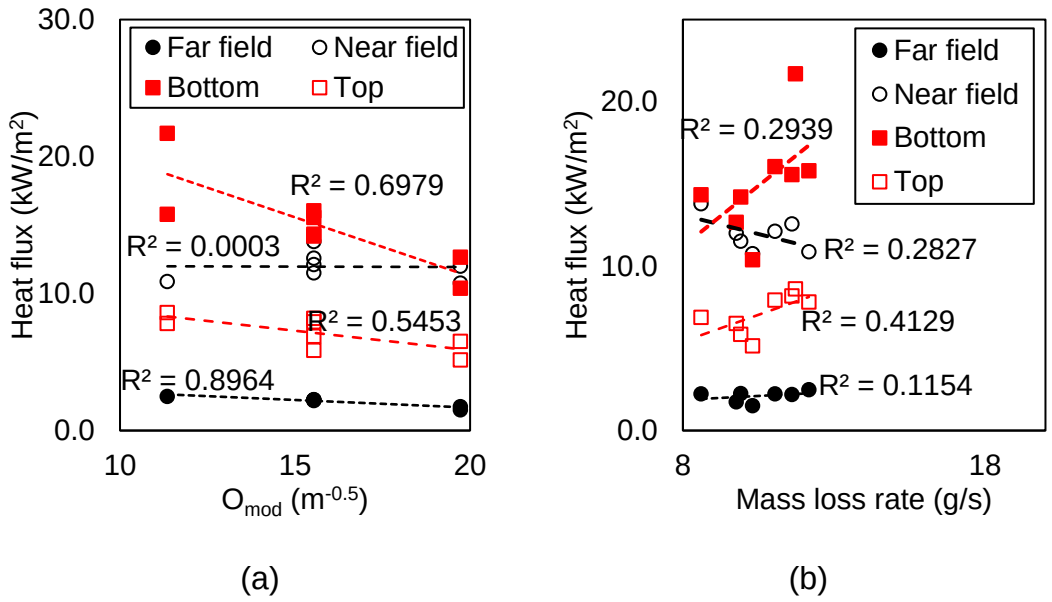

Figure 4.24. (a) Correlation of heat fluxes opposite the plume and on the façade with the modified opening factor; (b) Correlation of heat fluxes opposite the plume with the mean mass loss rate. (Opposite: near field at 650 mm; far field at 1300 mm. Façade: bottom at 940 mm; top at 1300 mm.)

A correlation of the heat fluxes from the plume, measured opposite the compartment, with the opening factor and the mass loss rate are shown in Figure 4.24. There appears to be a direct correlation of the heat fluxes from the plume (far field measurements) to the opening factor ($R^2 \approx 0.9$). This is potentially due to the fact that the far field measurements capture only the plume, excluding the opening. The modified opening factor (representing heat losses through the opening), which correlates to the mean compartment temperature, is shown here to have a relationship with far field heat fluxes. Far field heat fluxes are a product of the plume's irradiance, which is due to the plume temperature profile emitted to the heat flux gauge. The rest of the heat fluxes are not strongly related to the opening factor, potentially due to dependency on other factors as well. Notably, there appears to be practically no correlation of the opening factor to the near field measurements. This is no surprise, as it was mentioned previously that the radiation from the opening dominated the results; due to this fact, the relationship of the rest of the heat losses (conductive and convective) is not "translated" into this correlation.

On the other hand, the averaged mass loss rate does not appear to be linked to the resulting incident heat fluxes on any of the gauges. The correlations are weak (R^2<0.5), which indicate that further factors are needed to predict the heat flux distribution from the external plume.

4.3 Summary of findings

Preliminary conclusions from the Phase 1 experiments are divided in three categories: (1) compartment fire dynamics; (2) GER and the burning factor; and (3) external flaming.

4.3.1 **Compartment fire dynamics**

The heat release and mass loss rates are correlated with the ratio of exposed timber area to the total area of the compartment (excluding the floor); that is both at steady state and during the decay of the movable fuel load.

It was also observed that the exposed timber location seems to have affected the mass loss rate and the resulting total HRR. The CLT ceiling configurations presented higher values compared to the CLT back wall ones. This comes in contradiction with mean values produced from Gorska et al. [107]. However, accounting for error bars, their peak ceiling mass loss rate measurement is approximately equal to the peak back wall one. Therefore, this dataset adds to the observation of an equal (and in this case higher) mass loss rate for the CLT ceiling, compared to the CLT back wall.

It was found that the results achieved a good correlation regarding the A_{timber}/A_{total} ratio with both the net HRR (excluding the wood crib's contribution), and the HRR per unit area. When combined with data from other sources, the R^2 value was around 0.9.

4.3.2 **GER and burning factor**

The experimental data for the GER were not considered reliable as there was a large potential error associated with the data. GER was therefore calculated using two different ventilation formulae. When the Kawagoe method was used, the calculated values were at the lower boundary experimental range. The

Bartlett and Law method was more centrally located within the experimentally measured range (although some values were outside the bounds of the experimental data).

Irrespective of the different absolute values given by the various methods – each measurement showed that the GER was 12-38% higher for CLT lined compartments (depending on the number of exposed surfaces).

The burning factor devised by Bartlett and Law does not offer useful correlations for steady state with GER, as they also illustrated in their work. At the same time, the burning factor correlates well with GER in the decay phase, similar to Bartlett & Law's observations for large scale experiments.

4.3.3 **External flaming**

4.3.3.1 Façade

On average, heat fluxes on the façade were 20-30% higher for one CLT surface, compared to inert compartments; and 60% for two exposed surfaces.

Heat fluxes at the centerline of the façade strongly correlate with flame height. Heat fluxes and flame heights appear to be slightly out of phase; generally though, TSCs follow the flame height fluctuations.

At the bottom of the façade, centerline heat fluxes appear to be higher for exposed ceiling; they converged to similar values as the height above the opening increases.

4.3.3.2 Opposite

Near field measurements were approximately the same for all configurations; the opening dominated the near-field measurements, leaving no discernible contribution due to the external plume. Far-field measurements increased as more surfaces were exposed.

In this chapter the assumption of Margaret Law's work was explored (explained previously in Chapter 2) – that, if the compartment's (or opening's) temperature was known, this alone was sufficient to simulate the radiant emissions for a

compartment fire. This assumption was based on observations that external flaming did not last long and that the opening radiation was overestimated. This is not the case where timber is exposed as the plume had a longer duration and bigger dimensions compared to the plume from inert compartments.

The far-field measurements of plume radiation correlate well with the modified opening factor; none of the other heat fluxes presents the same correlation. No notable correlation exists for heat fluxes and the mass loss rate. Limitation for the instrumentation used to calculate the air inflow rate, video analysis, species measurements at the compartment opening, as well as the imposed fuel load need to be addressed.

Addressing these can aid characterisation of the plume and to, decouple effects of the fuel load on the velocity measurements, and focus the study on the understanding of the effect of exposed timber on external fire spread.

4.3.4 **Overall**

Overall the Phase 1 experiments demonstrated that there were substantial differences in GER and heat flux between compartments with inert linings and compartments with CLT linings. However, Phase 1 also demonstrated potential problems of experimental control and measurement when using timber as a fuel source. With the key magnitudes of burning rate and heat flux in a CLT lined wood crib compartment fire established – subsequent chapters will explore the plume dynamics in more detail.

This page intentionally left blank.

Chapter 5 – Creating a Baseline

5.1 Introduction

The previous chapter highlighted differences in external fire spread between “traditional” (i.e. inert) compartments and timber-lined compartments. Key differences in heat release rate, mass loss rate, heat fluxes, and flame heights were reported. The effect of timber linings in the compartment on the external plume was measured in terms of the heat flux and flame length. However, greater knowledge of the plume was required in order to gain greater physical insight about the parameters controlling the external fire spread hazard.

In order to establish the impact of timber linings on the external plume, it is firstly necessary to establish a baseline characterisation of the plume for a compartment with inert linings. The purpose of this is twofold – firstly, it will allow any differences associated with timber linings to be more easily detected. Secondly, it will allow the results from the current experimental programme to be compared against previous literature.

An experimental programme was therefore designed, with improvements and additions on the experimental system where necessary to lead to a more complete characterisation of the external plume.

The new apparatus design aimed to remove fuel-to-linings measurement dependencies. Additionally, the new fuel source would offer more control, and will not interfere with the flow measurements at the compartment opening. The fuel source was therefore switched from wood cribs to a propane burner – as described in Chapter 3. As will be described in this chapter, the propane burner also provided greater repeatability between repeats of the same experimental configuration.

A calibration of the cameras offered more reliable dimensional interpretation of the video data, thus aiding the plume spatial characterisation. Except for flame heights (and widths), the trajectory of the plume can provide additional

interpretable data to show whether or not trajectories are affected by the exposed timber inside the compartment.

The global equivalence ratio (GER) served as a crude metric for the indication for initiation of external flaming. In this experimental programme GER was used as a means to determine over- and under-ventilated conditions for the compartment, in order to examine a range of different scenarios; this aimed to identify a potential scenario for later use in the timber-lined experiments of Chapter 6.

A lack of gas phase measurements for the external plume was mentioned in the previous chapter. For this reason the *Tiresias* external thermocouple tree was employed (as fully described in the Methodology chapter). *Tiresias* allowed to have temperature readings of the plume without obscuring the direct view of the cameras to the plume.

The intent of the gas phase measurements was to allow temperature profiles such as those described in Yokoi's work to be constructed.

An iterative process was undertaken to determine the duration of the fire and the use of a single or multiple propane flow rate values. After this process, whereby the propane was gradually ramped up over the course of the experiments, it was found that more reliable data were obtained when each experiment was conducted using only single value of propane mass flow per experiment. This approach meant that after an initial period (between 10 and 15 minutes) where the compartment heated up, the compartment reached a reasonably steady state. All measurements within this steady state period oscillating around a steady value. The experiments were run for approximately 20 minutes; this time was found to be sufficient to achieve a steady state for all the measurements, through the iterative process, without damaging the equipment. The last 5 minutes of the experiment were used to extract what was considered steady state values. These values were smoothed over 120 seconds, resulting in the same smoothing as the previous experimental programme.

The flow rates were varied parametrically and set to achieve a GER (using Kawagoe's ventilation method) of 0.25, 0.50, 0.75, and 1.00 in this experimental programme.

Four propane flow rates were used. The peak flow corresponded to GER of 1.00. The rest of the flow rates were a percentage of the peak flow rate; these were as follows:

(a) 0.85 g/s (25% of peak flow rate);
(b) 1.70 g/s (50% of peak flow rate);
(c) 2.55 g/s (75% of peak flow rate);
(d) 3.40 g/s (peak flow rate).

These values aimed to ensure that any difference introduced by adding timber linings (as described in Chapter 6) would be measurable in the experiments. As a GER equal to 1.00 would ideally result in all fuel being consumed inside the compartment (which was disproved in the previous chapter), all additional fuel burning externally would be due to the presence of timber.

5.2 Results

5.2.1 **Heat release rate**

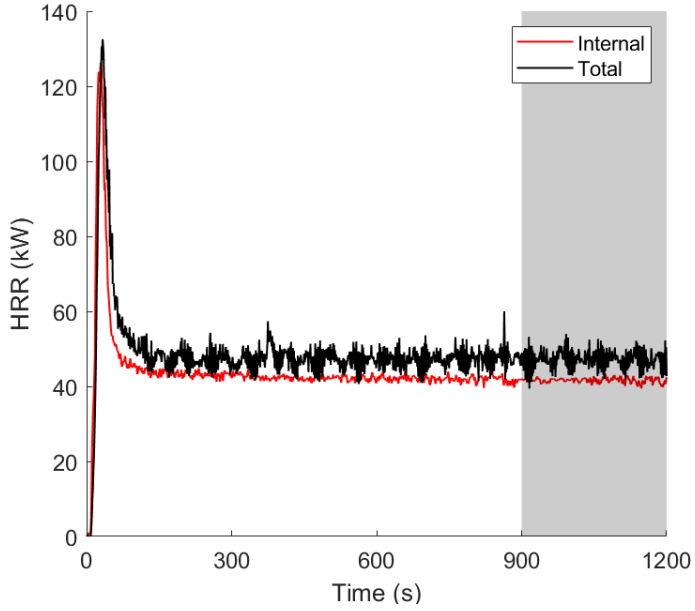

Figure 5.1. Example of internal and total HRR estimations for GER 0.25. The gray area represents the sampling interval.

Estimations of heat release rate (HRR) of both the compartment interior and the total were made. Capturing the internal HRR led to quantifying how much energy is released in the compartment interior (and as result also the exterior); this was especially useful for the timber experiments that will be described in Chapter 6. Figure 5.1 shows internal and total heat release for a GER of 0.25. As would be expected for such a low value of GER the measured values are very similar – indicating that most of the burning occurred internally. This agreement between the total heat release rate and the internal heat release rate gave confidence that the measurement technique was effective.

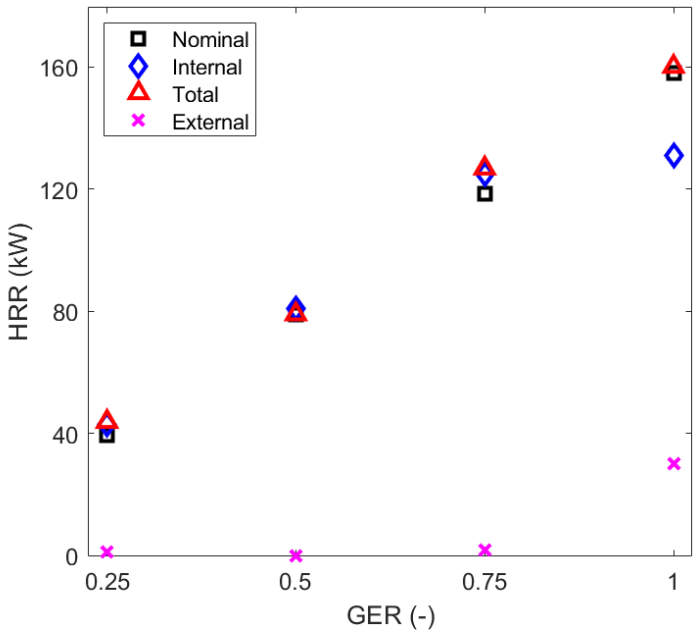

Figure 5.2. Heat release rate for different GER values.

Values from the last 5 minutes of the experiment are averaged, to acquire measurements at this steady state. Based on these, Figure 5.2 depicts the mean values from all GERs produced in the experiments.

The total HRR increases linearly; this is expected due to the linear increase of the propane flow rate. For the first two cases (GER 0.25 and 0.50) it is shown that the internal HRR matches the total, thus proving the observation that all

fuel is consumed within the compartment to be correct. Deviation of the calculated HRR (both internal and total) from the nominal HRR value are related to the cumulative error associated with the sampling and calculation process [101], [102]. Whereas internal HRR is shown to increase linearly until GER 0.75, it appears to reach a plateau at GER 1.00. The total HRR of GER 1.00 is higher than the internal, which means that fuel is also burning externally.

It was concluded from the measurements presented above that the system created can deliver reliable measurements. The quantification of internal and external HRR was essential for the parts of the analysis in the following chapters.

5.2.2 **Heat fluxes**

Heat flux measurements were made in order to have another form of comparison among the different experiments. The data can also be used as a comparison with the previous experimental phase; it is important to note that this can suffer in objectivity, as the emissivities of the fuel source and the compartment boundaries were different.

5.2.2.1 Façade

The instrumented façade of Phase 1 was used in these experiments. For the experiments of 0.25 and 0.50 GER, the lower TSC recorded very low values. The data from the upper instrumentation did not register sufficiently readings. For this reason, only the bottom TSC's data will be presented in comparison to the rest of the experiments that were conducted (Figure 5.3).

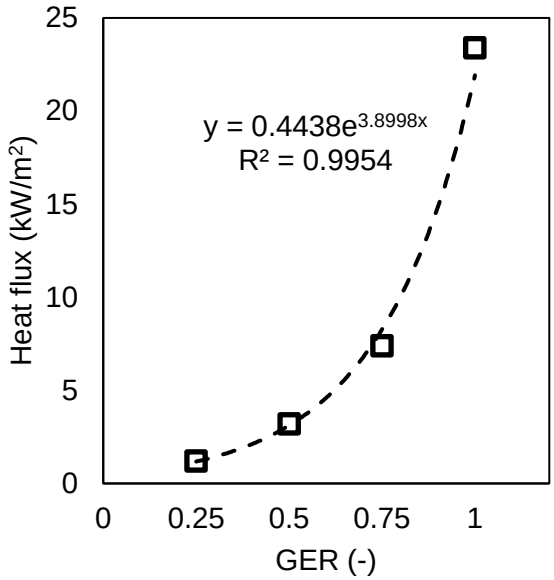

Figure 5.3. Heat flux at 820 mm height (from floor level) for all GERs.

The linear increase of GER led to a non-linear rise in heat fluxes on the façade (as shown in Figure 5.3).

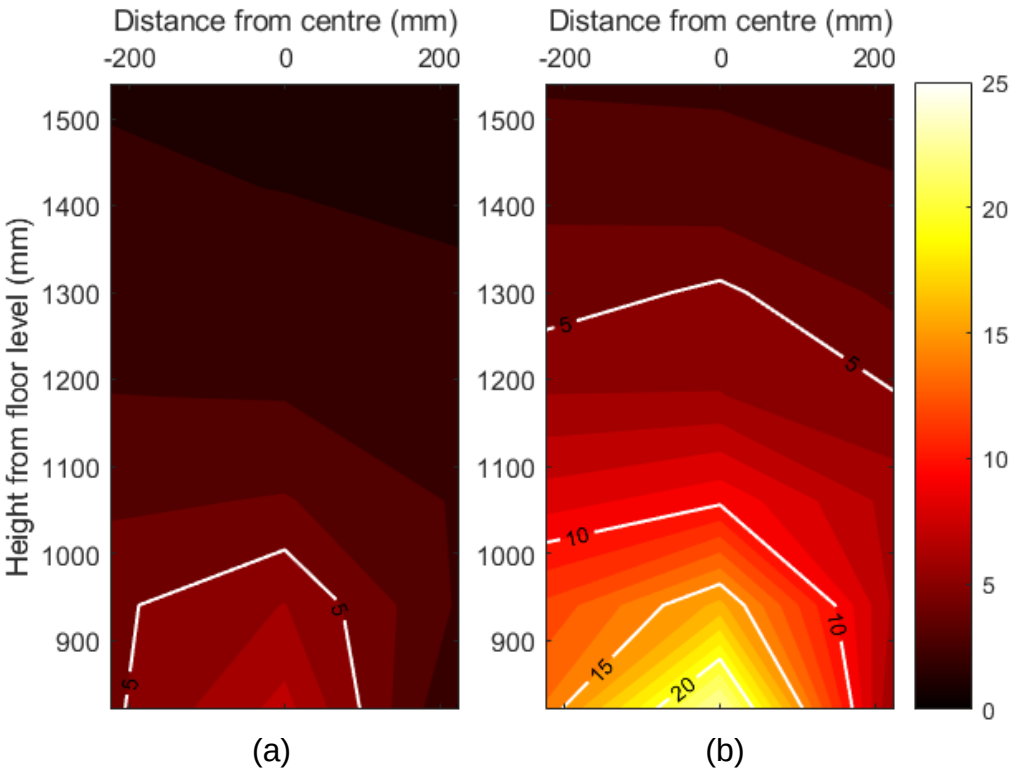

Figure 5.4. Heat flux distribution on the façade for: (a) GER 0.75; and (b) GER 1.00.

The heat fluxes on the façade for GER 0.75 and 1.00 are presented in Figure 5.4. As expected from Figure 5.4, the heat fluxes were higher, in general, for the experiment with the peak GER.

5.2.2.2 Opposite

Measurements of the total heat flux opposite the compartment were made. They aimed to demonstrate differences among the different fuel supplies; the measurements provided a baseline comparison for the Phase 3 experiments, which re-introduced timber in the compartment. Figure 5.5 shows the incident cumulative heat flux opposite (accounting for the opening and, where applicable, the external flaming).

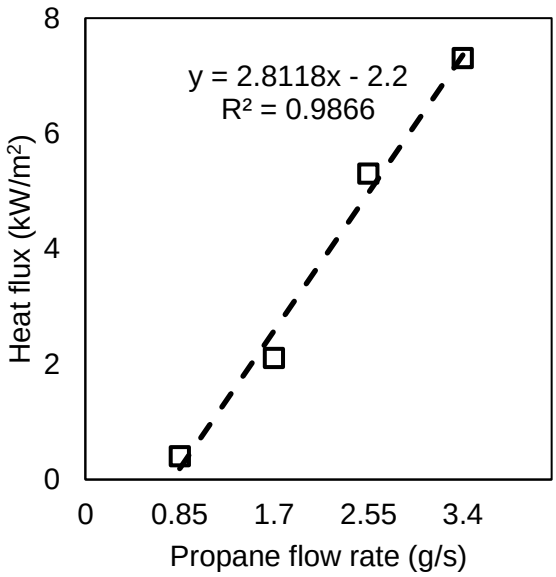

Figure 5.5. Incident heat fluxes opposite the compartment opening for all fuel supplies.

The results show a linear correlation of the fuel supply with the heat flux opposite. Although Chapter 4 (see Figure 4.24) demonstrated that no meaningful correlation exists between the heat fluxes and the mass loss rate, this does not appear to be the case here. Further investigation was done in Chapter 6 with experiments with timber linings.

5.2.3 External plume temperature profiles

Gas phase temperature measurements were made using the *Tiresias* tree. These measurements showed that a greater GER yielded high temperatures over a larger region. The *Tiresias* system logged the external plume temperatures for all GERs used. Temperature profiles are illustrated in Figure 5.6. Values between thermocouples are interpolated to create the contour plot.

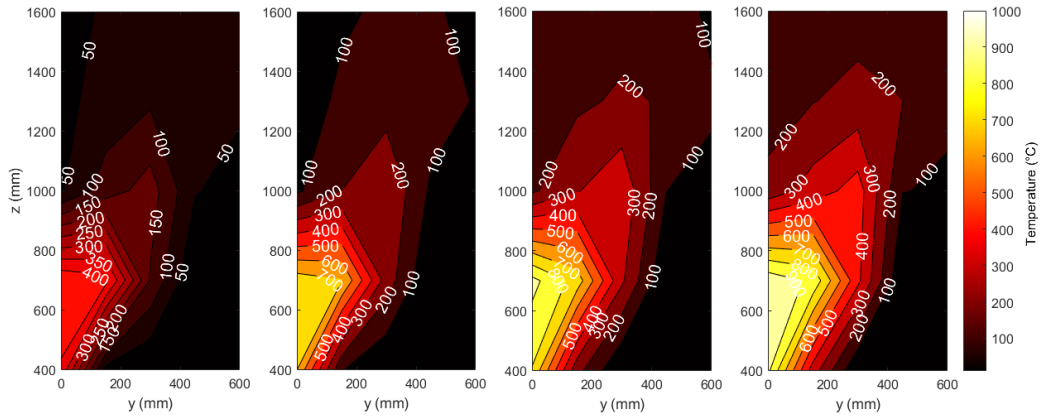

Figure 5.6. Time-averaged temperature profiles of the external plume for: (a) GER=0.25; (b) GER=0.50; (c) GER=0.75; (d) GER=1.00.

Tiresias was able to capture data that reflect both the overall shape and the dimensions of the external plume. This aids a direct comparison among the various GERs. Interestingly, the gas trajectory is also visible in these plots.

5.3 Analysis

5.3.1 External flaming

The temperature measurements from Tiresias allowed the gas temperature to be estimated. However, as noted in the literature review, flame height has been of key interest the practitioners and scientists alike. The extent of the flaming region is known to influence the heat fluxes on the façade. The videos that

were captured during the experimental programme allowed a detailed analysis of the dimensions of the plume.

Video analysis from the Phase 1 experiments revealed the importance of a proper calibration of the camera recorders. In this experimental programme, a checkerboard, of known square size, was used for the calibration procedure; this assured that measurements would be of a high fidelity. A representation of the calibration procedure is shown in Figure 5.7.

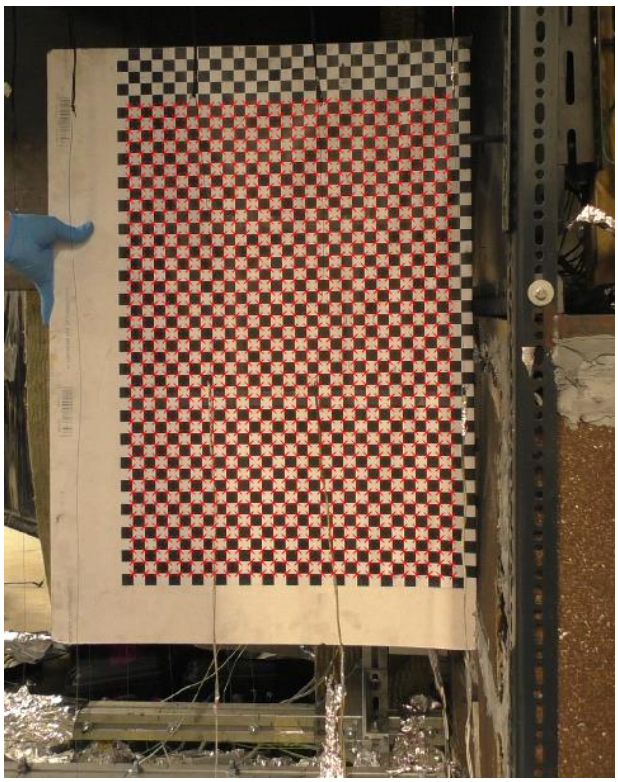

Figure 5.7. The calibration checkerboard points identified by MATLAB before the experiment.

The checkerboard was identified by the default command in MATLAB; the points of the squares are translated in coordinates. The coordinates lead to the pixel dimensions of the square edges; using these, a pixel-to-millimeter ratio can be calculated. On average, there were insignificant inherent errors in the camera measurements, as was evident by the calibration procedure. Since the cameras were set perpendicular to the opening, and the center plane was

used for calibration, the acquired data present a standard deviation of approximately 0.5 mm.

The flames' dimensions were determined using the same script as in Phase 1. The peak horizontal and vertical distances were recorded as flame standoff distance and height, respectively. Figure 5.8 shows an example of the analysis of flame height. This shows significant variation in terms of the detected maximum flame height – however this is to be expected given the inherent intermittency of diffusion flames. The data in Figure 5.8 show the raw data and the average flame height (i.e. the 50% intermittency).

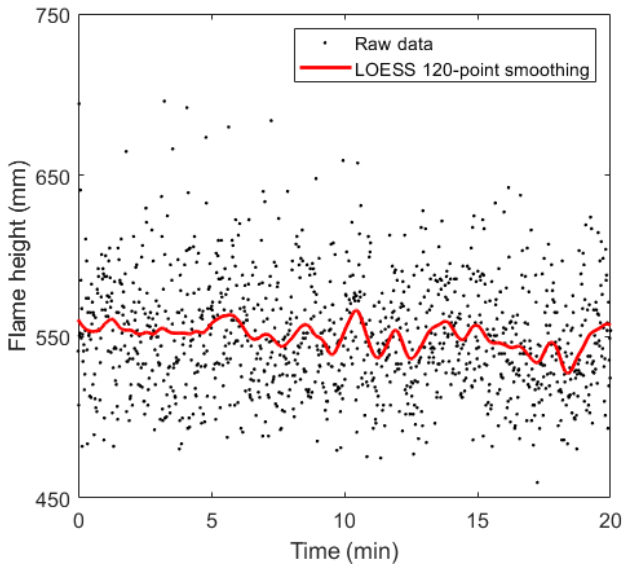

Figure 5.8. Example total flame height estimation for a GER of 1.00.

5.3.1.1 Dimensions

The first two fuel supplies (GER of 0.25 and 0.50) did not result in external flaming; thus no video analysis was performed. For the other two fuel supplies (GER 0.75 and 1.00) external flaming was visible. The data for flame heights and widths from these are presented in Figure 5.9 – with the average location (i.e. 50% intermittency) marked.

The difference between the two scenarios is more clearly illustrated with a contour plot (Figure 5.10) – where the overall shape of the flame is more

evident. To clarify, the contour plots depict clear flame heights (i.e. height of the flame above the top of the opening). It is clear from this data that (unsurprisingly) the greater the mass flow rate of fuel, the higher external flaming became. However, it is notable that the standoff distance was almost identical for the two experiments.

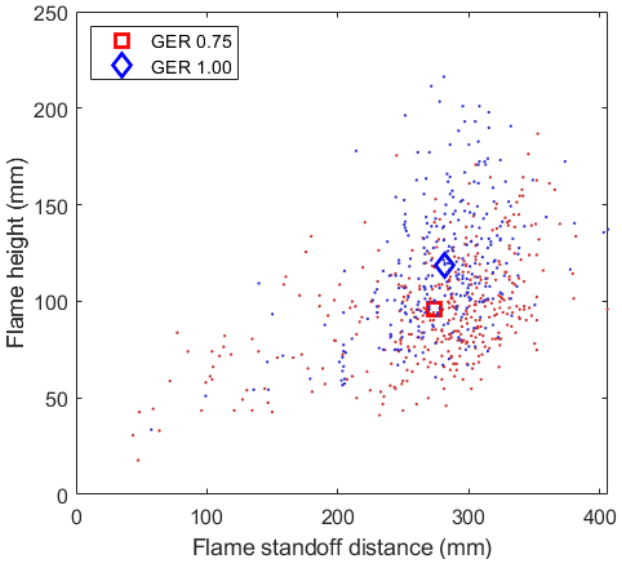

Figure 5.9. Relationship of flame standoff distance to height for the configurations that presented external flaming.

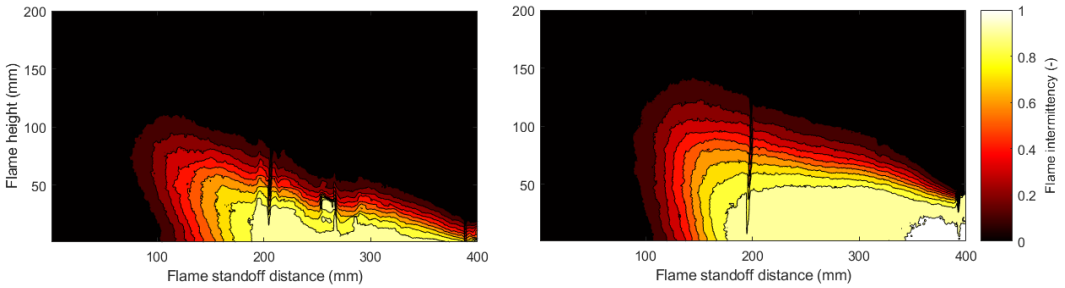

(a) (b)

Figure 5.10. Intermittency plots of (a) GER 0.75; and (b) GER 1.00 fuel scenarios. The compartment opening is at the right side of each contour plot.

5.3.1.2 Plume trajectory

Yokoi, in his extensive report on external plumes, identified certain patterns of the plume trajectory [76]. The patterns were related to the presence (or the lack there) of obstructions, and the ratio of the openings' dimensions. The original plot is shown in Figure 5.11.

a. No wall above the opening.
b. Wall above the opening; n=1
c. Wall above the opening; n=1.5
d. Wall above the opening; n=2
e. Wall above the opening; n=2.5
f. Wall above the opening; n=3
g. Wall above the opening; n=3.4
h. Wall above the opening; n=6.4

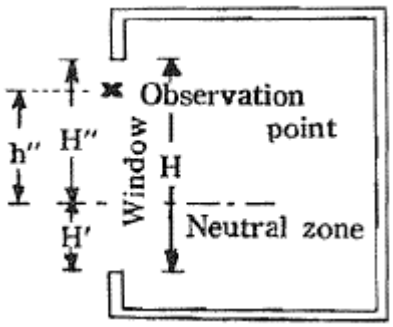

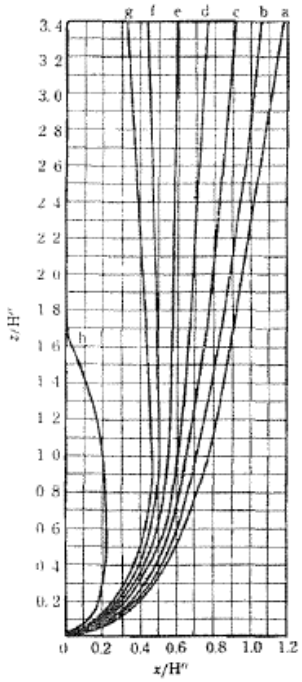

(a) (b)

Figure 5.11. Yokoi's model compartment cross section (figure 7.2 from [76]); (b) Trajectories of gases exiting various rectangular windows (figure 7.4 from [76]).

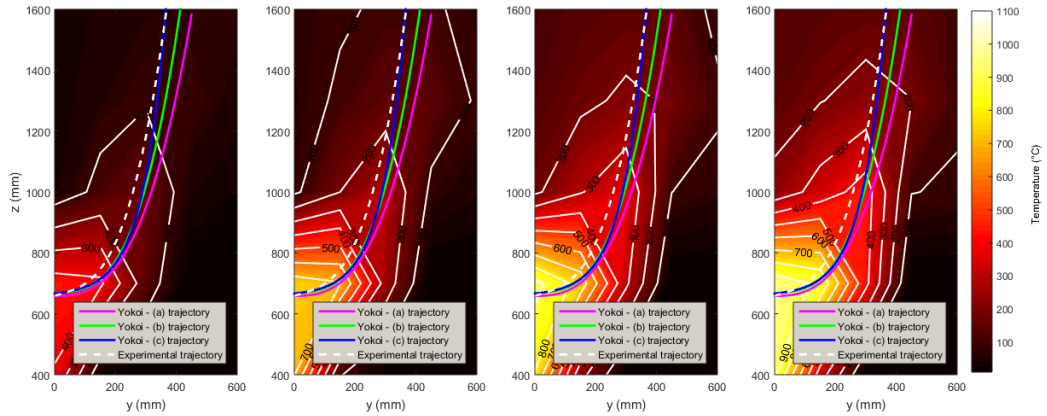

(a) (b) (c) (d)

Figure 5.12. Temperature profiles with multiple trajectories.
(a) GER=0.25; (b) GER=0.50; (c) GER=0.75; (d) GER=1.00.

The n number (hereafter referred to as a ‘shape ratio’) was described in Chapter 2. For the current compartment opening, the shape ratio is 0.14; this falls below what Yokoi has calculated for (n=1 is the minimum value). Using the ‘a’, ‘b’, and ‘c’ trajectory, plotted over the external plume temperature profiles, the accuracy of describing the plume trajectory is compared directly with the experimental data. This is shown in Figure 5.12. The centreline of the external plume, as this was manually drawn out over the centre points of plume using a dashed white line, is also included in the figure. This supports the decision to use the 'c' trajectory, as the one closest to the centreline.

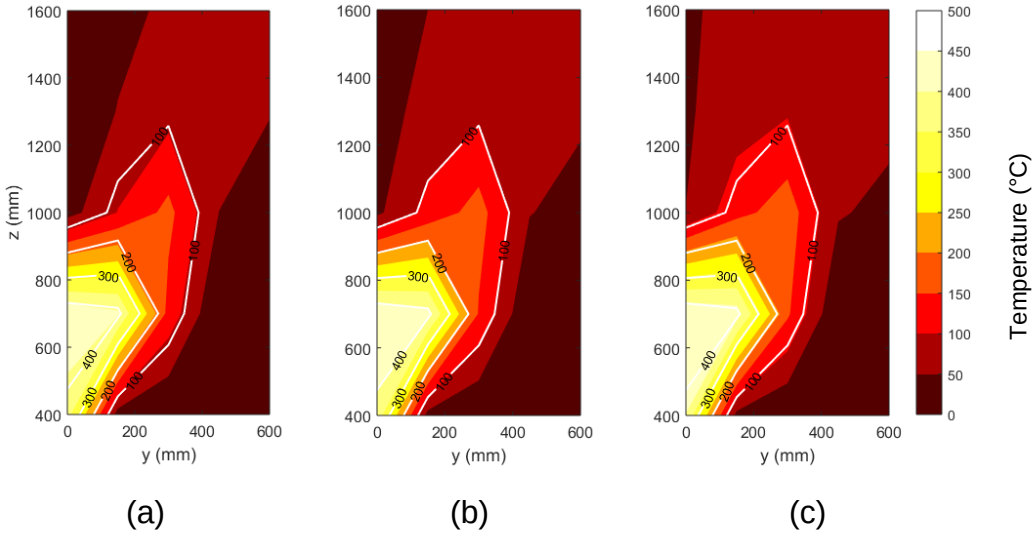

Figure 5.13. External plume variations: (a) time-averaged mean minus standard deviation; (b) time-averaged mean; (c) time-averaged mean plus standard deviation. The white contour lines represent the time-averaged mean temperature profile.

It is demonstrated in Figure 5.13 that there is slight difference when the standard deviation, calculated for the values used to get the time-averaged mean value, is added or subtracted from the mean. This establishes further confidence on the visual fit of a trajectory is fit for the purpose.

Despite the fact that Yokoi’s shape factor for the current opening can be considered to fall between the ‘a’ and ‘b’ trajectories, the experimental results contradict that. The data points are closer to Yokoi’s ‘c’ trajectory curve. This

information provides a baseline trajectory that will be used as a starting point for the timber evaluation in the next chapter.

In addition to the trajectory extracted from the thermal data of the plume, the video analysis yielded trajectory data. The trajectory from the video complements the one from the thermal plots; an envelope between the two was formed.

5.3.2 **Validation of current system with the classic plume theory**

As noted in the literature review, several researchers developed models to describe flame heights, in order to predict heat fluxes on façades. The current setup was compared with these models to establish a baseline; the baseline would provide a comparison point for the timber experiments.

5.3.2.1 Yokoi

Yokoi ran an extensive experimental series, covering various rising and ejected plume scenarios. In his work, the external plume was extensively studied and described on various cases. The common denominator on his experimental programmes was the lack of persistent external flaming (with the exception of flame tips ejected in some experiments). This initial approach aims to show similarities and identify differences in the presence of a flaming external plume.

5.3.2.1.1 Non-dimensional temperature

Yokoi created the concept of a non-dimensional temperature rise as a means to compare plume data from different compartments, regardless of internal dimensions, opening shape/size, and overall scale. The equation of the non-dimensional temperature is repeated here.

$$\Theta = \frac{\Delta\theta {r_0}^{5/3}}{\sqrt[3]{\frac{Q^2\theta_0}{{c_p}^2\rho^2 g}}} \tag{26}$$

where $\Delta\theta$ is the temperature difference (plume temperature minus ambient temperature) across the plume centerline [K]; r_0 radius of the orifice (or the

equivalent radius in the case of rectangular orifice) [m]; Q is the convective heat output [W]; θ_0 is the ambient temperature [K]; c_p is the specific heat of the hot gas [J/(kg·K)]; ρ is the hot gas density [kg/m^3]; g is the gravitational acceleration [m/s^2].

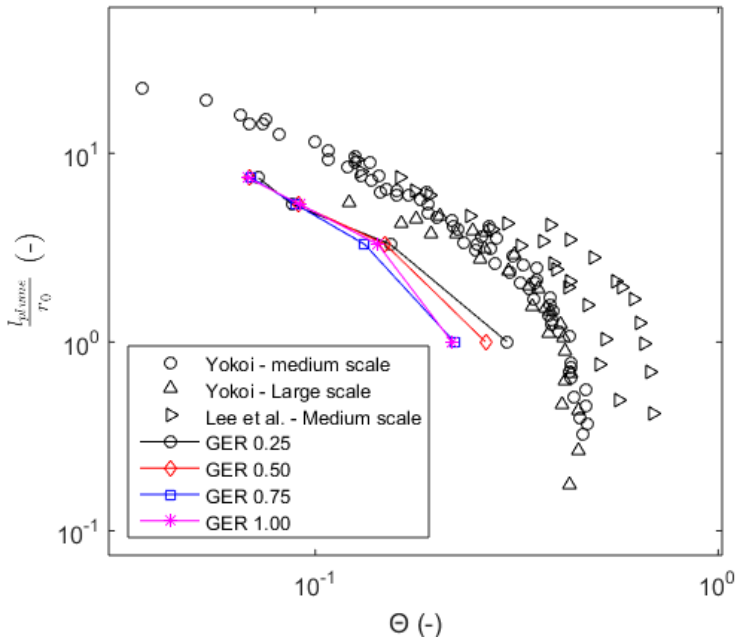

Figure 5.14. Plume non-dimensional temperatures plotted over the Yokoi datasets.

Yokoi proceeded with a double logarithmic plotting of his comprehensive dataset's non-dimensional temperatures to the respective distance on the centerline of plume. The natural next step for the dataset of this thesis was to compare the results to Yokoi's existing dataset; this was done in Figure 5.14.

The dataset was below the Yokoi model that can be extracted by his dataset. Nevertheless, a deviation of the data of Lee et al. to values higher than those of Yokoi is also seen in the same plot. Both experimental programmes (i.e. the current one and the one from Lee et al.) had external flaming. Yokoi mentioned in his work that this prediction model was to be used for rising hot currents, not external combustion. That means that both datasets deviate from the original purpose of the Yokoi model, thus possibly explaining these deviations. Moreover, all three programmes (Yokoi, Lee et al., present thesis experiments)

used different fuel sources. This could have been an additional factor for deviation between these datasets.

5.3.2.2 Thomas and Law

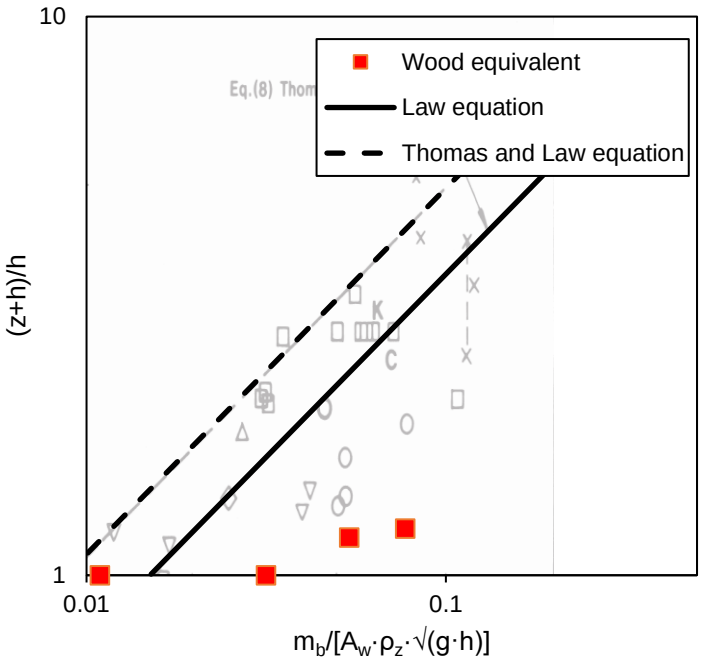

Figure 5.15. The Law correlation for flame heights and total burning rate (modified figure from [80]).

As described in the literature review chapter, at the same period Yokoi developed his model for the ejected plume, Thomas and colleagues were working on a similar project [77]. Thomas and Law used Yokoi's dataset and replotted it using their model for flame heights of the ejected external plume [79]. They concluded that their model was a suitable substitute for Yokoi's model; Law proceeded some time after that to develop her design approach [80]; she based this work on the joint work with Thomas [79]. The plot she created is shown next; the data from this chapter are plotted in this to demonstrate if the model is suitable for predictions.

The data used for the Law model development were based on compartments with no obstruction above the opening – that led to external plumes with different ventilation conditions compared to the one examined in this thesis.

This becomes apparent from Figure 5.15 that the dataset falls below the Law model.

5.3.2.3 Lee et al.

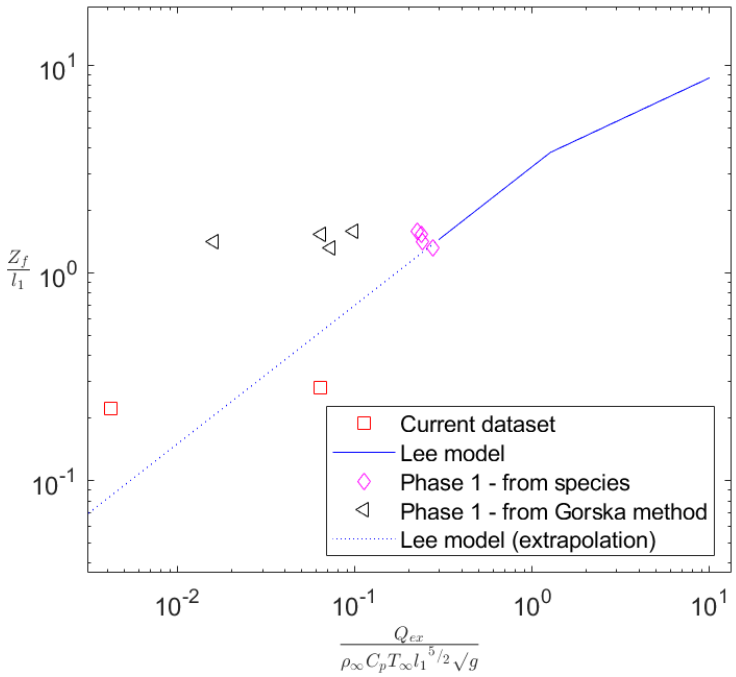

Figure 5.16. Model by Lee et al.; current dataset is plotted and compared to the extension of the current model.

Lee ran a series of experiments with inert compartments. These experiments included various compartment size ratios, opening shapes and fire sizes. The relation of the flame height to the external heat release rate was plotted by Lee et al. [82]; using her resulting model, data from this experimental programme are also plotted in the same fashion in Figure 5.16.

It is demonstrated that the Phase 2 setup follows the Lee model trend. External flaming and heat release rate were not significantly high, as the compartment was under well ventilated conditions. Despite this, as there was some external flaming, the model was applicable.

The Phase 1 experiments have a correlation, when the HRR from the species (oxygen consumption calorimetry) was used. This could be attributed to the

oxygen calorimetry estimating a result closer to the actual values, and thus appropriate to use in the model. As for the HRR from Gorska's ventilation method, the data appear be off.

5.4 Summary of findings

A novel system was designed to characterise the external fire plume. The system demonstrated competence in producing repeatable experiments with controlled burning, using a propane burner. The burner used with a prescribed propane flow rate per experiment. This provides an isolation of the fuel bed and any combustible linings (which were used and studied in the following chapter).

The system provided a characterisation of the gas phase temperatures of the external plume, as an addition to the previous experimental setup. Moreover, the external flaming was recorded by video cameras; the cameras were calibrated using a checkerboard of known square size, which provided more precise measurements, in relation, again, to the previous setup.

The classic plume theory correlations can be utilised, up to a certain extent for the current setup. As it was demonstrated, depending on the model used, a better or worse prediction can be made.

- Yokoi's model slightly overestimates the external flaming height or temperature, depending on the desired prediction target. This could be an inherent issue of Yokoi's model, since this was developed only for non-reacting external plumes; however, it appears that even for the cases where there was no external flaming, the dataset still deviates from Yokoi's. Fuel source could potentially affect the results. Yokoi used pool fires as a heat source; the present experimental programme used a propane burner, which could have resulted in higher exit velocities and therefore have affected the trajectory of the external plume.
- The Thomas and Law correlation was developed for compartment fires that did not have a façade above the opening. This is not applicable in

the current experimental programmes; however, it affords a comparison among the present work, with the work by previous researchers.

- Lee et al. developed a model for flame heights correlated with the external HRR, and is suitable to the present thesis work. Using the extension of the model, a prediction can be made for the Phase 2 experiments; however, the short flames and the low external HRR produced results that deviated from the Lee et al. model.

This page intentionally left blank.

Chapter 6 – Timber Linings

6.1 Introduction

In the previous chapter a system was designed to characterise external plumes from compartment fires. The design offered robustness in repetitive experimentations. The burner provided steady burning conditions throughout the duration of each experiment. The instrumentation captured the behaviour of external flaming and smoke in terms of trajectory, shape, temperatures, incident heat flux to the surroundings, and rate of heat released. In addition to all the above, the system provided the baseline for plume behaviour in the absence of timber linings. This can lead to an evaluation of the underpinning differences of combustibles only on the compartment floor, and combustibles simultaneously on the floor and other surfaces of the compartment.

In this experimental programme, a propane flow rate of 1.70 g/s (GER=0.50) was used. The purpose of using this GER was that minimal external flaming was observed for this flow rate for the inert compartment. In order to investigate the affect timber has on the external plume, the timber was exposed in two locations: (1) back wall; and (2) ceiling.

These two conditions correspond to commonly used arrangements within the construction industry – i.e. to expose a timber wall, or a timber ceiling. Initially those surfaces were thought to be sufficient for a direct comparison with each other as well as the propane supplies used in the previous phase. It was hypothesized that there would be an observable difference between the plume behavior depending on the location of the exposed timber.

To further elucidate any differences and the degree to which location of exposed timber may affect the behaviour of the external plume, the experimental programme included a series of arrangements where only a half panel of timber was exposed, but the location of this was changed from “ceiling-front” to “wall-base”. These configurations are shown in Figure 6.1.

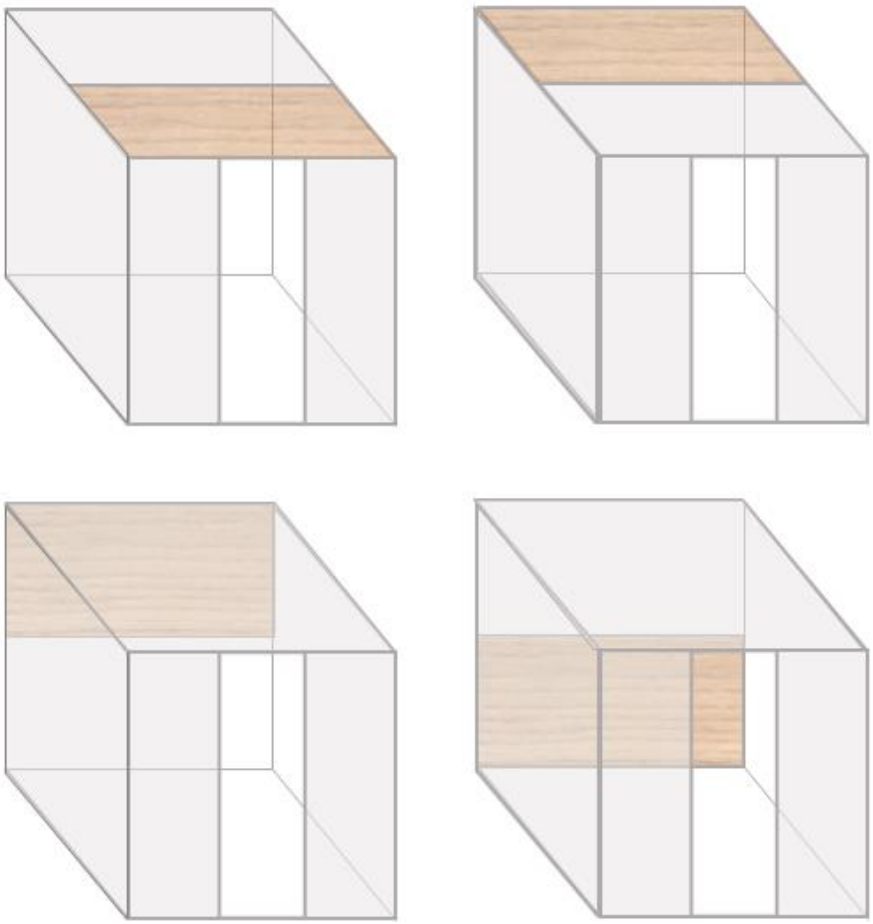

Figure 6.1. Half exposed timber surfaces in all the experimented configurations. Top row shows the exposed ceiling timber; bottom row the exposed back wall timber.

6.2 Results

6.2.1 **Initial observations**

This experimental programme used the same setup as in Phase 2 (Chapter 5). The propane flow rate used, in an inert compartment configuration, resulted in combustion inside the box, almost exclusively, as evident by video footage and calorimetry data.

Substituting the compartment ceiling or back wall insulation with a timber surface resulted in immediate visual changes of the external plume. The ceiling configuration resulted in a tall and slender flame; the wall configuration had a

shorter and thicker flame. Both compartments exhibited severe under-ventilated conditions.

The experiments that used half the length of exposed timber appeared to have different behaviours from each other; all of them demonstrated external flaming. As observed throughout the experimentation and the video footage, the shape of the external plume as well as the burning conditions inside the compartment deviated significantly. Starting with the front half of the ceiling, the flaming of the timber was visibly separated by the flames of the fuel bed (almost like a sample exposed to a radiant heat source from below). As the timber slab moved further backwards and downwards, the separation of the burning gases from the burner and the respective timber surface was indiscernible.

6.2.2 **Calorimetry**

Table 6.1 presents the values for total and internal heat release rate for experiments of Phase 3. As expected, the HRR for both the full ceiling and back wall experiments had approximately the same values; the internal HRR is also approximately equal in the two cases. The internal HRR for the top of the back wall both halves of the ceiling was approximately equal; the bottom half of the wall was lower, potentially indicating poorer mixing conditions inside the box. Total HRR were approximately the same for experiments with half-exposed surfaces (slightly lower for the front half of the ceiling, presenting an issue with mixing time, probably leading to less volatiles burning).

Table 6.1. Heat release rate (internal and total) for different configurations.

Configurations	A_{timber}/A_{total} (-)	HRR_{in} (kW)	HRR_{tot} (kW)
Ceiling – full	0.21	138.7	168.6
Back wall – full	0.21	139.9	171.5
Ceiling – front	0.11	106.8	120.2
Ceiling – back	0.11	106.3	127.3
Back wall – top	0.11	110.6	127.8
Back wall - bottom	0.11	96.7	128.8

The mass loss rate of the experiments with half-length exposed timber is shown in Table 6.2.

Table 6.2. Mass loss rate for the half-length experiments

	Ceiling		Back wall	
	Front	**Back**	**Top**	**Bottom**
Mass loss rate (g/s)	3.5 ± 0.4	3 ± 0.1	3.8 ± 0.8	3.5 ± 1

Values appear to be similar when one accounts for the measurement's deviation (included in the table). The ceiling presented slightly lower values compared to the back wall. This deviation comes in agreement to similar observations in the literature from Gorska and Bateman et al. ([9], [106] respectively).

6.2.3 **Heat fluxes**

The heat fluxes on the façade are shown in Figure 6.2. There is a noticeably higher heat flux on the bottom of the façade for the case where the front half of the ceiling was exposed. Despite the expectations for the heat fluxes would drop as the exposed timber was moved further back in the compartment, the case of the top half of the wall having exposed timber appears to have yielded the second highest heat flux profile.

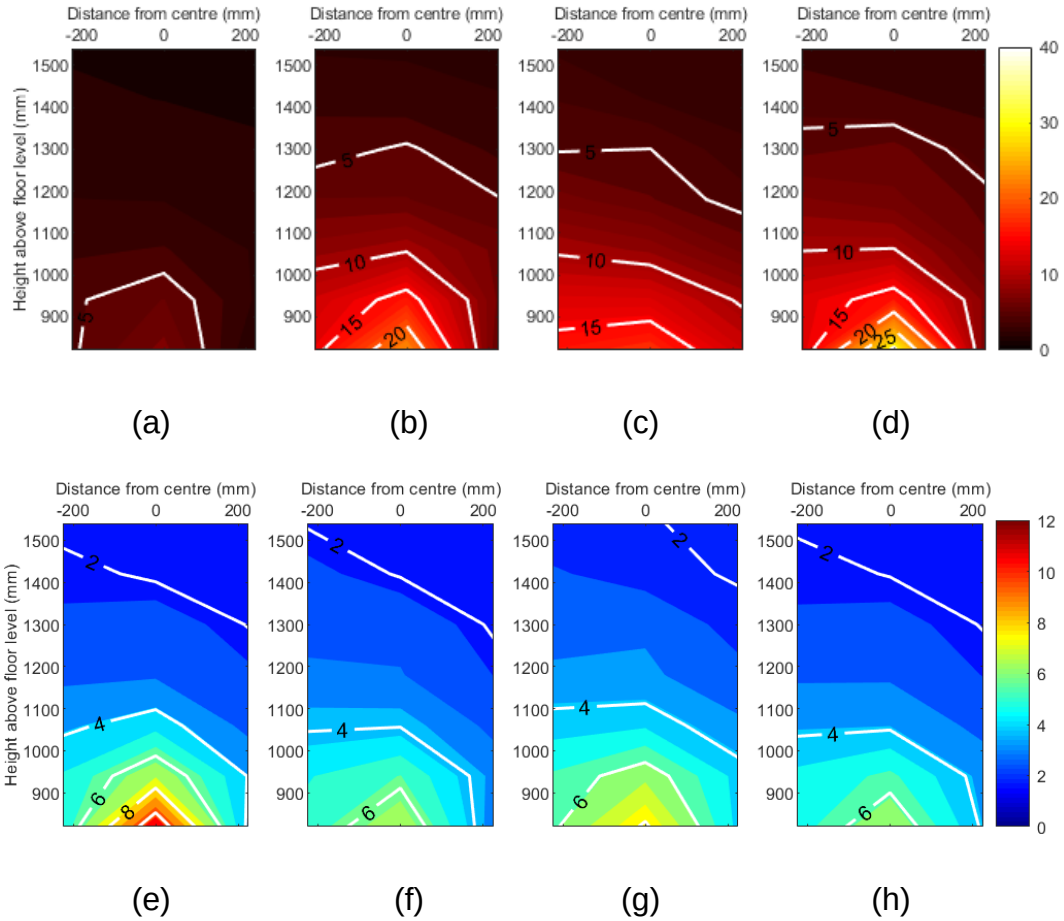

Figure 6.2. Heat fluxes on the façade for different configurations:
(a) Inert GER 0.75; (b) Inert GER 1.00; (c) Timber back wall; (d) Timber ceiling;
(e) Half timber ceiling (front); (f) Half timber ceiling (back);
(g) Half timber back wall (top); (h) Half timber back wall (bottom).

Figure 6.3 illustrates the incident heat flux opposite the compartment opening as a function of the time-averaged: (a) HRR; and (b) mass loss rate. Propane and timber have different heats of combustion. This leads to different HRR for the same mass loss rate. Due to the fact that the experiments included both materials, the mass loss rate of propane was transformed into an equivalent mass loss rate of wood, using the ratio of the two heats of combustion.

Heat flux measurements from the burning timber would be overestimated if the HRR was the only factor used to predict the heat flux opposite. It is shown in

Figure 6.3 (b) for the same HRR, propane leads to higher heat fluxes, compared to timber.

Following this, Figure 6.3 demonstrates that timber, when exposed in the back wall, always produces a higher heat flux compared to a ceiling configuration of the same dimensions (as the back wall values are higher than the ceiling ones). This could support the evidence that a back wall configuration produces a more momentum-driven external flaming, thus producing higher heat fluxes opposite an opening. Alternatively, the higher heat flux from the wall could be due to direct radiation from the burning wall, as temperatures at the opening were higher.

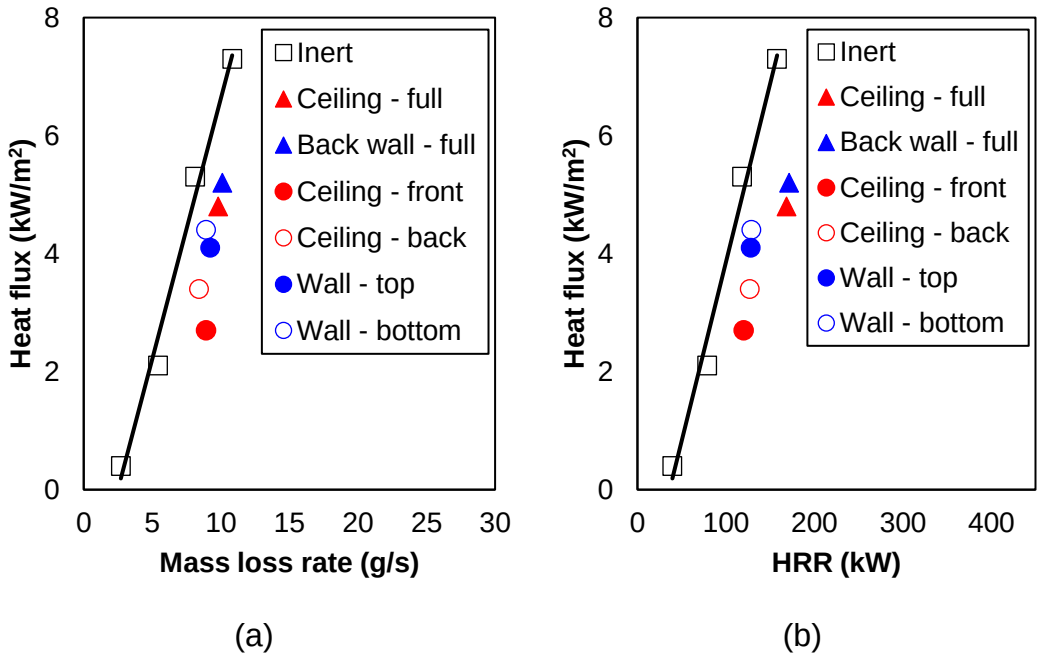

Figure 6.3. Heat flux opposite the compartment opening over (a) the average cumulative mass loss rate and (b) total HRR for different configurations.

6.2.4 External plume temperature profiles

The thermal profiles for the fully exposed linings were acquired by the *Tiresias* external thermocouple tree; these are shown in Figure 6.4. The temperature distribution of the external plume for the exposed ceiling configuration appears to be more buoyancy driven compared to the exposed back wall.

Yokoi recorded trajectories of ejected plumes for different opening shape factors [76]; the closest n-number shape factor to the current opening shape was ‘b’. This suggested trajectory was used in Figure 6.4 (a) – i.e. the ceiling configuration – showing that, indeed, Yokoi’s observation on trajectories is applicable for exposed timber ceilings. On the contrary, the back wall configuration (Figure 6.4 (b)) cannot be represented accurately with the same trajectory. The ‘c’ trajectory appears to be fitting better the thermal profile of this configuration. Nevertheless, as it was shown in Chapter 5, the compartment/burner system behaved similar to the ‘c’ trajectory. The ceiling configuration behaved in the “expected” manner from a geometric perspective; despite that fact, the back wall configuration was the one that followed the system’s behaviour more closely, as the same trajectory was applicable for the inert compartment fires.

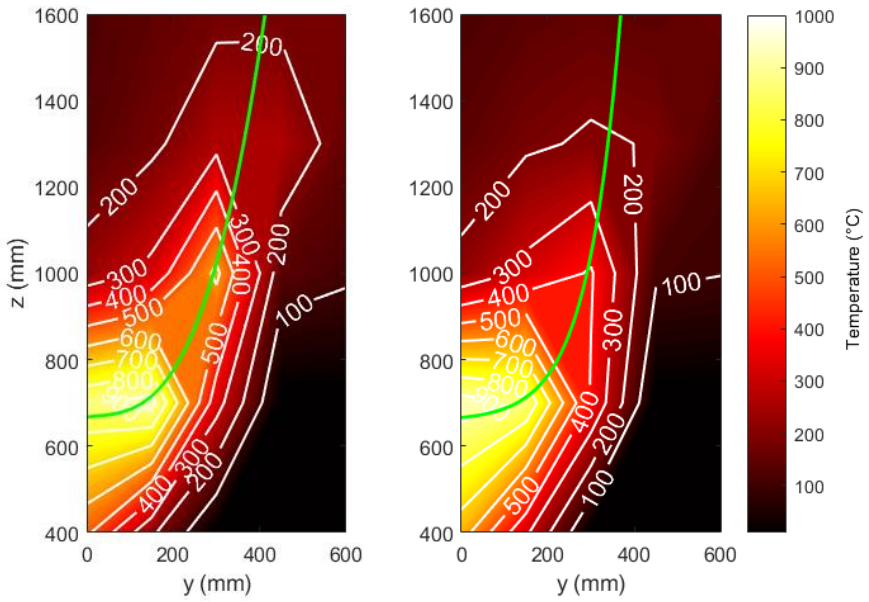

Figure 6.4. Temperature distribution in the external plume for exposed timber linings at (a) ceiling; and (b) back wall. Green lines indicate the gas centreline trajectory.

The temperature of the external plume for the half-length timber linings were also recorded, in order to complement the analysis and make a distinction of

differences between the two exposed surfaces. The temperature profiles are presented in Figure 6.6. The thermal profiles reflect what was captured in video: (1) the exposed ceiling configurations had a taller and more slender external flame; (2) the exposed wall configurations had manifested in slightly shorter but thicker external flames.

Regarding the plume trajectories, the exposed wall configurations seem to be adequately described by the ‘c’ trajectory (similar to the inert compartments and the full-length back wall). However, the exposed ceiling configurations appear to be better described by trajectories ‘d’ and ‘e’ (for the front and back exposed halves respectively). Yokoi related these trajectories to shorter and wider openings. During the experimentations, the half-exposed ceiling surfaces presented burning that was visually detached (as shown in Figure 6.5) from the burning of the fuel bed; this detachment, leading to a shorter hot layer exiting the compartment, could be the driving reason behind this shift of trajectory from the fully exposed lining.

Figure 6.5. Snapshot from an experiment of the exposed front half of the ceiling.

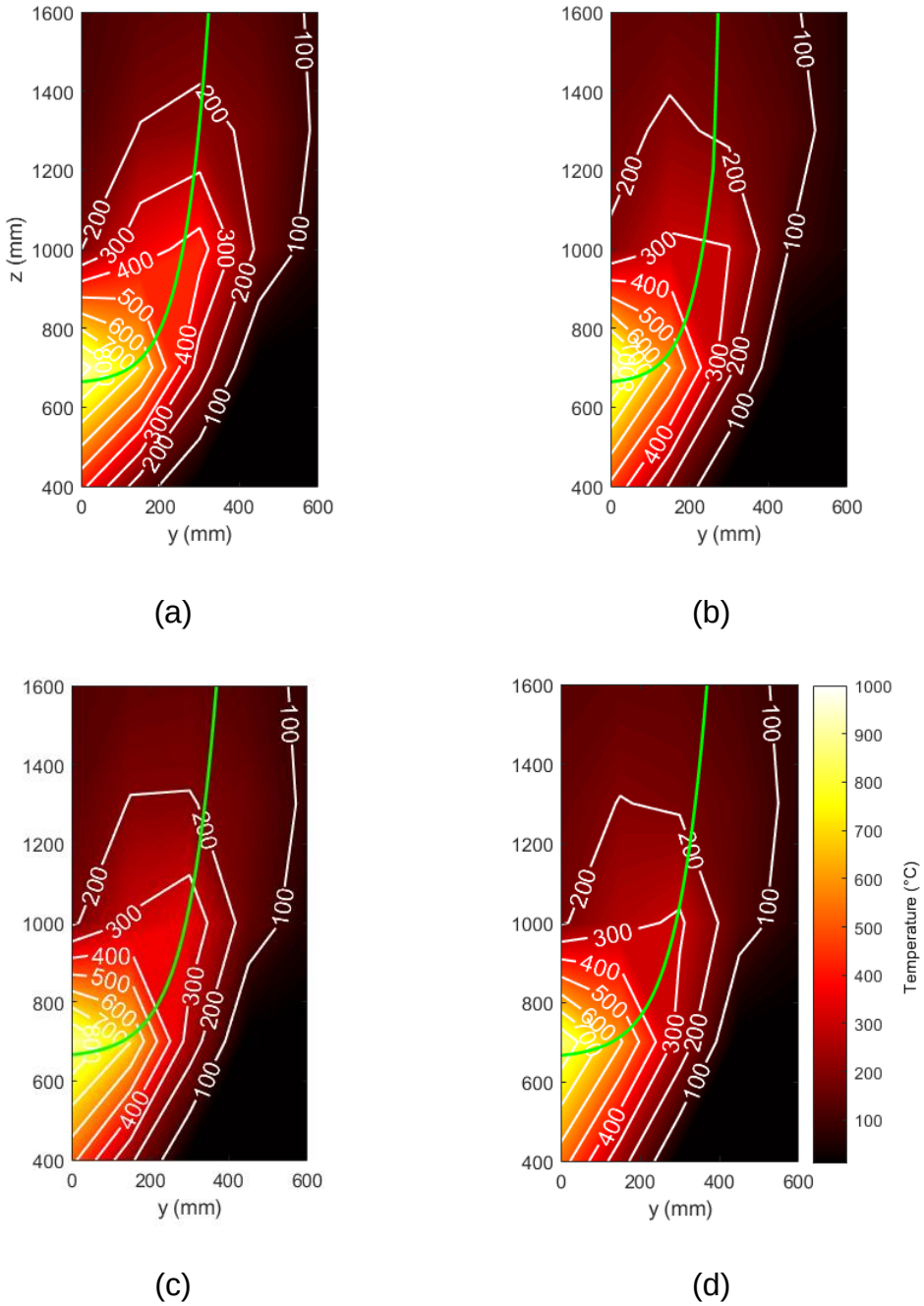

Figure 6.6. Thermal profiles and gas trajectories of different configurations: (a) front-half ceiling; (b) back-half ceiling; (c) top-half back wall; and (d) bottom-half back wall. Green lines indicate the gas centreline trajectory.

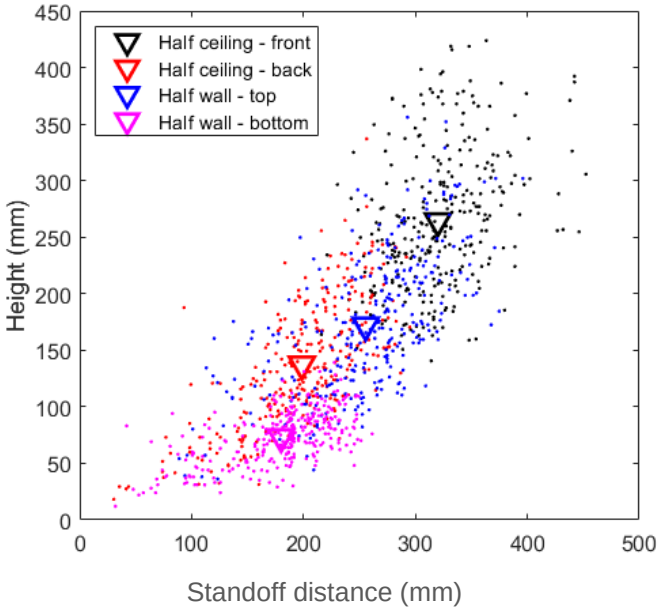

Figure 6.7. Average height and standoff distance of flames for all experimental configurations.

Figure 6.7 shows the average standoff distance-height of external flames for the experiments of this set. A clear favouring of the exposed front half of the ceiling over the rest of the configurations is depicted. In further support to the thermal profiles of the plume and the heat fluxes on the façade, the top half of the back wall has the second highest flame height (and protrusion), compared with the back half of the ceiling and the bottom half of the wall. An approximately 90% higher flame was recorded for the exposed back half of the ceiling compared to the bottom half of the wall; despite the markedly taller flaming, the standoff distance was approximately the same for these two surfaces, with a slightly higher value for the ceiling configuration.

6.2.5 **Velocity profiles at the opening**

Measurement of the velocities at the opening reveal some difference between the locations of exposed timber. The results of the full-length timber experiments are illustrated in Figure 6.8.

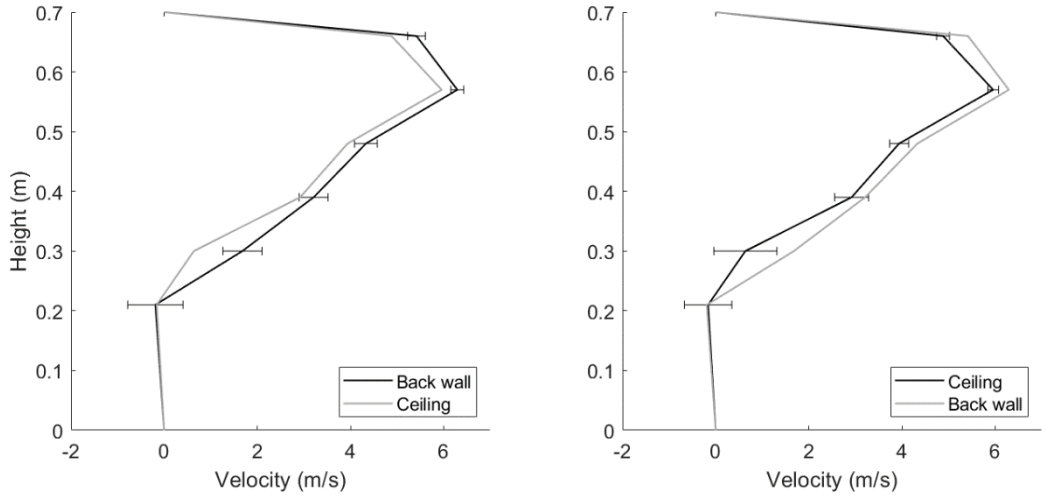

(a) (b)

Figure 6.8. Velocity profiles at steady state:
(a) Fully exposed back wall; (b) Fully exposed ceiling.

The exposed timber ceiling had a marginally smaller exit velocity compared to the exposed back wall. Error bars show fluctuations of measurements; nevertheless, instruments' inherent deviations from true value could account for the discrepancy. Further investigation was deemed necessary to underpin which part of each surface was driving the phenomenon.

Figure 6.9 shows the profile of the average velocities for all experimental configurations. For the front half of the ceiling, the neutral plane appears to be higher compared to the back counterpart; additionally, the peak velocity at the outflow is the lowest compared to the rest of the configurations. A more momentum-driven plume was produced when the exposed timber was at the back wall of the compartment. The peak velocity was almost identical for both halves of the wall; marginally higher velocities were recorded for the case of the top half.

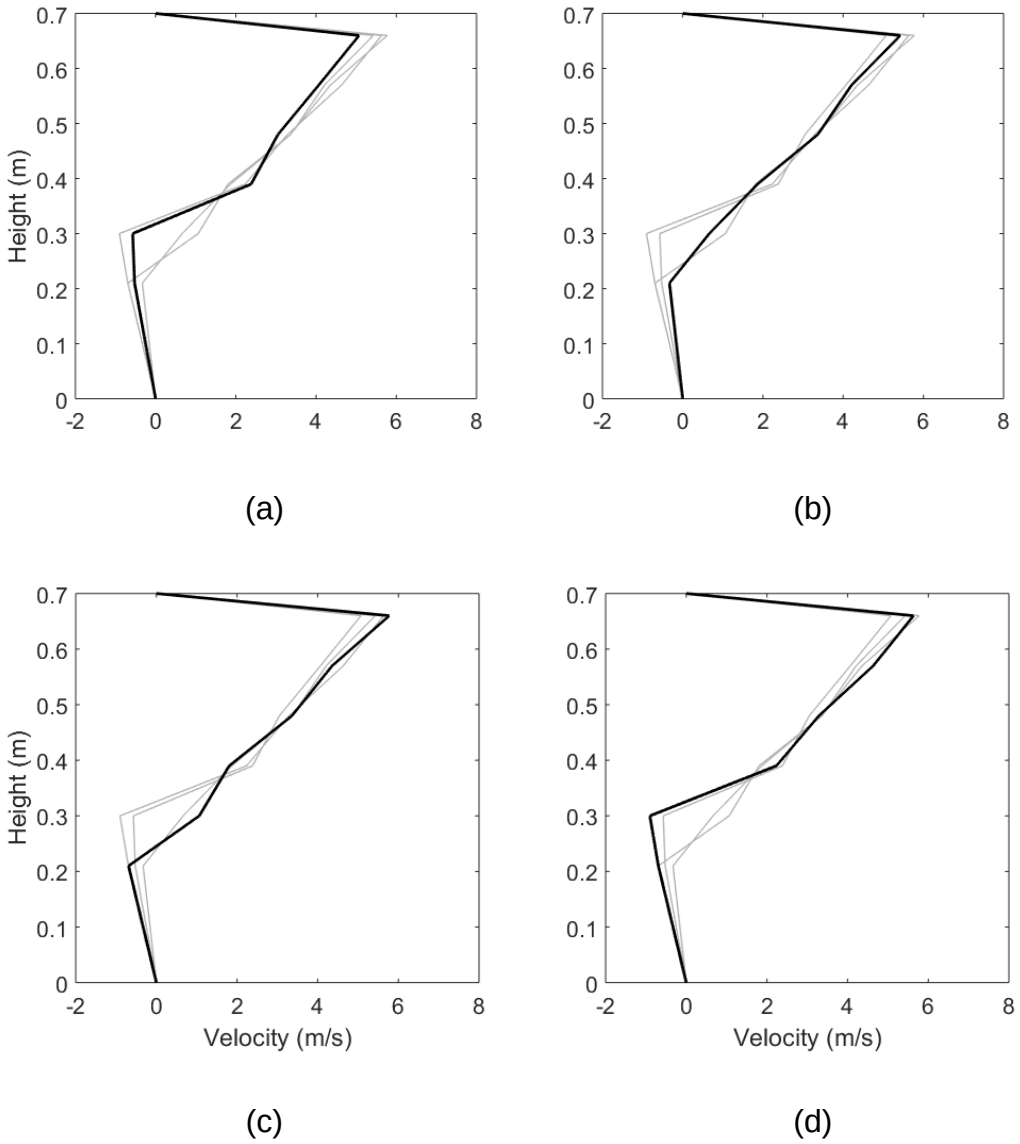

Figure 6.9. Velocity profiles at steady state: (a) Half ceiling – front; (b) Half ceiling – back; (c) Half wall – top; (d) Half wall – bottom.

6.3 Summary of findings

This experimental programme revealed some of the specific features of exposed timber in different locations in compartment fires. The burning rate is not grossly affected by the configuration of timber; nevertheless, slightly higher mass loss rates were recorded for the exposed back wall, which comes to support past literature findings.

Incident heat fluxes on the façade were higher for exposed ceiling compared to an exposed wall; the halves that appear to be the main contributors of this behaviour are the ones closer to the exit point for either configuration (i.e. the front of the ceiling and the top of the wall). Flame heights also supported these findings.

Upon examination of the heat fluxes opposite, exposed walls – either half- or full-length configuration – consistently recorded higher values, in comparison to the exposed ceiling; differences between the two locations were more pronounced for the smaller areas. This could be attributed due to the burning wall radiating directly towards the HFG, or due to the overall higher compartment temperatures recorded for exposed back wall experiments. Exit velocity values were higher for the back wall. That was a general trend, especially for the half-length exposed timber; as the piece was moving further back, the velocity was increased; this peaked for the top-half of the wall, as the bottom bit had a slightly lower peak velocity.

Finally, the trajectories appeared to have been affected by the location of exposed timber.

- For the full-length configurations, the trajectory of the back wall remained similar to that of the inert compartment. The ceiling's trajectory on the other hand was more projected, as it appears to fit better to Yokoi's 'b' trajectory instead of 'c', which has been the default for the inert compartments.
- For the half-length configurations, again, the exposed wall configurations behaved similarly to the inert compartments, as 'c' trajectory adequately describes the hot gas trajectory exiting the compartment. The exposed timber ceiling configuration presented trajectories more like Yokoi's 'd' and 'e', which suggest that there was less pressure pushing the hot gases out of the compartment.

All the above are analysed in full in the following chapter.

This page intentionally left blank.

Chapter 7 – Analysis

7.1 Introduction

Chapters 4 to 6 displayed different experimental programmes carried out to investigate timber-lined compartments.

Specifically, the first objective was to establish whether timber linings changed the external fire spread hazard of a compartment fire (demonstrated in full in Chapter 4). A series of compartment fires with wood cribs were conducted using different configurations of exposed timber. It was shown that timber linings changed the fire dynamics; more fuel was produced at a higher mass loss rate; this fuel was consumed partly inside the compartment and partly in the external plume. The fuel reacted externally and resulted in a plume with higher irradiance towards its surroundings compared to an inert compartment. This established an increase of the external fire spread hazard compared to a compartment with inert linings.

Once the difference of hazard due to the presence of timber was demonstrated, a method of tracking the changes and a system capable of characterising these changes was developed (Chapter 5). For this purpose, a compartment was built out of non-combustible insulation boards. A propane burner was created to introduce fuel in the compartment space. Modifications and additions were made to the instrumentation used in the first experimental programme; these changes made the external plume characterisation possible (temperature distribution, external flame dimensions, gas trajectory). Data complied with some parts of the classic plume theory, with an internally consistent behaviour. For other parts of the classic theory, there was significant deviation, and practically these could be disregarded; however, it will be shown in the following text that this afforded a relative comparison for the produced datasets.

Finally, combustible linings were used in this novel system and an external plume characterisation was performed (Chapter 6). Data demonstrated the difference in plume behaviour, which occurred due to timber linings having

been exposed at various locations within the compartment space. Full- and half-length pieces of timber were used, in an attempt to underpin critical locations in the compartment that drive the phenomena. The data acquired were considered useful to aid a comparison between inert and timber-lined compartments, showcasing differences in behaviour that can alter the external fire spread scenarios.

The observations and measurements made in the previous chapters produced a variety of data to proceed with further analysis in the present chapter. Due to the fact that velocities at the opening varied, based on the experimental configuration, the relationship of buoyancy to momentum was examined first, in an attempt to understand differences that might have occurred with the exposure of timber in the compartment.

7.2 Momentum vs. Buoyancy

A momentum calculation can be made by averaging the outflow velocities. This was done using the following equation:

$$M = \dot{m}_{out} v \tag{27}$$

where $\dot{m}_{out}$ is the mass outflow rate of gases from the opening (kg/s); and v is the average outflow velocity of gases (m/s). Moreover, based on the temperature data from the opening, the buoyancy at the opening can also be estimated by the following equation:

$$J = \dot{m}_{out} \frac{\Delta T_g}{T_\infty} g \tag{28}$$

where ΔT_g is the temperature difference of the hot gases compared to the ambient temperature (K); T_∞ is the ambient gas temperature (K); g is the gravitational acceleration (m/s^2). Based on these the following figure was created.

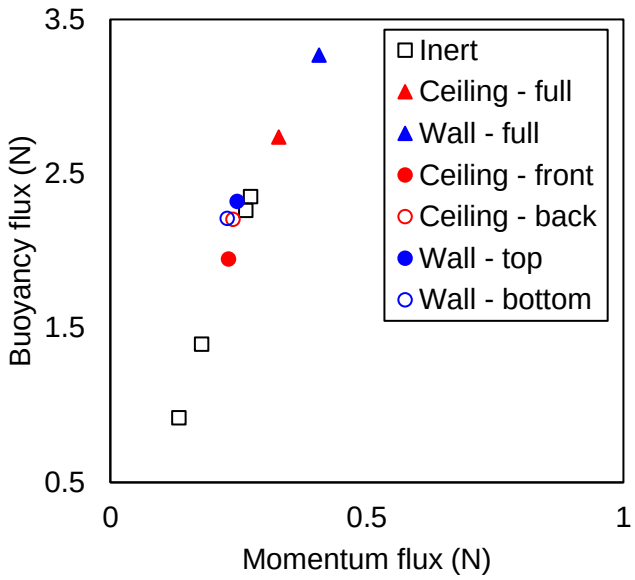

Figure 7.1. Buoyancy flux and momentum flux correlation for inert and timber-lined compartments.

Figure 7.1 shows that the exposed timber produces higher buoyancy and momentum at the outflow. This is responsible for trajectory changes, as demonstrated previously (see Figure 6.4 and Figure 6.6). It is observed that the halves at the back of the ceiling and the bottom of the wall were virtually the same. Whereas momentum was approximately equal for the top of the wall and the front of the ceiling (since exit mass and velocity was similar), the former had a higher buoyancy, which was affected by the temperatures at the opening.

Radiant heat flux on the façade and opposite is a combination of plume temperatures and the configuration factor, which is affected by the shape and distance of the plume from the targeted area/point. For this reason, a lower momentum plume can grossly influence the heat fluxes on the façade; at the same time, highly buoyant plumes lead to longer external flames, which affect both the façade and the building surroundings

Tabulating the ratio of buoyancy to momentum, an interesting observation arises. The results are shown in Table 7.1.

Table 7.1. Ratio of buoyancy to momentum for all experimental configurations of Phases 2 and 3.

	GER (Inert)				Ceiling (timber)			Back wall (timber)		
	0.25	**0.50**	**0.75**	**1.00**	**Full**	**Front**	**Back**	**Full**	**Top**	**Bottom**
J/M (-)	6.9	7.9	8.6	8.6	8.3	8.5	9.2	8.0	9.4	9.7

The values range from 6.9 to 9.7; especially once there is flaming in the external plume, the range becomes narrower (8.0 - 9.7). This might suggest that as more fuel exits the compartment (and thus developing a higher momentum), temperatures also rise (leading to a higher buoyancy).

7.3 Analysis

7.3.1 **Classic plume theory correlations**

The previous chapter demonstrated how the present compartment and instrumentation setup performs compared to previous work [76], [79], [82]. It also demonstrated that the experimental setup was capable of capturing the plume measurements necessary to assess this compartment against the classic plume theory correlations. The same calculations were carried out for the experiments of this phase of the experimental programme that included the combustible linings.

7.3.1.1 Yokoi

Figure 7.2 illustrates the baseline data acquired from the inert compartment fires in the previous chapter (in grey). The baseline data include two propane flow rates that strictly result in combustion inside the compartment; the other two flow rates have combustion both inside and outside the box. Figure 7.2 also presents the data when timber linings were exposed in the compartment.

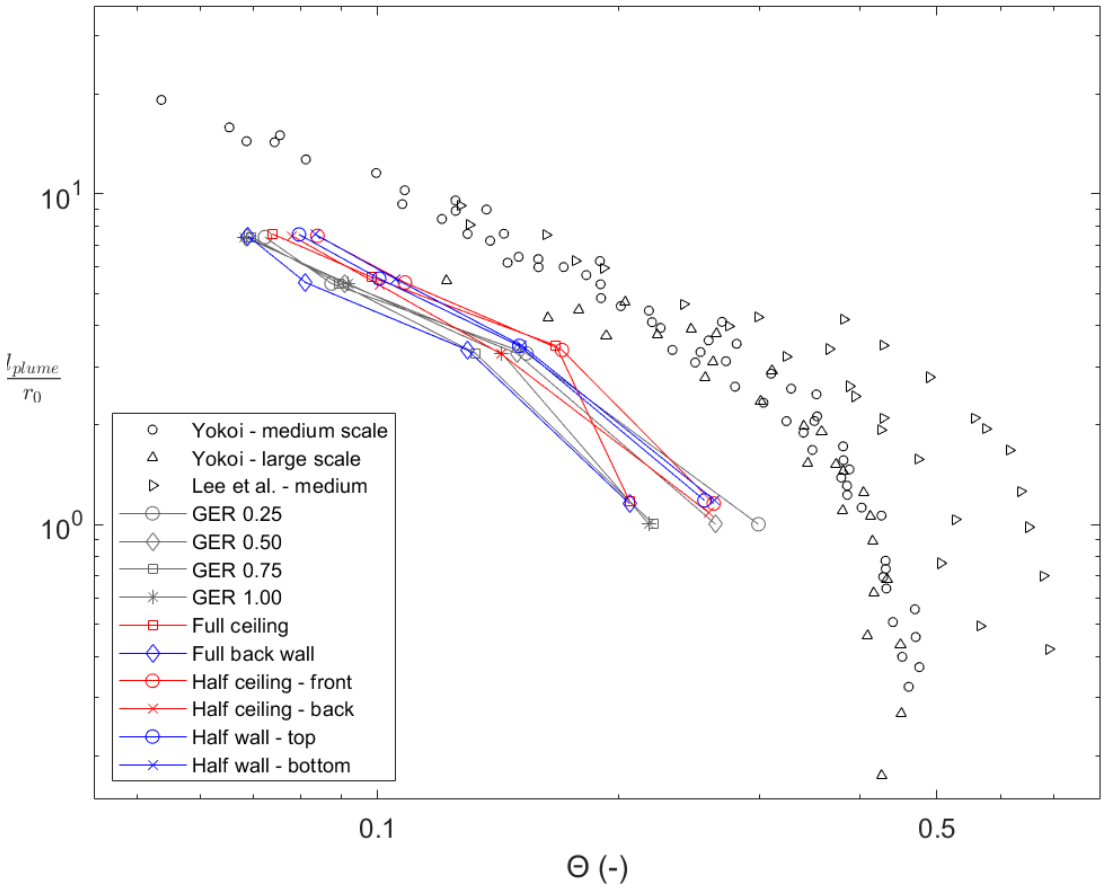

Figure 7.2. Normalised axis distance over non-dimensional temperature – Data from Phase 2 and Phase 3 experiments.

It is observed that, for the lowest height measurements, both the inert and timber-lined compartments performed similarly to each other. However, as the plume rises, the compartments with exposed linings persistently showed slightly higher non-dimensional temperatures. This validates the argument that timber changes the external fire spread hazard, as it shows that plume temperatures are affected in a non-dimensional level. Notably, after a certain height, both for inert and timber-lined compartments values of the non-dimensional temperature Θ converged in different values respectively. In the case of the inert compartment that was regardless of the fuel supply; in the timber compartments that was regardless of fuel location (as fuel supply was the same).

7.3.1.2 Law

Using Margaret Law's correlations from her work [80], the mean burning rates and the respective flame heights of all Phase 2 and 3 compartment fires are plotted in Figure 7.3.

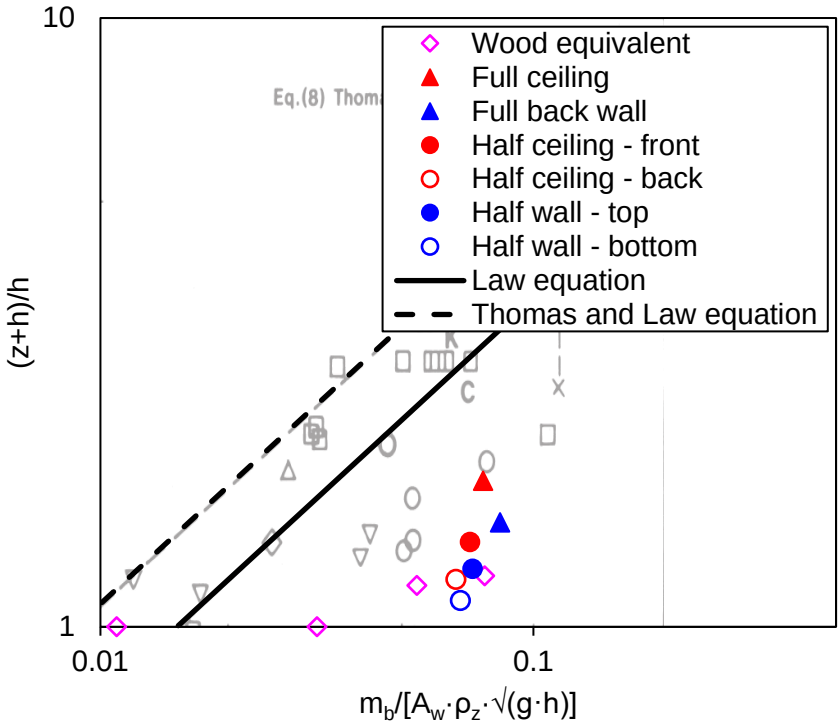

Figure 7.3. Law correlations for experiments of Phase 2 and 3.

The presence of timber on the ceiling (both fully and half exposed length) led to taller flaming regions in the external plume. A higher burning rate and higher temperature gases resulted in higher normalised mass loss rate values for the exposed timber wall.

Remarkably, the normalised mass loss rate for the ceiling and wall halves had almost the same values for the configurations that were closer to the opening (i.e. the front half of the ceiling and the top half of the wall, respectively). As external flames were higher for the ceiling scenarios, it demonstrates that the ceiling presents the most ominous exposed configuration for external fire spread, when compared to the wall of the same dimensions.

7.3.1.3 Lee et al.

Lee et al. [82] proposed a correlation of the external flame height to the external HRR. Potentially, this model could be used to predict flame heights for timber lined compartments. The full dataset of the present thesis was used with the proposed model and plotted in Figure 7.4.

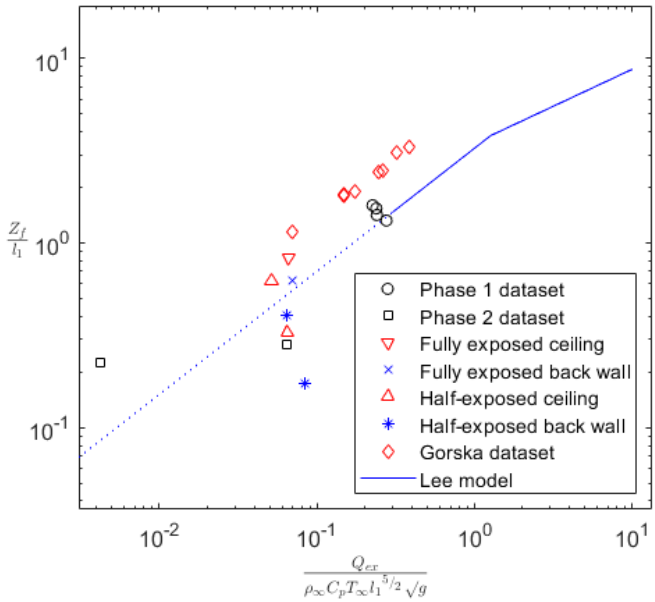

Figure 7.4. Flame height to external HRR model by Lee et al.; all datasets are plotted and compared to the extension of the current model.

There seems to be a trend in the data generated by this model; nevertheless, there is deviation of the model where data from timber compartments were used (for the present experimental campaigns and Gorksa's dataset). This indicates that compartments with exposed linings present a challenge for the model to accurately capture their behaviour. Alongside this, compartments that did not have severely under-ventilated conditions (i.e. all the half-exposed linings and the inert compartment experiments) were not represented adequately by the model's extension for low values.

Lee et al. also informed Yokoi's model with the modern understanding on plume theory. The updates included the consideration of the gas density used in the calculations. Modern plume theory dictates the use of the ambient gas

density, instead of the hot gas density. Furthermore, Lee et al. developed two different length scales:

- l_1 represents the width (parallel to the opening width) of the base of a virtual, equivalent plume burning outside the compartment.
- l_2 represents the required length for the buoyancy to dominate over the momentum, leading the plume to a vertical spread instead of horizontal. This length scale is the length (perpendicular to the compartment opening) of the base of the virtual plume burning outside the compartment.

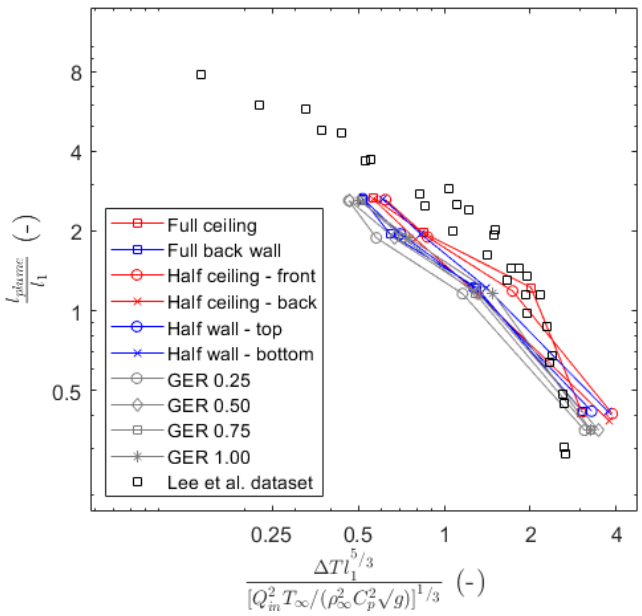

Figure 7.5. Non-dimensional temperatures compared to the normalised axis length of the plume's centerline for the current dataset and Lee et al..

They reported better data correlation [84] using these length scales (l_1 in particular), compared to the r_0 scale proposed by Yokoi. Figure 7.5 shows the present datasets plotted in the proposed equation formation by Lee et al., and in comparison with their dataset; this affords a relative comparison of the two experimental programmes.

The timber configurations present slightly higher non-dimensional temperatures for the lower heights in comparison to the inert configurations.

Furthermore, both the current dataset and that of Lee et al. collapse into one trendline; this demonstrates that both the contemporary understanding of entrainment and the proposed length scale by Lee et al. can capture the phenomena for the current datasets more adequately.

There are no pronounced deviations among the inert and timber-lined experiments of the present dataset, and the dataset of Lee et al.. The agreement shows that the current models satisfactorily capture the behaviour of both inert and lined compartments.

7.3.2 The Lee et al. heat flux model and Gorska's modifications

Lee et al. developed a heat flux model for the façade [82], based on the external heat release rate, the average flame height, and the characteristic length scale l_1. This model was developed for inert compartments, using a methane and/or propane burner. The main assumptions used in this model were that (1) the compartment is ventilation-controlled; and (2) the fuel, and as a result the fire, is located on the compartment floor.

Gorska performed an experimental campaign, using a pool fire as the fuel/heat source. The key difference was that she included combustible timber linings; that changes one of the fundamental assumptions of the model by Lee et al., that the fuel is only located at the floor. Gorska's dataset deviated from that of Lee et al.; she observed a pattern regarding timber compartments' continuous and intermittent external flaming, and the smoke plume regions. The lined compartments consistently exhibited higher heat fluxes in the continuous region; the discrepancy was less in the intermittent region; finally, in the plume region the inert compartments exhibited higher normalised heat fluxes compared to the timber-lined counterparts.

In an attempt to show where the current thesis' experimental results fit within the aforementioned experimental programmes ([9], [82]), all datasets produced, for which external flame heights and heat fluxes were reported, are plotted in Figure 7.6.

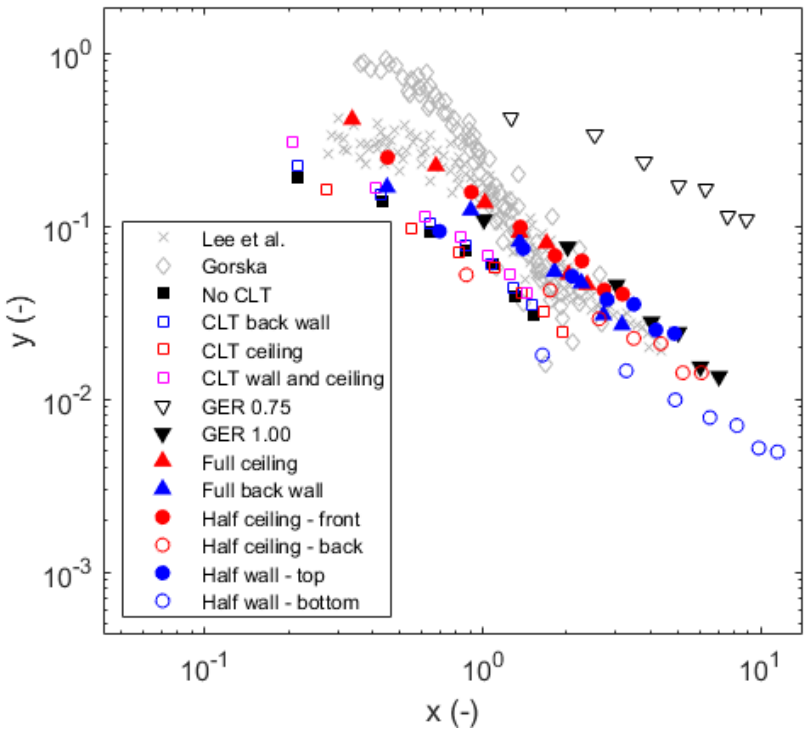

Figure 7.6. Proposed heat flux model for façades by Lee et al. for 'x' and 'y' terms.

In Figure 7.6, the Lee et al. model [82] correlates two terms:

- The 'x' term is the normalised height $\frac{Z}{Z_f}$, where Z is the net height above the top of the opening (m); and Z_f is the mean recorded flame height (m).
- The 'y' term is $\frac{\dot{q}''_t Z_f e^{0.6(\frac{H}{l_1})}}{\dot{Q}_{ex}/l_1}$, where $\dot{q}''_t$ is the normalised heat flux at height Z above the opening (kW/m^2); H is the height of the opening (m); l_1 is the proposed length scale by Lee et al. [82] (m); $\dot{Q}_{ex}$ is the external HRR (kW).

To some surprise, the results of the inert compartment's experimentations did not completely fit over the dataset by Lee et al.; in fact, the GER 0.75 was an outlier from the trendline of this dataset and the ones used for a comparison. At the same time, compartments with exposed timber did not match at all Gorska's data – in fact, there was a match of the data from Phases 2 and 3 (in

some cases) with Lee's inert compartment experiments. The Phase 1 experiments were consistently lower than Lee's data.

The experiments of this phase (Phase 3) violated Lee's model assumption in one of two ways:

- For the full-length lined compartments, only the assumption about the fuel location was no longer valid, as the compartments were under-ventilated;
- For the half-length lined compartments, both assumptions collapse. This is due to the fact that (a) multiple surfaces were burning and (b) the compartment's oxygen concentration at the door was, on average, 5%.

If one was to use the full dataset to create a heat flux model, this could be done with a single line prediction, as presented in Figure 7.7.

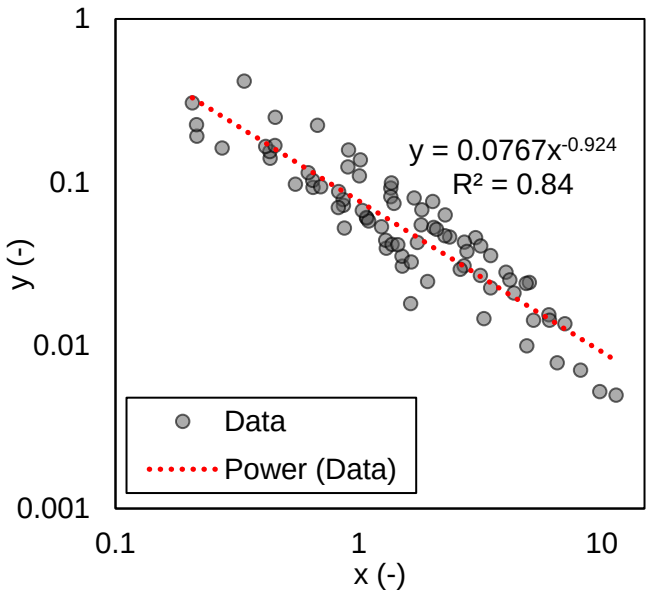

Figure 7.7. Different fit model based on all the data of this thesis

(x = $\frac{Z}{Z_f}$; y = $\frac{\dot{q}''_t Z_f e^{0.6(\frac{H}{l_1})}}{\dot{Q}_{ex}/l_1}$).

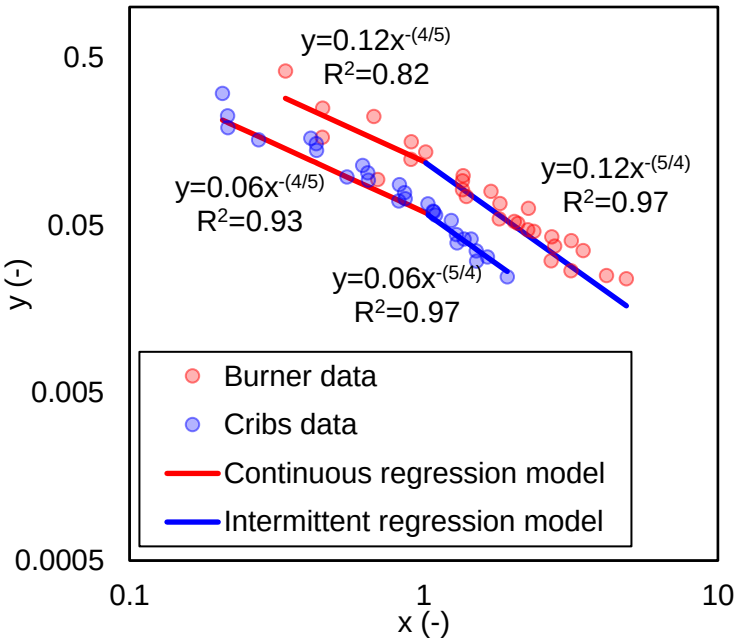

Figure 7.8. Wood crib and propane burner data with the resulting regression models for the continuous/intermittent flaming region and the intermittent/smoke plume region (x = $\frac{Z}{Z_f}$; y = $\frac{\dot{q}''_t Z_f e^{0.6(\frac{H}{l_1})}}{\dot{Q}_{ex}/l_1}$).

Upon closer examination of the dataset, a pattern arose. The data could be divided in two distinct categories: (1) the wood crib experiments; and (2) the propane burner experiments. Once the two datasets are split, a two-line trend becomes more apparent. This is shown in Figure 7.8.

The data used in the case of the burner study were the full-length timber experiments, and the half-length of the ceiling front and the top of the back wall; these were more in-line with the full-length respective surfaces. Apart for the continuous front of the burner, where the data were more scattered in relation to the regression model, the rest of the models had a very strong correlation to their respective datasets ($R^2 \approx 0.95$).

Notably, the individual regression model for the crib experiments is half of the propane burner experiment. The deviation could be an indication of the different fuel source. The burner ejected propane into the compartment space through small holes at the full length of the burner's pipes. This could have

affected the velocities in the compartment, since the average velocity of the burner was approximately 30 mm/s; a mean mass loss rate of the crib experiments was 0.4 mm/s (two orders of magnitude lower). Higher ejected velocity of the gases from the compartment could lead to less fuel burning in the compartment; more fuel exiting would lead to taller flames externally, and as a result, higher non-dimensional heat fluxes.

An average two-line regression model of the two datasets was produced and the correlation to all the data (with exception of the GER 0.75 ones) is illustrated in Figure 7.9. This two-line model is based on the following equations:

$$\begin{cases} y = 0.09x^{-\frac{4}{5}}, for\ x < 1\ (continuous\ flame\ front) \\ y = 0.09x^{-\frac{5}{4}}, for\ x > 1\ (intermittent\ flame\ front) \end{cases} \quad (29)$$

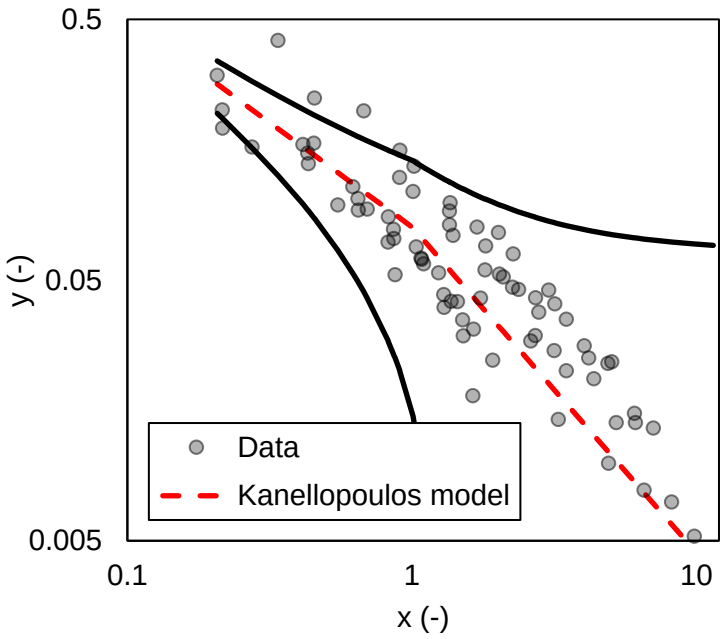

Figure 7.9. Two-line model for the full dataset of the thesis (black lines indicate the standard deviation of the model) (x = $\frac{Z}{Z_f}$; y = $\frac{\dot{q}''_t Z_f e^{0.6(\frac{H}{l_1})}}{\dot{Q}_{ex}/l_1}$).

The correlation of the two-line model to the complete dataset is strong ($R^2 \approx 0.85$). Using this model, data prediction was attempted, in order to demonstrate the model's performance. The model of Gorska was also used as a comparison of prediction.

To begin with, certain variables should be estimated in order to work on the final model. These are as listed below.

- The external heat release rate: there are two ways to pursue this. The first is to measure it directly at the opening, which is possible in a lab scenario, but not practical from a real life perspective. The second way would be to try and estimate it. This presents an issue with whether the compartment is ventilation controlled or not; this is a challenge for all the half-length experiments.

  It is mentioned in Gorska's work that the external HRR is the most critical variable of the heat flux model equation. This might present a specific challenge for the aforementioned reasons. Gorska's suggested model is:

$$\dot{Q}_{ex} = \dot{Q}_{tot} - 3000 \cdot 0.4 \cdot A_w \sqrt{H} \qquad (30)$$

  where $\dot{Q}_{tot}$ is the total convective HRR (kW); and $\dot{Q}_{ex}$ is the external HRR (kW).

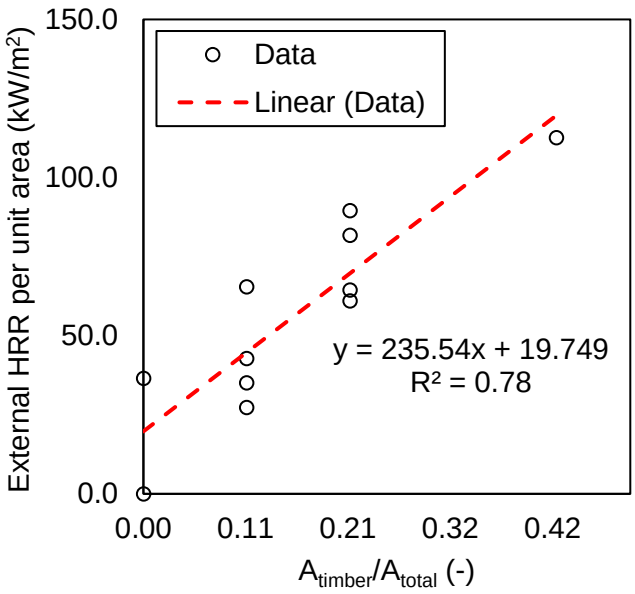

Figure 7.10. Correlation of the calculated external heat release rate per unit floor area to the ration of exposed timber to the total internal area (excluding floor and opening area) in the current experimental setup.

Alternatively, a relationship based on the total exposed timber surfaces in the enclosure could be used, using the experimental products of this thesis. The correlation is depicted in Figure 7.10.

A linear correlation of the $\dot{Q}_{ex}$ (multiplying the equation with the floor area in these experiments, i.e. 0.49 m^2) and the percentage of exposed timber in this experimental programme is:

$$\dot{Q}_{ex} = 115.4 \frac{A_{CLT}}{A_{total}} + 9.7 \quad (31)$$

- The average flame height: that can be determined from a relationship with the measured external HRR. Plotting measured flame heights to the measured external HRR has a correlation as shown in Figure 7.11.

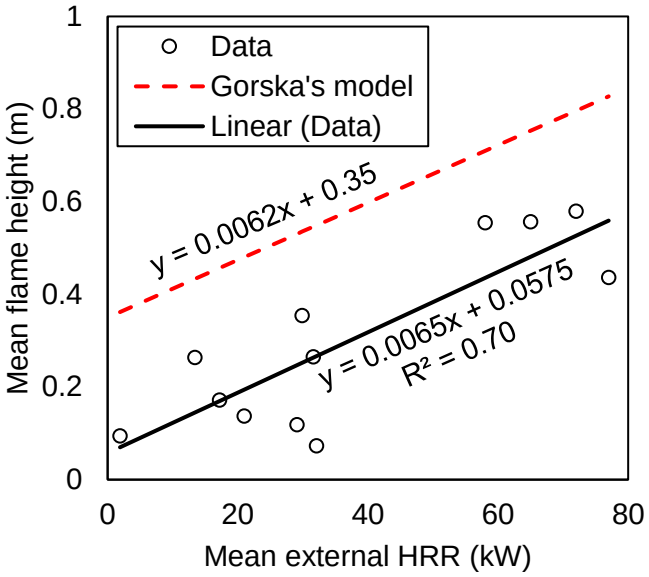

Figure 7.11. Time-averaged flame height to external HRR for the experimental configurations in all different experimental programmes. The Gorska model is plotted as a comparison to the resulting correlation (red dashed line).

The resulting relationship of flame height to external HRR is:

$$z_f = 0.0065 \cdot \dot{Q}_{ex} + 0.0575 \tag{32}$$

There is a visible deviation of the above flame height prediction equation to the one Gorska proposed, based on her dataset. Nevertheless, both shall be used to demonstrate their fitness (or lack thereof) for the purpose of a working prediction model.

- The heat flux model, based on equation (29) is:

$$\dot{q}''_{inc} = \frac{0.09\left(\frac{z}{z_f}\right)^m \dot{Q}_{ex}}{l_1 z_f e^{0.6\left(\frac{H}{l_1}\right)}} \tag{33}$$

The value of m is dependent of the z/z_f ratio:

- for values below 1, $m = -4/5$;
- for values above 1, $m = -5/4$.

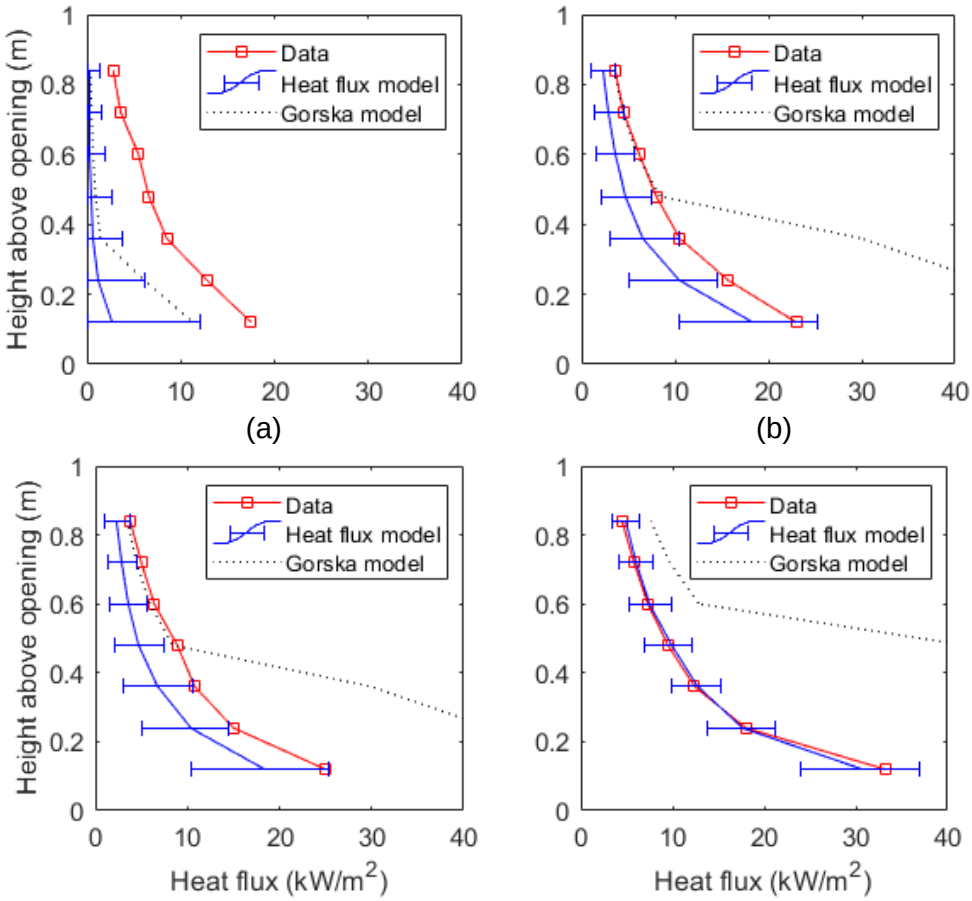

Figure 7.12. Heat flux model comparison for all Phase 1 (wood cribs) configurations: (a) No timber; (b) Timber back wall; (c) Timber ceiling; (d) Timber wall and ceiling.

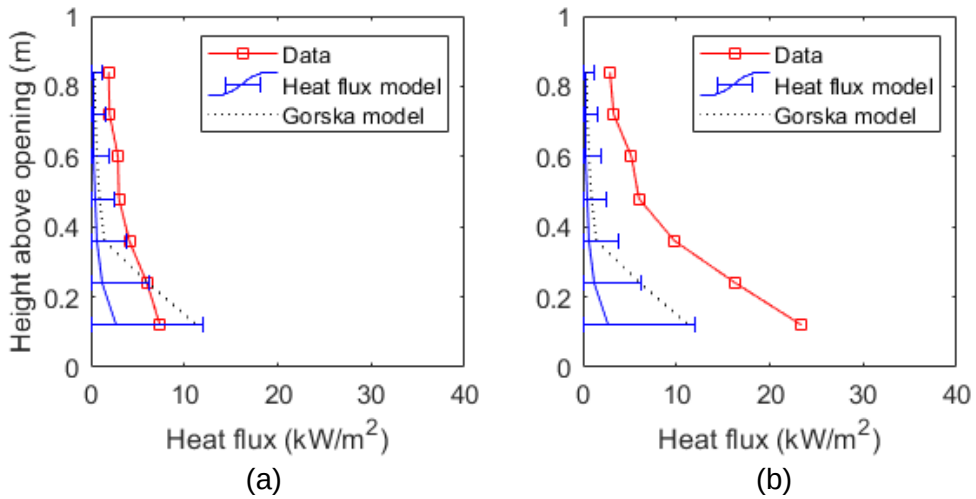

Figure 7.13. Heat flux model comparison for Phase 2 (propane burner) configurations that had external flaming: (a) GER 0.75; (b) GER 1.00.

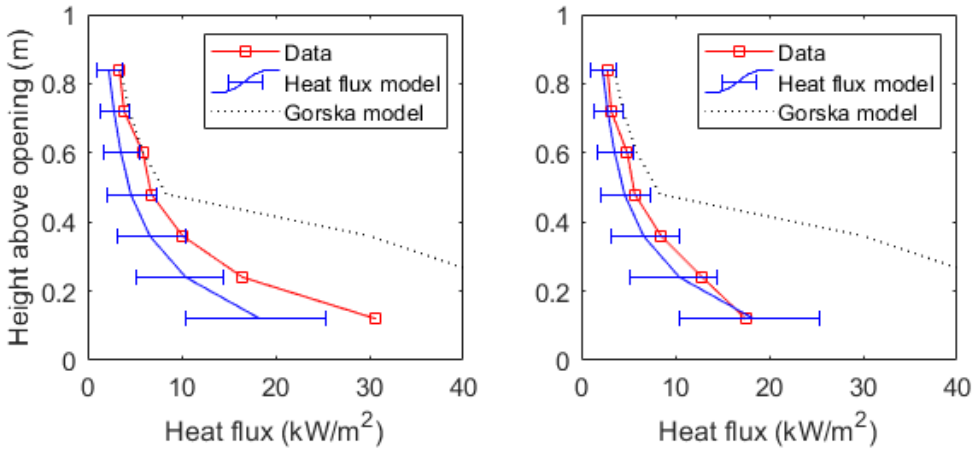

Figure 7.14. Heat flux model comparison for the fully exposed experiments of Phase 3 (propane burner) configurations: (a) Ceiling; (b) Back wall.

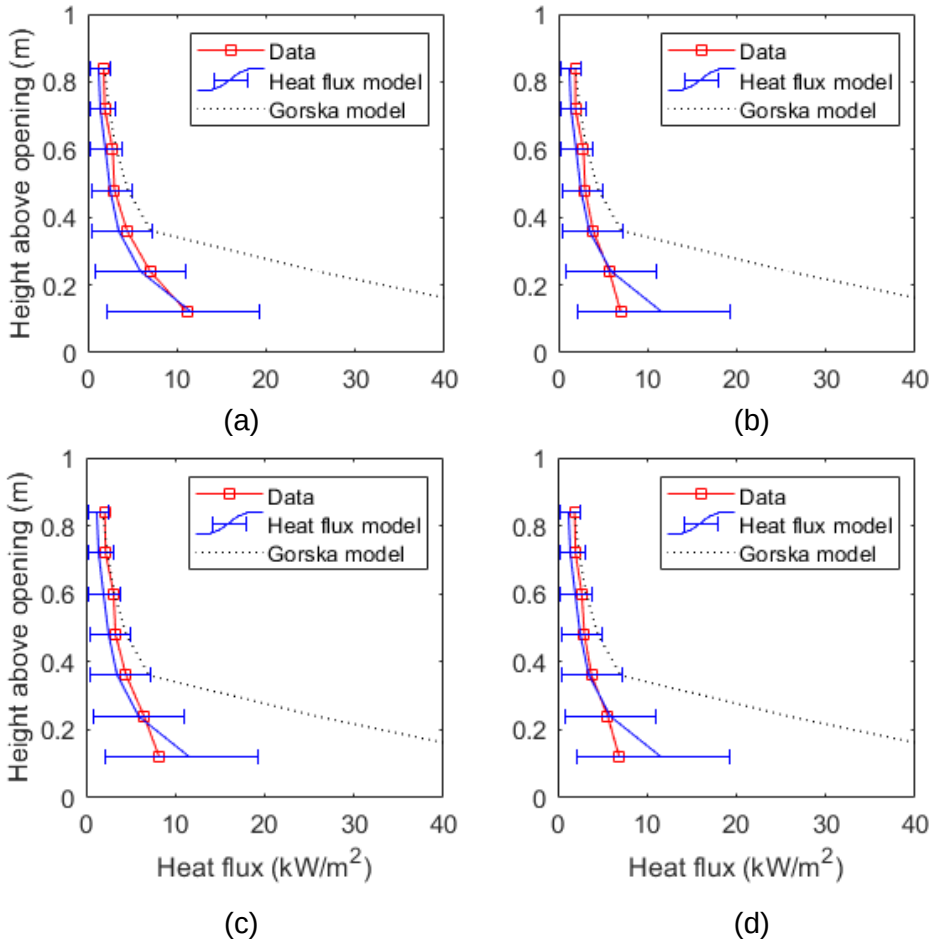

Figure 7.15. Heat flux model comparison for the half-length exposed timber experiments of Phase 3 (propane burner) configurations: (a) Ceiling - front; (b) Ceiling – back; (c) Back wall – top; (d) Back wall - bottom.

The resulting values of applying the newly formed model are plotted against the measured values in Figures 7.12 – 7.15. Gorska's model was used as a comparison, following the method as reported in her dissertation [9, pp. 171–172]. The external HRR was input into her model based on the equation (31).

7.3.2.1 Wood crib experiments

The inert compartment case was not represented appropriately by the heat flux model. However, models, like the one suggested by Lee et al., could be applicable, as that model was designed based on inert compartment fires. The rest of the exposed timber experiments are fitted well by the new model (accounting for the standard deviation).

7.3.2.2 Propane burner experiments

Similarly to the wood cribs experiments, the inert boundary experiments with the propane burner also failed to be captured by the heat flux model. The data from the GER 0.75 experiment were almost within the bounds of the model; the ones from the GER 1.00 are not represented appropriately by either model.

The model provides more predictions for the case of full-length exposed timber surfaces. It satisfactorily captures the trend of the exposed back wall and the error bars envelope the recorded heat fluxes, thus providing a conservative estimation. On the other hand, the model fails to capture the incident heat fluxes from the exposed ceiling. It becomes clear that there is an underestimation of the hazard from the exposed ceiling, as the model only considers the relation of HRR to the ratio of A_{timber}/A_{total}, not accounting for orientation.

Finally, the model centerline appears to be close to the actual heat flux measurements made for the half-length exposed timber. If one was to take the error bars into consideration, the model provides a prediction that errs to the side of caution, by overestimating, in some configurations, the incident heat flux.

Overall, comparing to the pre-existing models by Lee et al. and Gorska, the currently developed model shows a good prediction with regards to the

exposed timber surfaces (especially for the half-length parts, which fall in the range of the well-ventilated compartments). Gorska's model has merits and is applicable for the smoke region of the plume, as the predictions were closely matched to the actual measurements. However, the model struggled to fit over the measured data at the lower levels close to the flaming region as, with a few exceptions, it over-predicts the timber's contribution.

7.4 Summary of findings

The analysis presented herein aimed to: (1) assess whether classic plume theory adequately represents the external plume behaviour from timber-lined compartments; (2) reveal the drivers behind external plume behaviour; and (3) provide models to predict plume temperatures and incident heat fluxes on the façade from exposed timber compartments.

7.4.1 **Classic plume theory**

Yokoi's method is valid for estimating flame temperatures; however, the measurements deviate, when different experimental setups are used. Lee et al. suggested updates to incorporate the current perception of plume theory and introduced a new length scale. The data satisfactorily collapse in a more compact trend, suggesting that dependencies on experimental setup can be removed with the suggested modification by Lee et al..

Law's correlation is only fit for compartments with no obstructions above the opening (i.e. façade). Despite this fact, it became a tool for comparison for different timber lined configurations. The compartments that had the same normalised mass loss rate would present different flame heights, depending on the timber configuration inside. Ceilings always had higher values when compared with a wall configuration with the same normalised burning rate.

7.4.2 **Modern approaches to external plumes**

Lee et al. also proposed a model to predict the mean flame height based on a normalised external HRR. This model fails to account for the location of timber.

Aside from the flame temperature distribution and average flame heights based on the HRR, Lee et al. also presented a heat flux model for the façade. Gorska showed that adjustments need to be made, if one intends to use this for timber construction. In the present work, a dependency was revealed; this was either based on the scale of the experiment or the experimental setup and fuel source used. The fuel source dependency could be more strongly suggested, as the datasets produced in this thesis could be split in two distinct categories: (1) the wood crib experiments; and (2) the propane burner experiments. Based on these, a two-line exponential model was developed, as an average of the two distinct datasets (cribs and burner).

This newly developed model (Section 7.3.2) was used to predict the heat fluxes on the façade. For the wood crib experiments, the model was challenged as the predictions were underestimating the inert and the exposed ceiling configurations. A better prediction was made for the back wall; the two exposed surfaces had a strong fit with the model centreline. For the propane burner experiments, again, the inert compartments were challenging. Where timber was exposed, the model was able to predict the trend and values were close to the experimental data. The exposed ceiling presented more of a challenge to the model, as flames were taller and closer to the façade; this is not something that can be predicted only by a ratio of exposed timber in the compartment, as the dimensions were identical for the back wall. Nevertheless, the model gave a good prediction for the back wall. The model also expanded the previous predictive capabilities of both Lee et al. and Gorska, as it included timber lined compartments with well-ventilated conditions. These were covered by the model centreline; any over-estimation simply gives a more conservative estimation of the actual values.

This page intentionally left blank.

Chapter 8 - Conclusions and future work

The dissertation covered a range of different experimental approaches, in order to understand if and how external fire spread is affected by the presence of timber linings.

8.1 Conclusions

To begin with, the literature review showed the knowledge gap between timber-lined compartment fires and external fire spread. So far, these two topics have been studied separately. Research in compartment fires with timber linings has been more focused on extinction, with exception of the latest work by Gorska [9]. External fire spread has been studied extensively for compartments with non-combustible linings. The two research topics needed to be coupled; this work aimed to fill in some of the knowledge gaps in this joint research area.

As it was established throughout three experimental programmes, timber changes the hazard of a compartment fire with respect to external spread. The first experimental campaign definitively showed that excess fuel is produced, when timber is exposed in the compartment interior. Excess fuel, unless the compartment is well-ventilated, it will exit through openings and burn outside; this produces higher heat fluxes, as more energy is released in the form of heat and light.

8.1.1 **Mass loss rate**

The mass loss rate is affected by exposing timber linings in the enclosure. The mass loss rate of exposed timber was estimated; depending on the type of fuel used and the nature of the linings, values on the back walls differed from the exposed ceiling ones. The propane burner experiments with low density insulation led to higher mass loss rate for the exposed back wall; this supports the literature perception for medium-scale experiments. On the other hand, the exposed ceiling had higher mass loss rate when high density inert linings

where used with wood cribs; this aligned with the large-scale experimentation from Gorska and co-workers [9].

8.1.2 **Heat fluxes**

External flames had more volume for timber-lined compartments, as higher mass loss rates and under-ventilated conditions led to more fuel burning outside. The configuration of the exposed timber affected the shape of the external plume; taller and thinner flames were produced from exposed ceilings whereas shorter and thicker ones were observed for exposed back walls.

Heat fluxes on the façade are generally higher for exposed timber compartments; approximately 60% for two exposed surfaces; 20-30% higher for one exposed surface. For one exposed surface, heat fluxes were higher for a fully exposed timber ceiling. Where half surfaces were used, the front of the ceiling created higher heat fluxes; the top half of the wall was responsible for the second higher heat fluxes, potentially indicating a mixing-time issue, since both bits are closest to the exit point.

In the case of heat fluxes opposite, the distance from the opening is of paramount importance; very close-range measurements tend to be dominated by the opening's irradiance; further field measurements reveal that heat fluxes rise proportionally as more timber gets exposed. Heat fluxes were consistently higher for the back wall configurations (whether fully or partly exposed). Higher velocities were recorded for these configurations; this helps to explain the phenomenon, as the heating surface would be closer to the measuring point opposite.

There are no notable correlations of the mass loss rate to the heat fluxes on the façade, indicating a weaker correlation as noted in Drysdale's book [75].

The Lee et al. proposed model to correlate flame heights with external HRR failed to describe the inert compartment datasets. The extrapolation of the model's line could be proven beneficial for timber compartments, however requiring further investigation.

8.1.3 Global equivalence ratio

The global equivalence ratio (GER) can only serve as an indicator of external flaming. It is strongly dependent on the accuracy of mass loss rate used and entrainment into the compartment; for this, it cannot be used as a prediction tool, but more like an indicative metric. GER was increased 12-38% for exposed timber compartments, depending on the inflow calculation technique used and the number of exposed timber surfaces.

The burning factor was devised by Bartlett and Law. Similar to their findings, the burning factor does not produce a meaningful correlation with GER at the steady state phase; however, it was established that it does correlate well with GER at the decay phase.

8.1.4 Buoyancy, momentum, and gas trajectories

Timber presence on the ceiling affects the hot gas trajectory. All the exposed back wall configurations just followed the trajectory of the baseline, potentially indicating a shift of the trajectories only with exposed timber on the ceiling.

Compared to a baseline with the inert compartments, fully exposed timber drove flames further away from the opening. Conversely, part-exposed timber on the ceiling had lower velocities and generally was just driven up by buoyancy, resulting in plumes that were closer to the opening plane.

Analysis of the buoyancy and momentum forces showed an upward trend, when timber is exposed in the compartment space. However, the ratio of the two forces is similar regardless of position. This could suggest that the external combustion is influenced by the mixing time of fuel and air.

8.1.5 Yokoi, Lee et al., and Gorska's models

Yokoi’s model was proven adequate in the general sense; however, it lacks refinement since experiments undertaken by different researchers (present work included) do not fall under the same model line as his dataset. The Thomas and Law correlation is only helpful as an internal assessment tool, due to the fact that their formula is applicable only for compartments without a

façade above the opening. On plume behaviour, the complete dataset showed that Yokoi's model, with some alteration suggested by Lee et al., can be a valid tool to calculate external temperature distribution. The current dataset coincided with the one from Lee et al. when the modified Yokoi/Lee et al. model was employed.

Lee also developed a heat flux model correlated to external HRR; Gorska modified this to fit her timber dataset. Due to the fact that this model fails to capture the behaviour of the present dataset, alterations were made.

8.1.6 **Novel model**

The novel model fails to predict the inert compartment heat flux distribution on the façade, as data used to develop the correlations are in majority from timber-lined compartments. However, good predictions (accounting for the error bars) are made for the exposed timber compartments in almost all cases. This model appears to be sensitive on the input parameters (HRR, flame heights); due to this, a larger dataset is needed to remove the variations of that can (and did) occur with just two datasets.

8.2 Future work

Work in the future can solve ambiguities and uncertainties that arose in this thesis. The author suggests some potentially interesting ways forward:

- The trajectories appeared to be affected by the presence of timber on the ceiling that could not be explained by momentum and buoyancy alone. Further investigation could reveal whether that was a specific setup dependency, or an effect of the timber in the specific configuration.
- There is an ambiguity when different datasets are examined on which surface (if any of them) presents a higher burning rate. Experimental scale was suggested by data to come into effect with this issue, effectively promoting further questions.
- Experimental setup dependencies appear to exist for the heat flux model by Lee et al. These can be removed by understanding the extent

to which the fuel source, the compartment boundaries, and the combustible linings are responsible for changes in the model.

- Lack of large-scale experimentation leads to questions of whether these medium scale compartment fires are adequately representing reality. More real scale programmes should be carried out, to clarify the validity or not of the smaller scale experiments.
- This dataset produced during this experimental programme comes to complement missing information of datasets by other researchers. These datasets can be used to develop and/or validate modelling tools, and thus furthering the communities understanding of the phenomenon.

This page intentionally left blank.

References

[1] F. Mills, “Top 5: The World’s Tallest Timber Buildings,” 2017. https://www.theb1m.com/video/top-5-the-world-s-tallest-timber-buildings (accessed Jun. 15, 2018).

[2] T. Ravenscroft, “What is Cross Laminated Timber (CLT)?,” 2017. https://www.theb1m.com/video/what-is-cross-laminated-timber-clt (accessed Jun. 17, 2018).

[3] R. Cavendish, “The Great Fire of Rome | History Today.” https://www.historytoday.com/archive/months-past/great-fire-rome (accessed May 08, 2019).

[4] “After The Fire • Great Fire Of London,” *Great Fire Of London*. https://greatfireoflondon.net/after-the-fire/ (accessed May 08, 2019).

[5] H. com Editors, “Chicago Fire of 1871,” *HISTORY*. https://www.history.com/topics/19th-century/great-chicago-fire (accessed May 06, 2019).

[6] R. Emberley, “Fundamentals for the Fire Design of Cross Laminated Timber Buildings,” PhD Thesis, 2017.

[7] R. M. Hadden *et al.*, “Effects of exposed cross laminated timber on compartment fire dynamics,” *Fire Saf. J. - Proc. 12th Int. Symp.*, vol. 91, no. February, pp. 480–489, 2017, doi: 10.1016/j.firesaf.2017.03.074.

[8] A. I. Bartlett, “Auto-Extinction of Engineered Timber,” PhD Thesis, The University of Edinburgh, 2018.

[9] C. Gorska, “Fire dynamics in multi-scale timber compartments,” PhD Thesis, The University of Queensland, Brisbane, QLD, Australia, 2019.

[10] F. Wiesner, F. Randmael, W. Wan, L. A. Bisby, and R. M. Hadden, “Structural response of cross-laminated timber compression elements exposed to fire,” *Fire Saf. J.*, vol. 91, pp. 56–67, Jul. 2017.

[11] F. Wiesner *et al.*, “Requirements for engineered wood products and their influence on the structural fire performance,” Seoul, Republic of Korea, Aug. 2018.

[12] F. Wiesner, D. Bell, L. Chaumont, L. A. Bisby, and S. Deeny, “Rolling shear capacity of clt at elevated temperature,” Seoul, Republic of Korea, Aug. 2020.

[13] “Trends in wood buildings.” https://www.awc.org/pdf/greenbuilding/wood_and_greening.pdf (accessed Apr. 18, 2019).

[14] N. Keipour, H. R. Valipour, and M. A. Bradford, “Experimental study of steel-timber composite (STC) beam to steel column joints having a flush end-plate,” *Eng. Struct.*, vol. 174, pp. 906–918, Jan. 2018.

[15] “Dalston Works - The world’s largest CLT building,” 2017. http://waughthistleton.com/dalston-works/ (accessed Jul. 29, 2018).

[16] “Engineered wood.” https://en.wikipedia.org/wiki/Engineered_wood (accessed Apr. 21, 2019).

[17] P. Hargest, “Making the cut: Is cross-laminated timber safe?” https://buildingresiliencecoalition.org/making-the-cut-is-cross-laminated-timber-safe/ (accessed Apr. 30, 2019).

[18] “Forte Living.” https://www.woodsolutions.com.au/inspiration-case-study/forte-living (accessed Jul. 11, 2018).
[19] D. Shearing, “Dalston Works.” http://www.architecturetoday.co.uk/dalston-works/ (accessed Apr. 30, 2019).
[20] Naturally:wood, “Brock Commons Tallwood House.” https://www.naturallywood.com/emerging-trends/tall-wood/brock-commons-tallwood-house
[21] A. Frearson, “Hawkins\Brown pairs cross-laminated timber and steel for record-breaking apartment block.” https://www.dezeen.com/2015/09/25/hawkins-brown-cross-laminated-timber-steel-apartment-block-housing-shoreditch-london/ (accessed Apr. 30, 2019).
[22] “The Cube / Hawkins\Brown.” https://www.archdaily.com/774172/the-cube-hawkins-brown/5601f561e58ece38c1000090-the-cube-hawkins-brown-photo (accessed Apr. 30, 2019).
[23] F. Maier, “Jackson Hole Airport in Wyoming.” https://www.detail-online.com/article/jackson-hole-airport-in-wyoming-16648/ (accessed Apr. 30, 2019).
[24] M. Green, “Why we should build wooden skyscrapers,” 2013. https://www.ted.com/talks/michael_green_why_we_should_build_wooden_skyscrapers/transcript (accessed Jul. 11, 2018).
[25] J. McKnight, “Michael Green completes largest mass-timber building in United States.” https://www.dezeen.com/2016/12/02/michael-green-architecture-t3-largest-mass-timber-building-usa-minneapolis-minnesota/ (accessed Jan. 05, 2019).
[26] “Rethinking Timber Buildings,” Arup, London, Mar. 2019.
[27] Waugh Thistleton Architects, “100 projects - UK CLT.” 2018.
[28] F. Mills, *Top 5: The World’s Tallest Timber Buildings*. 2017.
[29] “First Timber Arrives at the World’s largest Engineered Timber Office Building,” 2018. https://brisbanedevelopment.com/first-timber-arrives-at-the-worlds-largest-engineered-timber-office-building/ (accessed Jan. 05, 2019).
[30] “Hackney puts wood first,” 2012. http://apps.hackney.gov.uk/servapps/newspr/NewsReleaseDetails.aspx?id=2437 (accessed Jul. 11, 2018).
[31] “The Cube / Hawkins\Brown,” *ArchDaily*, Sep. 28, 2015. http://www.archdaily.com/774172/the-cube-hawkins-brown (accessed May 02, 2019).
[32] “Leilighet type 1 | Treet.” http://treetsameie.no/om-leilighetene/ (accessed May 02, 2019).
[33] “Brock-Commons-Interior,” *Archpaper.com*. https://archpaper.com/2018/01/united-states-timber-industry-europe-canada/brock-commons-interior/ (accessed May 02, 2019).
[34] P. H. Thomas and A. J. M. Heselden, “Fully Developed Fires in Single Compartments - A co-operative research programme of the Conseil International du Batiment (CIB report No. 20),” *Fire Res. Note*, no. 923, Aug. 1972.

[35] J. L. Torero, A. Majdalani, C. Abecassis-Empis, and A. Cowlard, “Revisiting the compartment fire,” *Fire Saf. Sci. - Proc. Elev. Int. Symp.*, pp. 28–45, 2014.

[36] R. M. Hadden *et al.*, “Effects of exposed cross laminated timber on compartment fire dynamics,” *Fire Saf. J. - Proc. 12th Int. Symp.*, vol. 91, no. February, pp. 480–489, 2017, doi: 10.1016/j.firesaf.2017.03.074.

[37] A. I. Bartlett *et al.*, “Auto-extinction of engineered timber: Application to compartment fires with exposed timber surfaces,” *Fire Saf. J.*, vol. 91, no. February, pp. 407–413, 2017, doi: 10.1016/j.firesaf.2017.03.050.

[38] R. Emberley *et al.*, “Description of small and large-scale cross laminated timber fire tests,” *Fire Saf. J.*, no. February, pp. 1–9, 2017, doi: 10.1016/j.firesaf.2017.03.024.

[39] D. Drysdale, *An introduction to fire dynamics*, Third edit. John Wiley & Sons, Ltd., 2011. doi: 10.1016/0379-7112(86)90046-9.

[40] X. Dai, S. Welch, and A. Usmani, “A critical review of ‘travelling fire’ scenarios for performance-based structural engineering,” *Fire Saf. J.*, vol. 91, pp. 568–578, Jul. 2017, doi: 10.1016/j.firesaf.2017.04.001.

[41] C. L. Wu and R. Carvel, “An experimental study on backdraught: The dependence on temperature,” *Fire Saf. J.*, vol. 91, pp. 320–326, Jul. 2017, doi: 10.1016/j.firesaf.2017.04.003.

[42] “The Great Fire of Rome | Background | Secrets of the Dead | PBS,” *Secrets of the Dead*, May 29, 2014. https://www.pbs.org/wnet/secrets/great-fire-rome-background/1446/ (accessed May 06, 2019).

[43] “Did Emperor Nero Really Start the Great Fire of Rome?,” *History Hit*. https://www.historyhit.com/did-nero-really-start-the-great-fire-of-rome/ (accessed May 06, 2019).

[44] “The Great Fire of London.” https://www.london-fire.gov.uk/museum/history-and-stories/the-great-fire-of-london/ (accessed May 05, 2019).

[45] “Chicago fire of 1871 | American history,” *Encyclopedia Britannica*. https://www.britannica.com/event/Chicago-fire-of-1871 (accessed May 06, 2019).

[46] “The O’Leary Legend,” *The Great Chicago Fire & The Web of Memory*. https://www.greatchicagofire.org/oleary-legend/ (accessed May 06, 2019).

[47] “Early fire brigades.” https://www.london-fire.gov.uk/museum/history-and-stories/early-fire-brigades/ (accessed Jan. 13, 2020).

[48] N. G. Society, “The Chicago Fire of 1871 and the ‘Great Rebuilding,’” *National Geographic Society*, Jan. 25, 2011. http://www.nationalgeographic.org/news/chicago-fire-1871-and-great-rebuilding/ (accessed May 08, 2019).

[49] G. Spinardi and A. Law, “Beyond the stable door: Hackitt and the future of fire safety regulation in the UK,” *Fire Saf. J.*, vol. 109, p. 102856, Oct. 2019, doi: 10.1016/j.firesaf.2019.102856.

[50] M. Law, “Heat Radiation from Fires and Building Separation,” Department of Scientific and Industrial Research and Fire Offices’ Committee, Joint Fire Research Organisation, Borehamwood, UK, Fire Research Technical Paper No. 5, 1963.

[51] K. Kawagoe, “Fire behaviour in rooms,” Tokyo, Japan, 27, 1958.
[52] L. A. Ashton and H. L. Malhotra, “External walls of buildings - Part I: The protection of openings against spread of fire from storey to storey,” Fire Research Station, Boreham Wood, Herts, 436, 1960.
[53] C. T. Webster and M. M. Raftery, “The Burning of Fires in Rooms - Part II: Tests with cribs and high ventilation on various scales,” no. 401-Fire Research Note, 1959.
[54] J. H. McGuire, “St. Lawrence Burns - Radiometer measurements,” Division of Building Research, Ottawa, 153, Dec. 1959.
[55] G. W. Shorter, J. H. McGuire, N. B. Hutcheon, and R. F. Legget, “The St. Lawrence Burns,” National Research Council, Ottawa, Ontario, Research Paper 98, Jun. 1960.
[56] J. H. McGuire, “Heat transfer by radiation,” *Fire Res. Spec. Rep. No 2*, 1953.
[57] M. Law, “Paper 2. Heat radiation from fires and building separation (Fire Research Technical Paper No. 5).” https://www.arup.com/perspectives/publications/books/section/engineering-fire-safety-some-selected-papers-from-margaret-law (accessed Jan. 13, 2020).
[58] *Approved Document B - Fire Safety (Vol. 1: Dwelling Houses)*. HM Government, 2010.
[59] *Approved Document B - Fire Safety (Vol.2 - Buildings Other Than Dwelling Houses)*. HM Government, 2009. doi: 10.1016/B978-0-7506-8580-1.00027-0.
[60] R. Chitty, “BR 187: External fire spread: Building separation and boundary distances,” BRE Trust, 187, 2010.
[61] “Fire Grading of Buildings - Part I: General principles and structural precautions,” His Majesty’s Stationery Office, London, Post-war Building Studies 20, 1946.
[62] L. A. Ashton, “A multi-storey building for experiments on the spread of fire and smoke,” Fire Research Station, Borehamwood, UK, Fire Research Note 279, Dec. 1956.
[63] British Pathé, *Fire Research (1961)*. Accessed: Jun. 05, 2019. [Online]. Available: https://www.youtube.com/watch?v=Z2gI2Wx9N4E
[64] A. Law and G. Kanellopoulos, “The rise and fall of the UK’s spandrel panel,” *Fire Saf. J.*, vol. 115, 2020, doi: 10.1016/j.firesaf.2020.103170.
[65] S. Yokoi, “Study on the prevention of fire-spread caused by hot upward current,” The Building Research Institute, Tokyo, Japan, 1960.
[66] D. Yung and I. Oleszkiewicz, “Fire spread via exterior walls of buildings,” presented at the The Fourth Conference on Building Science and Technology, Toronto, Ontario, Feb. 1988.
[67] I. Oleszkiewicz, “Fire Exposure to Exterior Walls and Flame Spread on Combustible Cladding,” *Fire Technol.*, pp. 357–375, Nov. 1990.
[68] J. Ondrus, “Fire Hazards of Facades with Externally Applied Additional Insulation,” Lund Institute of Technology, Lund, Sweden, LUTVDG/(TVBB-3021), Jun. 1985.

[69] P. H. Thomas and A. J. M. Heselden, “Fully-developed fires in single compartments - a co-operative research programme of the Conseil International du Batiment,” Aug. 1972.

[70] E. G. Butcher, G. K. Bedford, and P. J. Fardell, “Further experiments on temperatures reached by steel in building fires,” in *Joint Fire Research Organisation Symposium No. 2*, London, 1968, pp. 2–17.

[71] M. L. Bullen and P. H. Thomas, “Compartment fires with non-cellulosic fuels,” *Symp. Int. Combust.*, vol. 17, no. 1, pp. 1139–1148, 1979, doi: 10.1016/S0082-0784(79)80108-3.

[72] W. M. Pitts, “The global equivalence ratio concept and the formation mechanisms of carbon monoxide in enclosure fires,” *Prog. Energy Combust. Sci.*, vol. 21, no. 3, pp. 197–237, 1995, doi: 10.1016/0360-1285(95)00004-2.

[73] G. Kanellopoulos, A. I. Bartlett, and A. Law, “Investigation into global equivalence ratio and external plumes from timber lined compartments,” St. Petersburg, 2019, pp. 468–477. doi: 10.18720/SPBPU/2/k19-68.

[74] E. K. Asimakopoulou, D. I. Kolaitis, M. A. Founti, and K. Chotzoglou, “Characteristics of Externally Venting Flames and Their Effect on the Facade: A Detailed Experimental Study,” *Fire Technol.*, no. 52, pp. 2043–2069, Feb. 2016, doi: 10.1007/s10694-016-0575-5.

[75] D. Drysdale, *An introduction to fire dynamics*, Third edit. John Wiley & Sons, Ltd., 2011. doi: 10.1016/0379-7112(86)90046-9.

[76] S. Yokoi, “Study on the prevention of fire-spread caused by hot upward current,” The Building Research Institute, Tokyo, Japan, 1960.

[77] P. H. Thomas, C. T. Webster, and M. M. Raftery, “Some experiments on buoyant diffusion flames,” *Combust. Flame*, vol. 5, pp. 359–367, 1961, doi: 10.1016/0010-2180(61)90117-1.

[78] P. H. Thomas, “On the heights of buoyant flames,” Fire Research Station, Borehamwood, UK, Fire Research Note 489, Dec. 1961.

[79] P. H. Thomas and M. Law, “The projection of flames from burning buildings,” Fire Research Station, Borehamwood, UK, Fire Research Note 921, Jan. 1972.

[80] M. Law, “Fire safety of external building elements - The design approach,” *AISC Eng. J.*, no. Second quarter, pp. 59–74, 1978.

[81] K. M. Frank, H. Park, G. Baker, and C. Wade, “Vertical external fire spread from flames extending out of an opening,” BRANZ - Building Research Association of New Zealand, Judgeford, New Zealand, BRANZ Study Report SR 360.

[82] Y. P. Lee, M. A. Delichatsios, and G. W. H. Silcock, “Heat fluxes and flame heights in facades from fires in enclosures of varying geometry,” 2007. doi: 10.1016/j.proci.2006.08.033.

[83] M. A. Delichatsios, G. W. H. Silcock, X. Liu, M. Delichatsios, and Y. P. Lee, “Mass pyrolysis rates and excess pyrolysate in fully developed enclosure fires,” *Fire Saf. J.*, vol. 39, no. 1, pp. 1–21, 2004, doi: 10.1016/j.firesaf.2003.07.006.

[84] Y. P. Lee, M. A. Delichatsios, and Y. Ohmiya, “The physics of the outflow from the opening of an enclosure fire and re-examination of Yokoi’s

correlation," *Fire Saf. J.*, vol. 49, pp. 82–88, 2012, doi: 10.1016/j.firesaf.2012.01.001.

[85] A. H. Majdalani, "Compartment fire analysis for contemporary architecture," PhD Thesis, The University of Edinburgh, 2015. [Online]. Available: https://era.ed.ac.uk/handle/1842/9969

[86] R. Emberley *et al.*, "Description of small and large-scale cross laminated timber fire tests," *Fire Saf. J.*, no. February, pp. 1–9, 2017, doi: 10.1016/j.firesaf.2017.03.024.

[87] P. H. Thomas and A. J. M. Heselden, "Fully-developed fires in single compartments - a co-operative research programme of the Conseil International du Batiment," Conseil International du Batiment, CIB report 20, Aug. 1972.

[88] C. J. Bateman, A. I. Bartlett, L. Rutkauskas, and R. M. Hadden, "Effects of Fuel Load and Exposed CLT Surface Configuration in Reduced-Scale Compartments," 2018.

[89] R. M. Hadden *et al.*, "Effects of exposed cross laminated timber on compartment fire dynamics," *Fire Saf. J. - Proc. 12th Int. Symp.*, vol. 91, no. February, pp. 480–489, 2017, doi: 10.1016/j.firesaf.2017.03.074.

[90] A. I. Bartlett and A. Law, "Influence of excess fuel from timber lined compartments," *Constr. Build. Mater.*, no. 235, pp. 117355–117364, 2020, doi: 10.1016/j.conbuildmat.2019.117355.

[91] M. Law, "Heat Radiation from Fires and Building Separation," Department of Scientific and Industrial Research and Fire Offices' Committee, Joint Fire Research Organisation, Borehamwood, UK, Fire Research Technical Paper No. 5, 1963.

[92] C. Gorska Putynska, A. Law, and J. L. Torero, "An investigation into the effect of exposed timber on thermal load," in *24th Australasian Conference on the Mechanics of Structures and Materials*, 2016, pp. 939–944.

[93] "Micalite - Fire resistant board." https://www.fluehouse.com/pdfs_141/micalite-vermiculite-boards-datasheet.pdf (accessed Feb. 28, 2022).

[94] B. J. McCaffrey and G. Heskestad, "A robust bidirectional low-velocity probe for flame and fire application," *Combust. Flame*, vol. 26, no. C, pp. 125–127, 1976, doi: 10.1016/0010-2180(76)90062-6.

[95] R. Gardon, "An Instrument for the Direct Measurement of Intense Thermal Radiation," *Rev. Sci. Instrum.*, vol. 24, 1953, doi: https://doi.org/10.1063/1.1770712.

[96] "SBG01 heat flux meter." https://www.hukseflux.com/products/heat-flux-sensors/heat-flux-meters/sbg01-heat-flux-meter (accessed Feb. 15, 2020).

[97] A. I. Bartlett, G. Kanellopoulos, and A. Law, "Heat flux distribution on a facade from timber-lined compartments," Royal Holloway College, London, UK, Jul. 2019.

[98] J. P. Hidalgo, C. Maluk, A. Cowlard, C. Abecassis-Empis, M. Krajcovic, and J. L. Torero, "A Thin Skin Calorimeter (TSC) for quantifying irradiation during large-scale fire testing," *Int. J. Therm. Sci.*, vol. 112, pp. 383–394, 2017, doi: 10.1016/j.ijthermalsci.2016.10.013.

[99] T. Laschütza, “Numerical and experimental investigation of a Thin Skin Calorimeter (TSC),” Master’s thesis, The University of Edinburgh, Edinburgh, UK, 2017.
[100] “INCONEL® alloy 600,” *specialmetals.com*. https://www.specialmetals.com/documents/technical-bulletins/inconel/inconel-alloy-600.pdf (accessed Jul. 14, 2021).
[101] M. Janssens, “Calorimetry,” in *SFPE Handbook of Fire Safety Engineering*, Fifth., M. Hurley, Ed. New York, 2016, pp. 905–951.
[102] M. Dahlberg, “The SP Industries Calorimeter - For rate of heat release measurements up to 10 MW,” Swedish National Testing and Research Institute, SP Report 43, 1992.
[103] A. Glew, “The effect of timber compartment linings on external fire plumes,” Master’s thesis, The University of Edinburgh, 2019.
[104] F. Tang, L. Hu, Q. Wang, X. Zhang, K. Lu, and M. A. Delichatsios, “An experimental study on buoyant spilled thermal plume temperature profile from over-ventilated enclosure fires in a reduced air pressure,” *Procedia Eng.*, vol. The 9th Asia-Oceania Symposium on Fire Science and Technology, no. 62, 2013, doi: 10.1016/j.proeng.2013.08.058.
[105] E. K. Asimakopoulou, D. I. Kolaitis, and M. A. Founti, “Thermal characteristics of externally venting flames and their effect on the exposed façade surface,” *Fire Saf. J.*, vol. 91, no. 6, pp. 451–460, 2017, doi: 10.1016/j.firesaf.2017.03.075.
[106] K. Kawagoe, “Fire behaviour in rooms,” Tokyo, Japan, 27, 1958.
[107] C. Gorska, J. P. Hidalgo, and J. L. Torero, “Fire dynamics in mass timber compartments,” *Fire Saf. J. - Proc. 13th Int. Symp.*, doi: https://doi.org/10.1016/j.firesaf.2020.103098.
[108] C. J. Bateman, A. I. Bartlett, L. Rutkauskas, and R. M. Hadden, “Effects of Fuel Load and Exposed CLT Surface Configuration in Reduced-Scale Compartments,” 2018.